Studies of the Interaction between a Magnet and a High T_c Superconductor

A Thesis

in Partial Fulfillment of

the Requirements for the Degree of

Doctor Scientiarum

by

ZhongJin YANG

Department of Physics, University of Oslo

P.O. Box 1048, Blindern, 0316 Oslo 3, NORWAY

1991

Preface

The work presented in this dr.scient. dissertation has been carried out in the Low Temperature Laboratory of the Solid State Group, Department of Physics, University of Oslo, in the period 1988-1991.

The historical discovery of oxide superconductors in 1986 has triggered a revolution in condensed matter science. A great number of scientists have been working in this stimulating field. As a young scientist, I joined the scientific "gold-rush" in the beginning of 1987. Before August of 1988, I was mainly working on the materials preparations of the $Y_1Ba_2Cu_3O_{7-\delta}$ (Y123) superconductors. After coming to Norway in August of 1988, I have been directing my research into the preparation of Bi-base superconductors and the magnetic properties of the high transition temperature superconductors (HTSC).

This dissertation consists of two parts. The last part is eight research papers, which involve two topics related to the HTSC studies. The topic in the Supplement relates to the preparation and magnetic properties of the Sb-doped Bi-Pb-Sr-Ca-Cu-O superconductors, and the main topic describes the interaction between a permanent magnet and a HTSC studied by a mechanical pendulum. The first part of this dissertation has two purposes. One is to give a brief introduction and background to the research papers, and the other is to outline my scientific findings from the HTSC studies. Besides this thesis, in the past years, I have also done some theoretical work, which is not discussed here.

This research work has received financial support from the Norwegian Research Council for Science and the Humanities (NAVF), which is gratefully acknowledged. I am deeply grateful to Harald G. Bratsberg and Arne T. Skjeltorp who have been my scientific advisors and they are also co-authors on the research papers in this dissertation. Their support, encouragement and guidance have been of invaluable help in my training as a scientist. I am indebted to Tom Henning Johansen and Geir Helgesen for helpful stimulating discussions and a lot of support through all the years of my studies. My warm thanks go to P.M. Hatlestad and K. Nilsen for their invaluable help in the experiments. I wish to convey my sincere thanks to all the members of the Solid State Group at the University of Oslo. I also would like to gratefully thank C.W. Lung and all the other teachers, colleagues and friends of mine, both in China and in Norway, for their support, help and encouragement. In addition, I would like to express my greatest respect and thanks to my parents, who have brought up their children through a great hardship, and to my brothers and sisters, who took responsibility of taking care of my studies in the past years. Finally, my deepest gratitude goes to my wife, Jie, for her unlimited love and support throughout these years, and without her support, patience and help, this work could not have been done.

Oslo, August 1991 ZhongJin YANG

Contents

List of Scientific Papers

1. *Vibrations of a Magnet Levitated over a Flat Superconductor*, **Z.J. Yang**, T.H. Johansen, H. Bratsberg, G. Helgesen and A.T. Skjeltorp, *Physica* **C160** 461-465 (1989).

2. *Comment on "Lateral Restoring Force on a Magnet Levitated above a Superconductor"*[J. Appl. Phys. **67** 2631 (1990)], **Z.J. Yang**, T.H. Johansen, H. Bratsberg, G. Helgesen and A.T. Skjeltorp, *J. Appl. Phys.* **68** 3761-3762 (1990).

3. *The Lateral Force on a Magnet Placed above a Planar $YBa_2Cu_3O_x$ Superconductor*, T.H. Johansen, **Z.J. Yang**, H. Bratsberg, G. Helgesen, and A.T. Skjeltorp, *Appl. Phys. Lett.* **58** 179-181 (1991).

4. *Investigation of the Interaction between a Magnet and a Type-II Superconductor by Vibration Methods*, **Z.J. Yang**, T.H. Johansen, H. Bratsberg, G. Helgesen and A.T. Skjeltorp, *Physica* **C165** 397-403 (1990).

5. *Potential and Force between a Magnet and a Bulk $Y_1Ba_2Cu_3O_{7-\delta}$ Superconductor Studied by a Mechanical Pendulum*, **Z.J. Yang**, T.H. Johansen, H. Bratsberg, G. Helgesen, A.T. Skjeltorp, *Supercond. Sci. Technol.* **3** 591-597 (1990).

6. *Effect of Current on Collective Motion of Flux Lines in a Bulk $Y_1Ba_2Cu_3O_{7-\delta}$ Superconductor*, **Z.J. Yang**, H. Bratsberg, T.H. Johansen, G. Helgesen, and A.T. Skjeltorp, *Jpn. J. Appl. Phy.* **30** L92-L95 (1991).

7. *The Effect of Pb-doping in Bi-Sr-Ca-Cu-O and Sb-doping in Bi-Pb-Sr-Ca-Cu-O Superconductors*, **Z.J. Yang**, H. Bratsberg, T.H. Johansen, N. Norman, J. Taftø, G. Helgesen, I. Lorentzen and A.T. Skjeltorp, *Physica* **C162-164** 1587-1588 (1989).

8. *Preparation and Magnetic Properties of the Sb-doped Bi-Pb-Sr-Ca-Cu-O Superconductors*, **Z.J. Yang**, H. Bratsberg, T.H. Johansen, N. Norman, J. Taftø, G. Helgesen and A.T. Skjeltorp, *J. Magn. Magn. Mater.* **89** 309-314 (1990).

Part I
General Introduction

Since the historical discovery of the La-Ba-Cu-O superconductor by Bednorz and Müller [1] in 1986, due to the great potential for applications, a great number of scientists have been working in this exciting field. Several thousand research articles have been published in a variety of journals. The tidal wave of research into the newly found phenomena took off in several directions. The theorists began to examine the BCS theory and its implications, and almost everyone was synthesizing materials. The experimentalists were studying relations among electrical and magnetic properties while the pure materials scientists began to examine the microstructures, and the dependences of one or two measurable quantities on the processing procedures. The engineering and system community were preparing real conductors and designing the needed components. Each of the communities was holding between two and three annual meetings to discuss most recent results.

Since the early days of 1987, I have been engaged in this stimulating field. My research in this dissertation involves two subjects: The subject in the Supplement is a study about the preparation and magnetic properties of Pb-doped Bi-Sr-Ca-Cu-O and Sb-doped Bi-Pb-Sr-Ca-Cu-O superconductors (P.7 and P.8). The main subject relates to the theoretical and experimental investigations of the interaction between a permanent magnet and a HTSC. This involves several topics, such as vibrations of a superconducting bearing system (P.1), the forces on a small magnet above a big HTSC disk (P.2 and P.3), the potential and force of a magnet-HTSC system (P.4 and P.5), and transport current effect on the collective motion of flux lines (P.6).

In the following sections I am going briefly to state the physical background of these investigations and to summarize the results we have obtained.

1 Introductory Remarks

Superconductivity was first discovered by Kammerlingh Onnes [2] in Leiden in 1911, who observed that the resistance of mercury disappeared to zero at and below a critical transition temperature $T_c = 4.2$K. A perfect diamagnetic property is the so-called Meissner effect. discovered by Meissner and Ochsenfeld [3] in 1933, when they observed that a superconductor in a weak magnetic field completely expels the field from the interior of the material. They also discovered that superconductivity can be destroyed at a critical magnetic field. This effect is a fundamental property of superconductivity and shows a great difference between a perfect conductor and a superconductor.

The critical magnetic field can be thermodynamically related to the free energy difference between normal and superconducting states in zero field, the so-called condensation energy of the superconducting state. Therefore, thermodynamics has been used to describe the superconducting transition [4]. In 1935, the London brothers [5] proposed two

equations that phenomenologically describe perfect conductivity and diamagnetic properties of superconducting phase in weak fields. Moreover, in 1950 Ginzburg and Landau [6] introduced a complex pseudowave function as an order parameter for the superconducting electrons, in the so-called Ginzburg-Landau second-order phase transition theory (GL theory). A microscopic theory of superconductivity was formulated in 1957 by Bardeen, Cooper and Schrieffer [7]. This so-called BCS theory showed that a weak attractive interaction between electrons mediated by phonons causes an instability of the normal electron ground state with respect to formation of bound pairs of electrons called Cooper pairs with equal and opposite momentum and spin.

Since Onnes' discovery, one of the primary objectives of superconductivity research has been to raise the transition temperature T_c. The discovery of T_c above 10 K in NbC and NbN was one breakthrough. The discovery of the A 15 compounds, with T_c finally breaking through the 20 K barrier in the later 1960s and early 1970s, represented the culmination of two decades intense search for higher transition temperature.

1.1 Two Types of Superconductors

Superconductors are classified in two types according to their magnetic behaviors. Type-I superconductors exhibit a pure diamagnetic, or Meissner, effect when the applied magnetic field is below the critical field, B_c,[1] as shown in Fig 1(a). In type-II superconductors, however, the diamagnetic effect is not complete when the field exceeds a critical value called the lower critical field, B_{c1}. The diamagnetism is then not destroyed until the field exceeds another critical value, the upper critical field, B_{c2}. Between B_{c1} and B_{c2} the material is in a mixed state as can be seen in Fig. 1(b).

According to the GL theory, the two types of superconductors can be clearly distinguished in terms of the GL parameter κ ($\kappa(T) = \lambda(T)/\xi(T)$): type-I for $\kappa < 1/\sqrt{2}$ and type-II for $\kappa > 1/\sqrt{2}$. Here $\lambda(T)$ and $\xi(T)$ are called the coherence length and penetration depth, respectively.

Abrikosov [8] first predicted the existence of type-II superconductivity in 1957. The mixed state occurs in the regime where κ is greater than $1/\sqrt{2}$ for the solution of the GL equations. For type-II superconductors there exists a negative surface energy between normal and superconducting regions that minimizes the total free energy. These normal cylindrical cores, or magnetic flux, exists in the form of isolated filaments, called flux lines, along the direction of the applied field at field values between B_{c1} and B_{c2}. Each flux line, where the superconducting order parameter rises from zero to unity over a distance $\xi(T)$, contains the basic unit of one magnetic flux quantum $\Phi_0 = h/2e$. The local magnetic field

[1] In this thesis, B denotes the applied magnetic field, which is similar to the notation used by C. Kittel in his book: "*Introduction to Solid State Physics*", (John Wiley & Sons, New York, 6th Ed., 1986) P 317. Values of B_c are given in teslas in SI units. In SI we have $B_c = \mu_0 H_c$.

penetrates over a distance $\lambda(T)$ from the center of the flux line. This distance is called magnetic penetration length. The vortex current with a radius $\lambda(T)$ is circulating as a result of a gradient of local magnetic flux. The current interacts with the magnetic field produced by the vortex current encircling any other flux line. This interaction results in the flux lines repelling each other. The flux lines eventually are self-organized in a triangular lattice with a periodic structure called the Abrikosov lattice, which has been observed directly by using the decoration method (*i.e.* the Bitter pattern method) in 1960's [9].

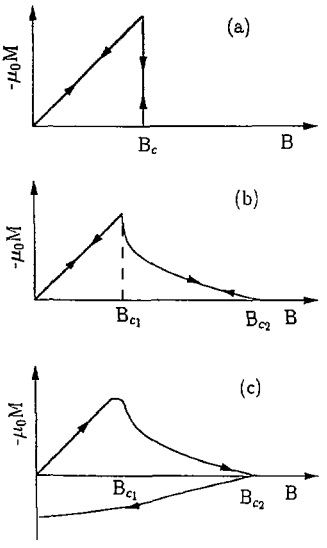

Fig. 1 Magnetization of long rod superconductors: (a) type-I, (b) ideal type-II, and (c) non-ideal type-II (irreversible magnetization). The applied field is along with the axis of the rod.

The magnetic structure of type-II superconductors in an applied field may be visualised as follows. In low fields $B < B_{c1}$ one has a Meissner effect, the energy of an isolated flux line being greater than the reduction in field energy that occurs if the flux line entered the superconductor. At the field B_{c1} this energy criterion is just satisfied, and flux lines

begin to enter. The equilibrium flux line density at a field above B_{c1} can be determined by the interactions that arise between flux lines as they come together. The flux lines approach with increasing field. Eventually the flux line cores touch and overlap, and the superconductivity disappears when the order parameter reduces to zero everywhere at B_{c2} [4]. The flux lines play a large role in the magnetic and transport properties of type-II superconductors.

The magnetic properties of type-II superconductors are shown in Figs. 1(b) and 1(c). At applied fields below B_{c1}, a type-II superconductor behaves exactly like a type-I superconductor with a perfect diamagnetization. When the field reaches B_{c1}, flux lines start to nucleate at the penetration layer and pass into the material. Since the flux is the same direction as that of the applied field, the induction inside is no longer equal to zero, and the magnitude of the magnetization suddenly decreases. As the strength of the applied field is further increased, the flux lines pack together more closely; thus the total induction increases, and the magnetization decreases smoothly with increasing applied field. When the field is reduced, the magnetization curve shows a reversible property, turning along the same path as the that increasing field. Based on the GL theory, the reversible magnetization can be theoretically predicted for ideal type-II superconductors.

1.2 Non-Ideal Type-II Superconductors

Impurities, defects, and inhomogeneities always exist in real superconducting materials. In the mixed state the flux lines can interact with these defects. This interaction leads to an irreversible magnetization behavior in most type-II superconductors. As the applied field increases below B_{c1}, the magnetization starts with flux exclusion. When the field is above B_{c1}, the magnetization peak rounds off as a result of the defects. Finally, the magnetization becomes zero at B_{c2} in the normal state. The magnetization follows a different path when the field is reduced from higher field. The magnetization versus field curve has, therefore, two different branches corresponding to increasing and decreasing field. respectively, as shown in Fig 1(c). This magnetic hysteresis can be understood in terms of the pinning of the flux lines by the defects. The superconductors with the departures from the reversible curve are called the non-ideal type-II superconductors, or hard superconductors.

In the presence of an applied current, the non-ideal type-II superconductors, show no resistance until a finite current is reached, since then the flux lines can be pinned by the defects. This current (or current density) is another important critical quantity of superconductors and is called the critical current (or critical current density, J_c). Anderson [10] and Gorter [11] were the first to make the microscopic argument that the critical current is reached when the Lorentz force on the flux lines is balanced by the pinning force as a result of the defects. Since the defects can be varied by different fabrication

techniques, the value of the critical current density depends on the preparation method. Hence, unlike the critical transition temperature and the critical fields, the critical current density is an extrinsic quantity and is mainly determined by the flux pinning properties of the material.

Although magnetic hysteresis [12] in superconductors had been observed in the 1930's, Bean's model [13] (1962) was the first one that successfully explained irreversible magnetization and its relation to the critical current density. In the corresponding reversible curve the flux lines enter abruptly at B_{c1}, and just above B_{c1} the flux density across the material is uniform. In the irreversible case, the effect of pinning tends to hold back the flux lines near the surface. There is a gradient of the flux density from the applied value at the surface to zero inside the material gradually. The Bean model assumes that the pinning strength determines the maximum gradient of flux density. By Maxwell's equations this means a maximum current density, the so-called critical current density.

The flux is held back by the pinning centers from reaching the equilibrium distribution. This means that the flux distribution at a point on an irreversible magnetization curve is always in a metastable state except in the ground state ($T = 0$K). However, the flux lines always vibrate and hop free from a pinned configuration as a result of a thermal activation. This jumping process can lead to an energy dissipation.

Above B_{c1}, type-II superconductors are not perfectly diamagnetic. The perfect conductivity is also lost. In the presence of a transport current, the flux lines experience a Lorentz force, $\mathbf{J}\times\mathbf{B}$, tending to move the flux lines. The motion of the flux lines generates a longitudinal dissipative voltage across the superconductor. In ideal type-II superconductors, the flux motion is hindered only by a viscous drag, and the superconductors then show a resistance comparable to that in the normal state. In non-ideal type-II superconductors, however, if the Lorentz force is larger than the pinning force on the flux lines, the flux lines follow with a corresponding resistance for any value of applied current. This can happen although the material is still in a superconducting state. An energy dissipation is caused by the resistance resulting from the flux flow.

1.3 Some New Features of HTSCs

After the introduction of the La-Ba-Cu-O superconducting system, many new systems have been synthesized, particularly the Y-Ba-Cu-O [14], Bi-Sr-Ca-Cu-O [15], and Tl-Ba-Ca-Cu-O [16] systems. In these materials the superconducting transition temperature (T_c) has been raised above liquid nitrogen (LN_2) temperature (77K), and practically the Tl-base oxides have reached the highest $T_c = 125$K. All these compounds have Cu-O planes or layers in either orthorhombic or tetragonal crystal structures, leading to unusually anisotropic physical properties.

Although each of these HTSCs has its own characteristics, all of them share a largely

common phenomenon: the superconducting state seems to be based on the Cooper pairs. However, the presence of anisotropy, the granular structure, and the higher operation temperatures produce completely different values for characteristic parameters relative to conventional superconductors.

The $YBa_2Cu_3O_{7-\delta}$ (Y123) and $Bi_2Sr_2CaCu_2O_x$ systems are good examples among these HTSCs. The Y123 has an orthorhombic structure with unit cell parameters a = 0.38591nm, b = 0.39195nm, and c = 1.18431nm [17]. The Cu-O_2 planes are primarily responsible for electron conduction. For the Y123, there is a structural phase transition to a tetragonal (non-superconducting) phase as the temperature is raised above 700°C in an oxygen atmosphere. The T_c strongly depends on the oxygen composition in Y123. Somehow, $Bi_2Sr_2CaCu_2O_x$ appears to have a relative stable tetragonal crystal structure with a = 0.3814nm and c = 3.052nm [18]. The oxygen composition in $Bi_2Sr_2CaCu_2O_x$ is much more stable than that in Y123.

The coherence length, ξ, is very short in the HTSCs. A typical value for ξ is of the order of 1nm, which is of the same order as the crystal unit cell's dimension. This small value implies that the superconducting properties will be much more sensitive to small scale structural and chemical imperfections than in conventional superconductors, whose $\xi \sim 10 - 10^3$nm. The short coherence length also leads to an extremely high value of the upper critical field, B_{c2}, with potential advantages for applications.

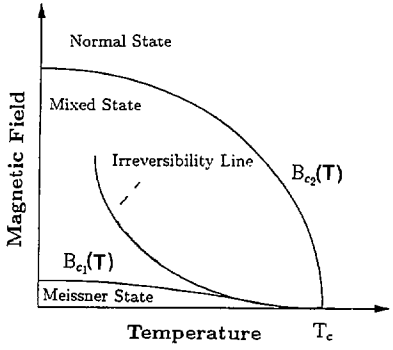

Fig. 2 Magnetic phase diagram of high T_c Superconductors.

The HTSCs are non-ideal type-II superconductors and exhibit many properties similar to those of conventional superconductors, such as the presence of the Abrikosov vortex line,

upper and lower critical fields, and magnetic hysteresis. However, the HTSCs have much more complicated magnetic properties. In the mixed state, unlike conventional type-II superconductors, the HTSCs show a very complicated phase diagram. A generally accepted distinguishing feature of the HTSCs from the conventional type-II superconductors is the existence of an irreversibility line between B_{c1} and B_{c2} in the $B-T$ diagram [19], which is not clearly understood yet. According to statistical physics, the probability of flux lines' hopping is proportional to the factor $\exp(-U/k_BT)$, where U is the pinning potential barrier and k_B is the Boltzmann constant. Therefore, the barrier controls the irreversibility line. It seems to be clear that the HTSC materials show a different feature about the barrier from the conventional superconductors. However, it takes more time fully to understand the differences. In the region near the irreversibility line, several phases such as vortex lattice, vortex glass, and vortex liquid etc. have been proposed [20][21][22][23].

Although there are various theories and experiments to explain some complicated properties of the HTSCs, the new phenomena have not been completely understood, and neither the experimental evidence nor the theories are fully consistent [24].

1.4 Magnetic Levitations and Related Vibrations

The history of bearings started from the dawn of human civilization. Since the Palaeolithic period, people have used mechanical bearings in their machine designs. Along with the progress in science and technology in this century, more and more physical means have been invented and developed in the applications of bearing designs. In a recent paper, Brandt[25] reviewed levitations in various physical systems, and stressed in particular the superconductor system.

A very important property of superconductors is their ability to levitate a magnet. The low T_c of conventional superconductors limits the applications of this phenomenon in many aspects. The discovery of the high T_c oxide superconductors exhibits the possibility to apply superconductor systems in popular technology, even in daily life [26].

There are always vibrations in a mechanical (physical) system no matter how the system is in a static or stationary motion status. Vibrations are also very common in engineering and constructions. Sometimes, they are so severe that constructions may be damaged. It is very important to avoid resonances in designing a new machine and to reduce vibrations in machine making.

Considering a small magnet-big superconducting plane system, we have utilized the dipole-dipole interaction model in P.1: (i) to analyse levitation forces; (ii) to study vibrations in connection with levitation; and (iii) to apply the vibration methods to type-II superconductors for exploring the physical properties of flux pinning. The methods, given in P.1 for studying the intrinsic vibrations of these kinds of systems, are also believed to be suitable for engineering design.

Following our theoretical investigation, Braun and co-workers have recently measured the vibration frequencies experimentally [27]. The experimental results are in semi-quantitative agreement with our theoretical predictions even though the magnets used in their experiments were not spheres but discs and cubes.

2 Experimental Setup

From the 1920's mechanical methods were introduced to study flux motion for conventional superconductors (for a review, see Ref. [28]). Two quite common techniques have been the use of a torsion pendulum and a vibrating reed. After the discovery of HTSCs, several new mechanical techniques have been introduced to characterize some physical properties related to levitation applications by using HTSCs. Some of these will be reviewed briefly below followed by a description of our experimental setup.

2.1 Other Mechanical Methods

The physical origin of the mechanical responses is the motion of the magnetic flux lines inside superconductors. From different starting points and with different application backgrounds, these mechanical techniques are used for different aims. The torsion pendulum was employed to probe the microscopic features of the flux motion. However, after the T_c exceeded LN_2 temperature, it became feasible to apply superconductors to the magnetic bearings. Concerning the research on macro-phenomena related to the superconducting levitation, some new methods have been invented to meet the requirements.

2.1.1 Torsion Pendulum

This section is a short review about the torsion pendulum technique used by Houston and Smith [29], and Wraight [28] to measure mechanical forces on superconducting films in a magnetic field.

A Nylon disc (lead used in Wraight's experiment) connected to a long steel wire was hung from a frame forming a torsion pendulum. The superconducting strips (a ring-shape specimen used by Wraight) were symmetrically mounted on the disc. Some slots were radially made on the disc. The inhomogeneous magnetic field on the specimens was produced when the field passed through the slots. In the experiments, the configurations of the magnetic fields could be oriented to be perpendicular to or parallel with the motion direction of the specimens. The top part connected with the wire had a mirror for recording the oscillations photographically. The specimen and connecting rod were suspended tautly between a single phosphor-bronze strip at the bottom and a bifilar suspension at the top. By varying the tension on the bifilar suspension the period of oscillation could

be altered during a run. The disc and specimen were suspended in helium gas at low pressures.

By measuring the energy loss versus applied field at various temperatures, they were able to characterize the pinning amplitudes of flux lines inside the superconductors.

2.1.2 Vibrating Reed

In the 1980's, Brandt et al.[30] introduced the vibrating reed technique to study the pinning of flux lines.

A cantilevered ribbon-shape superconductor and a pair of electrodes placed on each sides of the ribbon formed a vibrating reed. One electrode is used for driving the ribbon, and the other is used for detection. The pinning properties can be characterized by measuring the resonance frequency and the damping of the oscillations versus the applied magnetic field through the specimen at various temperatures.

In the beginning, the vibrating reed was used quantitatively to investigate the flux pinning for the conventional superconductors [31]. After the discovery of the HTSCs Gammel et al.[32] used this technique to observe a melting transition of flux lines in the $B - T$ diagram for an Y123 sample. Somehow, the later experiments showed that the melting line coincided with the depinning line reported by different groups [33].

2.1.3 Clamped Beam (Cantilever)

Moon's group [34] designed a cantilever to measure both the static (vertical and lateral) and dynamic forces on a magnet above a HTSC disc.

A small permanent magnet was mounted to one (free) end of an aluminum beam, which was fixed to a 3-dimensional motorized stage. Two strain gauges glued on the top and bottom surfaces of the cantilevered beam were used to measure the bending strain, which after calibration was used to indicate the levitation and lateral forces. An optical tracking camera (Optron) with a resolution of about 0.02 mm was used to measure the motion of the small magnet relative to the HTSC surface. The elastic beam was sensitive to a force of around 10^{-4}N. The calibrated data from the strain gauges and camera were plotted directly on an $x - y$ recorder.

Using the same experimental setup, they also measured the hysteretic behavior of the forces and the magnetic stiffness in the magnet-HTSC system. The same kind of setup has also been used to investigate the amplitude-dependent magnetic stiffness for the sintered, melt-textured and melt-quenched HTSC materials [35].

2.1.4 Magnet-Coil Resonance

The HTSC disc rested on a aluminum block in LN_2. When the system was well cooled, a magnet placed at the disc center floated there in a position of stable equilibrium above the surface. A coil supplied with a weak a.c. current was used to drive the levitated magnet. The coil could be oriented to be parallel with or perpendicular to the HTSC disc. The force (potential) in the magnet-HTSC system could be obtained by measuring the resonance frequency as a function of motion amplitudes of the magnet,

Williams and Matey [36] placed a coil horizontally (parallel with the HTSC disc) and studied the lateral force (potential) on a magnet levitated above a HTSC disk.

Braun et al.[27] placed a coil in different orientations and measured the resonance frequencies of a levitated magnet in different modes.

Nemoshkalenko et al. [37] placed a coil vertically (perpendicular to the HTSC disc) and measured the attenuation and nonlinearity of the vertical oscillation, which were interpreted in terms of the viscosity of the vortex lattice and the onset of the hysteretic damping related to the depinning of the flux lines for the HTSCs.

2.1.5 Torsion Balance

A torsion balance was introduced by Weeks [38] to measure the levitation force for the Y123 and Tl-Ba-Ca-Cu-O HTSCs.

The balance is essentially a torsion spring made with a tightly stretched piece of hardened steel wire. One end of the wire is fixed to a dial which can be twisted through a measurable angle. The other end of the wire is inserted into a retractable clamp that is used to tighten the wire. The clamp can also be rotated which provides overall calibration of the balance. One end of a hollow copper rod is clamped to the middle of the wire so that the rod and wire are perpendicular. A small magnet is fitted to the other end of the copper rod with its dipole axis in the plane perpendicular to the rod. When a HTSC disc is placed below the magnet, the force between the magnet and HTSC twists the wire. According to Hookes' law, the force is proportinal to the twist angle. The levitation force is thus obtained by measuring the twist angle by changing the separation between the magnet and the HTSC.

2.2 Our Apparatus: a Novel Computerized Pendulum

By extending the investigation on the vibrations of a free small permanent magnet levitated above a superconductor (P.1), we have designed and constructed a mechanical pendulum to investigate the interaction in a magnet-HTSC system.

The techniques of tbe pendulum with different operating modes have been described in P.3, P5, and P.6.

A permanent magnet, placed above a bulk (film) HTSC sample, is glued at the bottom end of a 4 mm diameter tubular quartz rod. At the other end, the rod ($\sim$ 50 cm) is attached to a metal frame that permits the rod to swing as a vertical planar pendulum. The horizontal axis of rotation is provided by a razor blade fixed to a support. The projected motion of the magnet onto the horizontal plane is parallel to the lateral displacement of the sample, the x-direction.

An expanded laser beam is sent through an aperture with a rectangular cross-section. Part of this light beam is intersected by the pendulum and focused by a lens onto a photodiode. The diode signal is amplified and recorded by a PC/AT.

The small permanent magnet, (M') and the adjacent coil were employed for controlling the motion of the pendulum (by using a PC/AT). In the experiments, three kinds of modes were used: (i) The feedback system (used in P.3) controls the current in the coil to attract the M' for measuring the lateral force on a long magnet bar above a big HTSC disk. (ii) The free oscillations (used in P.4, P.5, and P.6) were obtained via pulling the rod out to a fixed position ($< 0.4°$ from vertical) by supplying current to the coil. By switching off the current, the oscillations then started. (iii) The forced oscillations (used in [39]) were excited by supplying a.c. current in the coil to drive the M'.

In the experiments, the direction of the magnetic moment (M) could be made: (i) normal (N-configuration) and (ii) parallel (P-configuration) to the direction of motion of the pendulum. The P-configuration was used for measuring the lateral force, and the N- and P-configuations were used for the studies of potential (force) in a magnet-HTSC system and current effect on the collective motion of flux lines in HTSCs.

The performance of the pendulum was also checked with the samples in the normal state for clarifying the effects from the magnet-superconductor interaction. It was found that the free-damping Γ_0 was very small and negligible compared to the damping resulting from the superconducting sample. Also, no change in the oscillation frequency ν_0 of the free pendulum was observed. Thus, by a relatively rapid sampling rate of the amplitude signal (pendulum position), we could extract directly information about the magnet-HTSC interactions from frequency and damping changes.

Using this pendulum, we have studied: (i) the lateral restoring force on a bar-shaped permanent magnet above a big Y123 disk (P.3); (ii) the potential function and force between a (small) permanent magnet and a big HTSC disk (P.5); (iii) the current effect on the collective motion of fluxoids in HTSCs (P.6); and (iv) quasistatic fie'd responses of fluxoids in an Y123 film [39]

The advantages of the present pendulum compared with other mechanical methods are:

- It has the highest resolution (10^{-5}N) for macroscopic measurements on the lateral stability of the magnets above a HTSC. In a way, this is important for characteri-

zations of the HTSC materials before use in levitation or other applications.

- Currents can pass through the sample, by which one may investigate the combined motion of fluxoids.
- The sensitivity is sufficiently high to perform measurements on high quality film (single crystal) specimen for determining the pinning force on fluxoids and figureing out the profile of the pinning potential well.

3 Static Forces on a Small Magnet above a Big HTSC Disk

Before the discovery of the high temperature oxide superconductors (HTSC), major efforts were made to apply superconductors to magnetic bearing systems [25][40]. However, the expensive helium cooling systems for the conventional superconductors have limited the applications in many fields. For instance, the levitation train (Maglev) project employing conventional superconductors has for a large part been abandoned. The United States shut down their Maglev project more than 10 years ago. Germany has not used the superconducting system in their ongoing Maglev project either ([25][41] and references therein). (It should be pointed out that there are only two Maglev projects in the world, but, the Maglevs do not use the same levitation principle as we discuss in this thesis.) The historical discovery of HTSCs has stimulated more and more people to reconsider the possible applications of magnet-superconductor systems, in particular for levitation trains [42]. With the possibility of using liquid nitrogen as coolant, the building of cost-efficient superconducting levitation trains has come closer to realization.

While some theoretical analyses have been reported on the levitation and lateral forces, most papers have focused on experimental investigations.

In most cases, fundamental research on superconducting levitation has involved studies of systems formed by a small magnet and a large superconductor. Besides this, other systems have been considered and investigated, such as a ring-shaped magnet with a small HTSC body [43][44][45] and a ring-shaped superconductor with a small cylindrical magnet [46]

There has been considerable progress in engineering designs of levitation systems. For example, high-speed rotation of magnets on HTSC bearings have been investigated by some groups [47][48][49], and a micro superconducting actuator has been fabricated and tested [50]. A superconducting magnetic levitation system for the transport of light payloads has also been made and investigated [51].

Somewhat related to these topics, we have mostly focused our research on the small magnet and big HTSC plane system. Concerning this system, we have achieved results

relevant to some engineering problems.

3.1 Models for the Magnet-HTSC Interaction

Before the discovery of the HTSC, the image method was the only theoretical method to describe the magnet-superconductor interaction by using the dipole-dipole model. In this method, only the Meissner effect is taken into account. This model indeed provides a correct description for type-I superconductors, (or when $B < B_{c_1}$ for conventional type-II superconductors). After the discovery of HTSCs, more and more experiments have been performed to investigate the interaction with HTSCs. The results of the HTSCs are not consistent with the dipole-dipole model. Concerning the lifting force, Hellman et al [52] have introduced a complete penetration model. Following the experimental results [36], Davis [53][54] has suggested a model to calculate the lateral force based on Bean's critical state model [13].

3.1.1 Dipole-Dipole Model

It may be shown [55] that the field produced around a homogeneously polarized spherical permanent magnet (SPM) with moment $\mathbf{M}$ is the same as that created by a point dipole with moment $\mathbf{M}$ located at the center of the sphere. Considering a SPM with moment $\mathbf{M}$ over an infinite, flat superconductor as shown in Fig. 6 of P.5, the image method can be used to describe the interaction. The zeroth-order approximation is the dipole-dipole model. The potential can thus be expressed as (SI units hereafter):

$$V = \frac{\mu_0}{8\pi} \frac{\mid \mathbf{M} \mid\mid \mathbf{M}' \mid}{(2z)^3} [\cos(\alpha + \alpha') + 3 \sin\alpha \sin\alpha'], \tag{1}$$

where $\alpha' = \alpha$ is the inclining angle, and $\mathbf{M}'$ is the image dipole of the dipole $\mathbf{M}$ and $\mid \mathbf{M} \mid = \mid \mathbf{M}' \mid$. The potential can then be written

$$V = \frac{\mu_0}{64\pi} \frac{\mid \mathbf{M} \mid^2}{z^3} (1 + \sin^2\alpha) , \tag{2}$$

with minimum $\alpha = 0$, which is the equilibrium position. At the equilibrium position, the only force on the magnet is then given by:

$$\mathbf{F} = -\nabla V = \frac{3\mu_0}{64\pi} \frac{\mid \mathbf{M} \mid^2}{z^4} \mathbf{k} , \tag{3}$$

where $\mathbf{k}$ is the unit vector in the $z-$direction. No lateral force and twist torque can exist in the dipole-dipole model, but experiments show that there are a significant lateral force and a pronounced twist torque in the magnet-HTSC system [34][36][56] (P.3). Furthermore, the measured levitation force is much smaller than the value evaluated by using the dipole-dipole model ($1/5 \sim 1/2$) [57]. This means that the dipole-dipole model can not describe the magnet-HTSC system due to the penetration at very low fields, and a new model is required to interpret the observed phenomena.

3.1.2 Complete Penetration Model for Lifting Force

Studying the levitation height of a small magnet above a HTSC plane, Hellman et al. [52] have introduced a complete penetration model to calculate the levitation force. Considering that the energy cost of flux lines' penetration in the HTSC contributes to the origin of levitation, they showed that the levitation force is

$$F \propto z^{-2} \tag{4}$$

where z is the distance between the center of the SPM and the upper surface of the HTSC.

3.1.3 Davis Model for Lateral Restoring Force

Referring to Williams and Matey's work [56], Davis [53][54] has suggested a model to calculate the lateral force based on Bean's critical state model [13]. Davis has obtained the following expression for the force:

$$F_x(x_0) = -\frac{\mu_0}{4J_c}\left[H_0^3(0) - \int_{-\infty}^{0} dx \left(H_0(x-x_0)\frac{\partial H_0^2(x)}{\partial x} + H_0^2(x-x_0)\frac{\partial H_0(x)}{\partial x}\right)\right], \tag{5}$$

where $H_0(x)$ is the field profile produced by the magnet at the lateral displacement x. Davis evaluated the force numerically using the field profile of an infinitely long current carrying wire

$$H_0(x) = \frac{H_0(0)}{1+X^2}, \qquad X = x/h, \tag{6}$$

where x is the lateral displacement, and h is the height of the field source from the superconductor.

In fact, this can be calculated analytically (P.2):

$$\begin{aligned}\frac{-F_x(x)}{\mu_0 H_0^3(0)/4J_c} &= \frac{4+7X^2+X^4}{(4+X^2)^2} + \frac{X(20+X^2)}{(4+X^2)^3}(\pi - \arctan X) \\ &\quad - \frac{4(4+5X^2)}{X^2(4+X^2)^3}\ln(1+X^2).\end{aligned} \tag{7}$$

3.2 Lifting Force Experiments

Most activities on the force measurements in the magnet-HTSC systems have focused on the lifting (vertical) forces [34][38][52][57][58][59][60][61].

According to the complete penetration model of Hellman and co-workers, the lifting force is $F \propto z^{-2}$. However, to our knowledge, no experiments have confirmed this model.

Moon's group [47][62] have measured the levitation force as a function of separation (z) and the stiffness as a function of levitation force (F). After a series of experiments,

they have introduced an empirical exponential formula to express the relationship between the levitation force (F) and separation (z):

$$F = F_0 \exp(-\alpha z) , \tag{8}$$

and a phenomenological power-law formula to describe the stiffness (k spring constant) as a function of the lifting force (F):

$$k = CF^{\alpha'} . \tag{9}$$

However, so far they have not given a physical interpretation for their empirical formulae.

It should be pointed out that $k \neq -\partial F/\partial z$ (or $\partial F/\partial x$ for the lateral component) because the levitation force and lateral force measurements show hysteresis [34][57][63] due to the hysteresis in magnetization of the HTSCs. It is now clear that the magnetization hysteresis loop depends on the pinning of the flux lines in superconductors. A stronger pinning results in a larger area of the hysteresis loop and higher critical current density J_c. By using the melt-quenched preparation method, it has been possible to increase the J_c of ceramic (bulk) HTSCs, and the levitation force has been enhanced significantly [26][64][65].

Similar to Moon et al.'s measurements Weinberger and co-workers [48] have also measured the levitation force and its stiffness as functions of the separation using an analytic balance. They have also measured the vertical mechanical resonances of a freely levitated magnet above a HTSC sample. By measuring the levitation force as a function of temperature they have proved that, at a weak field condition (5×10^{-3} T), the force is correlated with the magnetization data measured by a SQUID.

Following the first reports of the suspension force in HTSCs [66][67], Adler and co-worker [68][69] have observed that a small piece of the conventional superconductor Nb_3Sn could also be suspended below a magnet. These results indicate that pinned flux lines must play a crucial role in levitation force of type-II superconductors.

It seems therefore reasonable that studying flux penetration is a good starting point to interpret the results found for the magnet-HTSC systems.

Johansen et al. [70] measured the levitation forces on a SPM placed above several $Y_1Ba_2Cu_3O_{7-\delta}$ (Y123) disks, and were able to confirm Moon et al.'s empirical formula (8), for both configurations: the magnetic moment of the SPM normal (N-state) and parallel (P-state) to the upper surface of the HTSC samples. Moreover, we observed a crossover behavior of two exponential coefficients when the maximum field on the Y123 disks reaches 8×10^{-3} T for both configurations. Based on the consideration for the interaction of fluxoids in the superconductor, we tried to formulate a phenomenological description [71].

3.3 Lateral Forces on a Long Bar-Shaped Magnet above a Big HTSC Disk

Due to the fact that the most important aspect of levitation applications is the ability of magnet-HTSC systems to lift "heavy" bodies, most studies have been focused on investigating levitation forces. Somehow, the lateral stability of a lifted body is very important in the levitation applications by using HTSCs. However, there are only a few published papers concerning the lateral force study. Williams and Matey [36] were the first to measure the lateral force on a small magnet floating above a HTSC disk using a resonance method. Moon and co-workers measured the hysteresis behavior of the lateral force [34].

Using the mechanical pendulum, we measured the lateral force on a long bar-shaped permanent magnet above a big Y123 disk (P.3).

We performed the experiments on a sintered Y123 disc sample (T_c = 90K, thickness 7 mm and diameter 70 mm). The maximum tangential field on the HTSC sample is $B_{max} = 1.3 \times 10^{-3}$ T for our measurements.

The experimental results of lateral force against displacement is shown in Fig. 2 of P.3. The curve of the lateral force versus displacement is quite similar to the behavior of the torque against the rotating angle of the applied field obtained in the $La_{1.85}Sr_{0.15}CuO_{4-\delta}$ and Y123 HTSCs by Giovannella et al.[72], which was interpreted in terms of the flux creep. Compared with Williams et al.'s result [36] and Moon et al.'s result [34], our experimental data have a higher resolution. A very important result is that the lateral stiffness is independent of the lateral displacement. The experimental data have been compared with Davis' model, which is the only theory treating the lateral force.

The x-component of the field profile from a permanent magnetic bar infinitely long in the y-direction and $x \times z$ dimensions of $2l \times 2w$, can be expressed as:

$$H_x = 2m_v \left(\arctan \frac{h-w}{x+l} + \arctan \frac{h+w}{x-l} - \arctan \frac{h-w}{x-l} - \arctan \frac{h+w}{x+l} \right) , \qquad (10)$$

where m_v is the dipole-moment volume density and h is the distance from the center of the bar magnet to the superconductor surface. When the vertical distance (h) is larger than $2w$, the field can be approximated by a dipole-line model (polarized along the x-direction and transverse to the line direction) and expressed as:

$$H_x = 2m_l h^2 \frac{X^2-1}{(X^2+1)^2} , \; X = x/h , \qquad (11)$$

where m_l is the dipole-moment linear density (per unit length), x is the lateral displacement, and h is the height of the dipole-line above the superconductor.

Since Davis' model is not valid for the fields which changes sign in the plane [54], we have tried several positive field profiles to evaluate the forces, such as rational polynomials and Gaussians, however, we have not found any one in agreement with the experimental

results even for the fractional field profile $H_0(x) = H_0(0)/(1+X^2)^3$, which is a good approximation for the infinite dipole-line model given by Eq. (11).

4 Magnet-HTSC Interaction

Due to the granularity, the bulk HTSCs show many new phenomena differing from the conventional superconductors [4]. It is generally accepted that the magnetic properties of the bulk HTSCs are dominated by the weak links between the granules at low external fields. The lower critical field of intergranules is $B_{c_{1J}} << B_{c_1}$ (the lower critical field of the intragranules). Tinkham and Lobb [73] have estimated $B_{c_{1J}} \sim 0.5 \times 10^{-4}$ T for a three-dimensional weak link cubic array model. Clem [74] has obtained the result $B_{c_{1J}} \sim 10^{-4}$T using the weak link Josephson coupling parameters.

This means that, if a permanent magnet is placed above a HTSC, the magnetic field from the magnet penetrates into the HTSC bulk materials for most cases. Furthermore, when the magnet is moved by an external force, such as the gravitational force, the flux lines in the HTSC will follow the motion. If the flux lines are in the vortex-liquid phase, the magnet will be influenced by the viscous force of the flux lines, but if the flux lines are in the vortex-glass phase, the magnet will be influenced by the pinning force of flux lines in the HTSC. These aspects are very important in levitation applications with motion between the magnet and the HTSC.

4.1 Potential and Force Between a Magnet and a HTSC

This research is an approach to investigate some macroscopic physical parameters (potential and force) by measuring the mechanical responses in a magnet-superconductor system.

In these experiments (P.4 and P.5), we used the same sample as that used in the lateral force measurements. The sample was immersed in liquid nitrogen (77K) and the distance z between the sample and permanent magnet could be adjusted by moving up and down the nitrogen reservoir containing the sample.

The magnet (M) used in these measurements had a cube-like shaped ($6.5 \times 6.5 \times 7.5\text{mm}^3$) Nd-Fe-B permanent magnet with rounded edges. The magnet was magnetized with a 1.3 T field along the longest side. The maximum remanent field on the surface of the magnet was measured to be 0.4 T using a Hall-probe.

The free oscillation operating mode was used in these experiments.

By varying the distances z between the magnet and the superconductor, the changes in frequency (ν) shift and damping (Γ) can clearly be seen.

In order to affirm that this is a specific interaction, normal metals and alloys (copper, aluminium, brass, etc.) were used as a substitute for the superconductor. Damping (due

to the eddy current) was observed for these, but frequency changes were never observed.

The results were confirmed by measuring other Y123 samples with various sizes made by different companies.

The experiments show that: (i) for the N-configuration, the frequency initially decreases slightly (this decrease is in the level of the resolution), and increases drastically with decreasing z; (ii) for the P-configuration, the frequency increases monotonically with decreasing z; and (iii) for both configurations, the frequency shifts show hysteresis for a cycling measurement (first decreasing z and then increasing z).

The frequency increase is due to some kind of attractive forces with lateral or vertical components. The physical reason for the frequency increase is due to the fact that the flux lines penetrates into the HTSC via the inter-granules or grain boundaries. The pinned flux lines attract the magnet and contribute to the frequency increase. (Unfortunately, we cannot perform this experiment with the small single crystals available at the present time).

4.2 Effect of Currents on the Motion of Fluxoids in HTSCs

Most applications of the type-II superconductors depend on the physical properties of the mixed state. An exotic picture of the HTSCs from the conventional type-II superconductors is the existence of an irreversibility line in the mixed state. (For a review about conventional superconductors, see Ref.[75].) It now seems clear that the irreversibility line determines the critical current density (j_c). For the present materials, j_c is very low and this limits the wide applications of the HTSCs for most cases.

Flux line (fluxoid) dynamics in type-II superconductors reveals information about the motion of vortices as influenced by various pinning effects from physical defects like inhomogenieties, strains, and vacancies. These effects are important for the depinning critical current and possible applications of HTSCs. Traditional a.c. susceptibility and magnetization measurements have revealed giant thermal flux creep in these materials [19][33][76][77][78][79].

Related to the dynamics of fluxoids in HTSCs, it is also of interest to find the relationship between the transport currents and the pinning barrier. Several experimental [80] and theoretical [81][82][83][84] papers have been published in journals and proceedings. All of these reports have focused on the behavior of the intragranules, i.e. the physical properties of single crystals and highly orientated thin films. This research is very important for the applications in microelectronics. The application of the bulk HTSC materials is equally important in other fields of science and technology.

As stated above, the lower critical field of the intergranules ($B_{c_{1J}} \sim 10^{-4}$T) is much lower than the lower critical field of the intragranules ($B_{c_1} \sim 10^{-2}$T for the Y-Ba-Cu-O and 2×10^{-3}T for the Bi(Pb)-Sr-Ca-Cu-O). When a relatively weak external field B in

the range $B_{c_{1J}} < B < B_{c_1}$ is applied to a bulk HTSC sample, the penetration takes place via intergranules. The pinning properties of the flux lines in this field range have not been understood yet.

By extending the pendulum experiments described in the previous sections, we have studied the effect of the transport currents on the "*dynamic*" responses of the flux lines in a bulk Y123 HTSC in the field range of $B_{c_{1J}} < B < B_{c_1}$ (P.6).

In all of the experiments, the sample current (I) direction was parallel with the light beam, and perpendicular to the direction of the motion of the magnet. Also the current could be in one direction (positive) or reversed (negative).

As stated previously, the interaction between a free-swinging permanent magnet and a superconducting disk leads to frequency change and strong damping. As shown below, this may be related to the flux bundle activation barrier U [10][81][84]. Specifically, we find that the predicted power-law dependence: $U(I) \propto I^{-\alpha}$ describes the data well for a certain range of currents.

The measurements of the oscillation frequency (ν) and damping factor (Γ) of the pendulum with sample currents from 0A to 5A in steps of 0.5A were performed with various distances between the magnet and the superconductor.

When the magnet is moved by the gravitational force, the fluxoids try to follow the magnet and perform a collective motion (hopping). The collective motion needs to overcome the pinnings at randomly distributed defects such as the interfaces of the intergranules. The pinned fluxoids attract the magnet, and as a consequence, the frequency ν increases due to the collective pinning of weak disorder. The frequency shift is thus a measure of the collective pinnings. From a classical point of view, $4\pi^2(\nu^2 - \nu_0^2)$ expresses the energy gain of the pendulum due to the collective pinnings in the HTSC sample. Therefore, we argue that the quantity $\delta\nu^2 = \nu^2 - \nu_0^2$ is proportional to the bundle activation energy U.

The collective pinning barrier U is of the order of the elastic energy of hopping flux bundles [10][81]. When a current is passed through the sample, the Lorentz force $\mathbf{F} = \mathbf{I} \times \mathbf{B}$ enhances the collective motion of fluxoids, which is equivalent to reducing the collective pinning barrier U. As a result of the reduced magnet-HTSC interaction, the "*effective stiffness*" of the pendulum is also reduced.

Feigel'man et al.[81] have studied the flux-creep phenomena in the case of collective pinning by weak randomly distributed defects. Based on the Anderson concept of flux bundle, they have shown that the bundle activation barrier U has a power-law dependence on current I: $U(I) \propto I^{-\alpha}$. For different regimes of currents, α changes from 1/7 to 7/9. Although they considered the single crystal materials, the physical basis for this theory is the pinning of weak disordered defects. The physical basis for the present results is also the randomly distributed pinning centers. Therefore, this theory should also be applicable for analyzing the present experimental data.

The field dependence of the barrier exponent (α) has also been measured, and the result is in qualitative agreement with Feigel'man et al.'s theory (P.6).

We found that the effect of sample currents on the frequency and damping is very different for weak fields ($B \sim B_{c_{1,J}}$ corresponding to $\nu \sim \nu_0$ without sample current and only a few penetrating flux lines present) and strong fields ($B \gg B_{c_{1,J}}$ corresponding to $\nu \gg \nu_0$ without sample current and with a certain amount of flux lines). It appears that when $B \sim B_{c_{1,J}}$, the frequency and damping factors are almost independent of sample currents. There seem to be a very small increase in frequency with an increase in sample current, but this is on the level of our experimental resolution. However, when the field is much higher than $B_{c_{1,J}}$, the effect of sample currents is significant.

Kes et al.[83] have introduced a theory to describe thermally assisted flux flow (TAFF). According to their theory, the activation barrier U is independent of the field for the TAFF at small driving forces. Kes et al.'s theory is a good description for isolated fluxoids. For the TAFF, the hopping of fluxoids is governed by the conventional linear diffusion equation. In this case the fluxoids relax individually, and the correlation of the fluxoids does not play an important role. The present experiments at low fields are consistent with Kes et al.'s theory. In the case of low fields, the fluxoid-fluxoid interaction is very weak since only a few fluxoids are present in the sample. The motion of fluxoids is similar to the TAFF in this case. However, when the fields are high enough, the correlation of fluxoids is more pronounced. As a consequence, the motion of fluxoids becomes collective, i.e. the flux-"creep" is the case of collective pinnings by weak disorder. As a result of an increase in fluxoid-fluxoid correlation, the barrier exponent α increases monotonically with increasing fields.

5 Concluding Remarks

The principal conclusions of the research presented in this thesis can be summarized as follows:

- The levitation forces of a magnet above a superconducting plane has been analysed, and the vibrations near equilibrium positions in a magnet-superconductor system have been investigated.
- Extending the research of vibrations in the magnet-superconductor system, we have constructed a novel mechanical pendulum to probe the interaction between a magnet and a HTSC, which includes several topics:
- *i)* The lateral force on a long magnet-bar above a HTSC disk. The stiffness of the force shows that HTSCs are much more stable laterally than had been predicted theoretically.

- *ii)* The potential and force in the magnet-HTSC system. The experimental results are consistent with the weak-link model for bulk HTSCs.
- *iii)* The effect of transport current on the collective motion of flux lines in a Y123 bulk sample. The experimental results have been interpreted based on the collective motion theory.

Many questions remain in the study of HTSCs. Theoretical investigations of the nature of the flux structure in HTSCs is under way. Layered structure, quasi two dimensional systems, short coherence length, and high operating temperature should play important roles in the flux dynamics. It may take a long time to fully understand these phenomena. It will probably take several years before it is possible to make practical high-current, wire-wound, high-temperature devices. The use of melt-quenched and melt-textured materials may be the first realization of the HTSC applications for levitation apparatuses (such as frictionless bearings, actuators, even the Maglev). In this sense, our pendulum can be modified to be a kind of standard technique to characterize the HTSC materials, which are to be used in engineering design.

There are many open questions related to flux dynamics in HTSCs. One direction of our research is to improve the pendulum for probing some physical properties of the HTSCs quantitatively, and further to figure out the mechanism of pinning. The construction of the low temperature facilities is ongoing in our lab. We believe that these new experimental facilities coupled with the use of high-quality samples will enable better understanding of the nature of the vortex structure in HTSCs.

6 Supplement: Pb- and Sb-doped Bi-Based Superconductors

After coming to Norway in August 1988, in the beginning I continued to do the research work related to materials science: trying to synthesize new materials and to characterize them. Later I shifted my main research topic, the study of the magnet-HTSC interaction has become my major investigation and is the main subject of this thesis. Somehow, in the past years, I have spent a lot of time on material processing, so that, the research results relevant to this are presented in this supplement.

Working on the new materials synthesis, scientists have tried many ways to enhance the superconducting transition temperature, T_c, and critical current density, J_c (for review, see Ref. [85]). On this topic, many efforts have been done in the Bi-Sr-Ca-Cu-O system. After the discovery of superconductivity in the Bi-Sr-Ca-Cu-O system by Maeda et al. [15], Tarascon et al.[86] have identified three superconducting phases in the Bi-Sr-Ca-Cu-O family referred to by their cation ratios as 2201, 2212 and 2223. Formation of the highest T_c (110K) phase, 2223, has been hampered by the relatively high stability of the 2212 (85K) phase. Sunshine et al.[87] have discovered that the addition of Pb enhances the content of the 2223 phase, but the mechanism for this still is an open question. Different groups have reported conflicting results. Some groups have claimed that the Pb occupies the Ca or Bi sites [88] [89], while some people argue that the final content of Pb and post-sintering procedure play important roles in the superconductivity [90].

Using dry and wet methods, we prepared a series of Bi-Pb-Sr-Ca-Cu-O superconductors. Using X-ray diffraction, SEM, TEM and a.c. susceptibility measurements, we have investigated the Pb-doped Bi-Sr-Ca-Cu-O superconductors (P.7). The X-ray emission studies of the SEM and TEM show that most of the Pb was lost in long term sintering time even though the starting compositions have a large percentage of lead. Our results show that the Pb seems not to occupy the Ca or Bi sites, but to be a catalyst in the high-T_c phase formation procedure.

Furthermore, several groups [91][92][93][94] have reported the effect of Sb-substitution in Bi-based superconductors, but with inconsistent results. One of these groups [91] have announced a record high T_c = 132 K in the Sb-doped Bi(Pb)-based superconductors, while others cannot repeat this result.

In order to clarify the effect of Sb-doping on the Bi(Pb)-based HTSCs, we have also prepared two groups of samples with nominal composition $Bi_{x_1}Pb_{x_2}Sb_{x_3}Sr_2Ca_3Cu_4O_z$ using the wet method (P.8). In the first group, $x_1 + x_2 + x_3 = 2$. Here x_1 ranges from 1.2 to 1.6 with x_2 varying from 0.72 to 0.12. The second group is characterisized by $x_1 + x_2 = 2$. Here x_1 was chosen to be 1.4 and 1.6 while x_3 ranges from 0.08 to 0.16. X-ray emission (SEM studies) was used to analyze the Pb content. A.c. susceptibility measurements

were used to show the effects of Sb-doping on the superconducting transition and the influences of external a.c. and d.c. magnetic fields.

Our experimental results indicate that: (i) high Sb content reduces the transition temperature; (ii) for small Sb contents the transition temperature is relatively constant, but the transition becomes sharper; (iii) the best sample (with $x_1 = 1.4$, $x_2 = 0.48$ and $x_3 = 0.12$) exhibits a very sharp transition with a peak in the imaginary component of the a.c. susceptibility at 108.4 K; and (iv) the transition of lightly Sb-doped material is strongly influenced by small external magnetic fields.

References

[1] J.G. Bednorz and K.A. Müller, *Z. Phys.*, **B 64** 189 (1986).

[2] H.K. Onnes, *Akad. van Wetenschappen* (Amsterdam), **14** 113, 818 (1911).

[3] Meissner and Ochsenfeld, *Naturwissenschaften*, **21** 787 (1933).

[4] M. Tinkham, "*Introduction to Superconductivity*", (McGraw-Hill, New York, 1975). D. Saint James, G. Sarma, and E.J. Thomas, "*Type-II Superconductivity*", (Pergamon, 1969).

[5] F. London and H. London, *Proc. Roy. Soc. (London)*, **A149** 71 (1935).

[6] V.L. Ginzburg and L.D. Landau, *Zh. Eksperim. i Teor. Fiz.*, **20** 1064 (1950).

[7] J. Bardeen, L.N. Cooper and J.R. Schrieffer, *Phys. Rev.*, **108** 1175 (1957).

[8] Abrikosov, *Soviet Phys.-JETP*, **5** 1174 (1957).

[9] H. Träuble and U. Essmann, *Phys. Stat. Sol.* **18** 813 (1968), N.V. Sarma, Phys. Lett. **A25** 315 (1968).

[10] P.W. Anderson, *Phys. Rev. Lett.*, **9** 309 (1962), P.W. Anderson and Y.B. Kim, *Rev. Mod. Phys.*, **36** 39 (1964).

[11] C.J. Gorter, *Phys. Lett.* 1 69 (1962), *Ibid* **2** 26 (1962).

[12] T.C. Keeley, K. Mendelssohn, and J.R. Moore, *Nature*, **134** 773 (1934), W.J. de Haas and J.M. Casimir-Jonker, *Nature*, **135** 30 (1935), F.G.A. Tarr and J.O. Wilhelm, *Can. J. Res.*, **12** 265 (1935).

[13] C.P. Bean, *Phys. Rev. Lett* **8** 250 (1962), C.P. Bean, *Rev. Mod. Phys.* **36** 31 (1964).

[14] M.K. Wu, J.R. Ashburn, C.J. Torng, P.H. Hor, R.L. Meng, L. Gao, Z.J. Huang and C.W. Chu, *Phys. Rev. Letter.* **58** 908 (1987).

[15] H. Maeda, Y. Tanaka, M. Fukutomi and T. Asano, *Jpn. J. Appl. Phys.* **27** L209 (1988).

[16] Z.Z. Sheng, A.M. Hermann, *Nature*, **332** 55 (1987).

[17] J.D. Jogensen, M.A. Beno, D.G. Hinks, L. Soderholm, K.J. Volin, R.L. Hitterman, J.D. Grace, I.K. Schuller, C.U. Segre, K. Zhang, and M.S. Kleefisch, *Phys. Rev.*, **B36** 3608 (1987).

[18] J.M. Tarascon, Y. LePage, P. Barboux, B.G. Bagley, L.H. Greene, W.R. McKinnon, G.W. Hull, M. Giroud, and D.M. Hwang, *Phys. Rev.*, **B37** 9382 (1988).

[19] K.A. Müller, M. Takashige and J.G. Bednorz, *Phys. Rev. Lett.* **58** 1143 (1987).

[20] Y.W. Xu and M. Suenage, *Phys. Rev.*, **B43** 5516 (1991).

[21] M.P.A. Fisher, *Phys. Rev. Lett.*, **62** 1415 (1989).

[22] T.R. Chien, T.W. Jing, N.P. Ong, and Z.Z. Wang, *Phys. Rev. Letter.*, **66** 3075 (1991).

[23] Z.J. Huang, Y.Y. Xue, P.H. Hor, and C.W. Chu, *Physica*, **C176** 195 (1991).

[24] P.W. Anderson and J.R. Schrieffer, *Physics Today* **44** No.6 55 (1991).

[25] E.H. Brandt, *Science*, **243** 349 (1989).

[26] F.C. Moon, *Nature*, **350** 270 (1991).

[27] M. Braun, P. Buszka, T. Motylewski, W. Przydróżny, and C. Śliwa, *Physica* **C171** 537 (1990).

[28] P.C. Wraight, *Phil. Mag.* **23** 1261 (1971).

[29] W.V. Houston and D.R. Smith, *Phys. Rev. Lett.* **16** 516 (1966), W.V. Houston and D.R. Smith, *Phys. Rev.* **163** 431 (1967).

[30] E.H. Brandt, P. Esquinazi, H. Neckel, and G. Weiss, *Phys. Rev. Lett.* **56** 89 (1986).

[31] P. Esquinazi, H. Neckel, G. Weiss, and E.H. Brandt, *J. Low Temp. Phys.* **64** 1 (1986), E.H. Brandt, P. Esquinazi, and H. Neckel, *J. Low Temp. Phys.* **64** 187 (1986).

[32] P.L. Gammel, L.F. Schneemeyer, J. Waszczak, and D. Bishop, *Phys. Rev. Lett.* **61** 1666 (1988).

[33] A. Gupta, P. Esquinazi, H.F. Braun and H.-W. Neumüller, *Phys. Rev. Lett.* **63** 1869 (1989), E. Rodriguez, C. Durán, J. Luzuriaga, F. de la Cruz, and C. Fainstein, *Physica* **C 165** 315 (1990).

[34] F.C. Moon, M.M. Yanoviak and R. Ware, *Appl. Phys. Lett.* **52** 1534 (1988).

[35] S.A. Basinger, J.R. Hull, and T.M. Mulcahy, *Appl. Phys. Lett.* **57** 2942 (1990), J.R. Hull, T.M. Mulcahy, K. Salama, V. Selvamanickam, B.R. Weinberger, and L. Lynds, Submitted to *J. Appl. Phys.*, (1991), Z.J. Yang, F.C. Moon, and M. Murakami, to be published (1991).

[36] R. Williams and J.R. Matey, *Appl. Phys. Lett.* **52** 751 (1988).

[37] V.V. Nemoshkalenko, E.H. Brandt, A.A. Kordyuk, and B.G. Nikitin, *Physica*, **C170** 481 (1990).

[38] D.E. Weeks, *Appl. Phys. Lett.* **55** 2784 (1989).

[39] Z.J. Yang, H. Bratsberg, T.H. Johansen, G. Helgesen, A.T. Skjeltorp, and F. Vassenden, *Solis State Commun.* (1991) in press.

[40] G.J. Homer, T.C. Randle, C.R. Walters, M.N. Wilson, and M.K. Bevir, J. Phys. **D 10** 879 (1977).

[41] F.C. Moon, "*Magneto-Solid Mechanics*", (John Wiley and Sons, New York 1984).

[42] L. Carlson, *Superc. Industry*, **3** No.2 19 (1990).

[43] H. Kitaguchi, J. Takada, K. Oda, A. Osaka and Y. Miura, *Physica* **C157** 267 (1989).

[44] A.N. Terentiev, Physca **C 166** 71 (1990).

[45] E.H. Brandt, Proceedings of the NASA-Conference "*Adv. in Mater. Sci. and Appl. of High Temp. Superconc.*", April 2-6, 1990, Greenbelt, MD., USA.

[46] P.J. Wojtowicz, J. Appl. Phys. **67** 7154 (1990).

[47] F.C. Moon and P.-Z. Chang, H. Hojaji, A. Barkatt, and A.N. Thorpe, *Jpn. J. Appl. Phys.* (1990) preprint.

[48] B.R. Weinberger, L. Lynds, and J.R. Hull, *Supercond. Sci. Technol.* **3** 381 (1990).

[49] G. Martini, A. Rivetti, and F. Pavese, Adv. Cryog. Eng. **35** 639 (1990).

[50] Y.K. Kim, M. Katsurai, and H. Fujita, Sensors and Actuators, **20** 33 (1990), Y.K. Kim, M. Katsurai, and H. Fujita, Proceedings of 9th Sensors Syposium, 121 (1990).

[51] D. Wolfshtein, T.E. Seidel, D.W. Johnson, Jr., and W.W. Rhodes *J. Supercond.* **2** 211 (1989).

[52] F. Hellman, E.M. Gyorgy, D.W. Johnson, Jr., H.M. O'Bryan and R.C. Sherwood, *J. Appl. Phys.* **63** 447 (1988).

[53] L.C. Davis, *J. Appl. Phys.* **67** 2631 (1990).

[54] L.C. Davis, E.M. Logothetis and R.E. Soltis, sl J. Appl. Phys., **64** 4212 (1988).

[55] Z.J. Yang, *Dept. Series Report No. 90-29*, **ISSN-0332-5571** (1990), Dept. of Phys., Univ. of Oslo.

[56] T.H. Johansen, H. Bratsberg, Z.J. Yang, G. Helgesen, and A.T. Skjeltorp, *Rev. Sci. Instrum.* **61** 3827-9 (1990).

[57] T.H. Johansen, H. Bratsberg, Z.J. Yang and G. Helgesen, Poster, Pres. at *EPS 10th Conf. Cond. Matt. Phys.*, Lisbon, April, 1990.

[58] W.G. Harter, A.M. Hermann and Z.Z. Sheng, *Appl. Phys. Lett.* **53** 1119 (1988).

[59] D.B. Marshall, R.E. DeWames, P.E.D. Morgan and J.J. Ratto, *Appl. Phys.* **A48** 87 (1989).

[60] D.B. Marshall, R.E. DeWames, P.E.D. Morgan and J.J. Ratto, *Appl. Phys.* **A 50** 445 (1990).

[61] S. Jin, R.C. Sherwood, E.M. Gyorgy, T.H. Tiefel, R.B. van Dover, S. Nakahara, L.F. Schneemeyer, R.A. Fastnacht, and M.E. Davis, *Appl. Phys. Lett.* **54** 584 (1989).

[62] P.-Z. Chang, F.C. Moon, J.R. Hull and T.M. Mulcahy, *J. Appl.Phys.* **67** 4358 (1990).

[63] E.H. Brandt, *Appl. Phys. Lett.* **53** 1554 (1988).

[64] M. Murakami, H. Fujimoto, T. Oyama, S. Gotoh, Y. Shiohara, N. Koshizuka, and S. Tanaka, pres. at *ICMC'90, High-Temperature Superc.* May 9, 1990, Garmisch-Partenkirchen, FRG.

[65] F.C. Moon, K.-C. Weng and P.-Z. Chang, *J. Appl. Phys.* **66** 5643 (1989).

[66] P.N. Peters, R.C. Sisk, E.W. Urban, C.Y. Huang, M.K. Wu, *Appl. Phys. Lett.* **52** 2066 (1988).

[67] Y. Shapira, C.Y. Huang, E.J. Mcniff Jr, P.N. Peters, B.B. Schwartz and M.K. Wu, *J. Magn. Magn. Mat.* **78** 19 (1989).

[68] R.J. Adler and W.W. Anderson, *Appl. Phys. Lett.* **53** 2346 (1988).

[69] R.J. Adler and W.W. Anderson, *J. Appl. Phys.* **68** 695 (1990).

[70] T.H. Johansen, H. Bratsberg and Z.J. Yang, *Proceedings of The 2nd World Congress on Supercond.*, Houston, Sept. 1990, C.G. Burnham ed. (World Scientific, Singapore, 1991).

[71] Z.J. Yang, T. H. Johansen, H. Bratsberg, G. Helgesen and A.T. Skjeltorp, *Proceedings of The 2nd World Congress on Supercond.*, Houston, Sept. 1990, C.G. Burnham ed. (World Scientific, Singapore, 1991).

[72] C. Giovannella, P. Rouault, A. Campbell, and G. Collin, *Appl. Phys. Lett.* **63** 4173 (1988).

[73] M. Tinkham and C.J. Lobb, *Solid State Physics*, **42** 91(1989).

[74] J.R. Clem, in "*Physics and Materials Science of High-Temperature Superconductors*", Eds. R. Kossowsky, S. Methfessel, and D. Wohlleben, (Kluwer Academic Publishers. Dordrecht, 1990), p 79.

[75] A.M. Campbell and J.E. Evetts, *Advanc. Phys.* **21** 199 (1972).

[76] Y. Yeshurum and A.P. Malozemoff, *Phys. Rev. Lett.* **60** 2202 (1988).

[77] A.P. Malozemoff, L. Krusin-Elbaum, D.C. Cronemyer, Y. Yeshurum and F. Holtzberg, *Phys. Rev.* **B38** 6940 (1988).

[78] T.T.M. Palstra, B. Batlogg, L.F. Schneemeyer and J.V. Waszczak, *Phys. Rev. Lett.* **60** 1662 (1988).

[79] M. Tinkham, *Phys. Rev. Lett.* **60** 1658 (1988).

[80] E. Zeldov, N.M. Amer, G. Koren, A. Gupta, M.W. McElfresh, and R.J. Gambino, *Appl. Phys. Lett.* **56** 680 (1990).

[81] M.V. Feigel'man, V.B. Geshkenbein, A.I. Larkin and V.M. Vinokur, *Phys. Rev. Lett.* **63** 2303 (1989).

[82] R. Griessen, *Phys. Rev. Lett.* **64** 1674 (1990).

[83] P.H. Kes, J. Aarts, J.van den Berg, C.J. van der Beek, J.A. Mydosh, *Supercon. Sci. and Tech.* **1** 242 (1989).

[84] T. Nattermann, *Phys. Rev. Lett.* **64** 2454 (1990).

[85] S. Jin and J.E. Graebner, *Mater. Sci. Eng.* **B7** 243 (1991).

[86] J.M. Tarascon, W.R. McKinnon, P. Barboux, D.M. Hwang, B.G. Bargley, L.H. Greene, G. Hull, Y. LePage, N. Stoffel and M. Giroud, *Phys. Rev.* **B38** 8885 (1988).

[87] S.A. Sunshine, T. Siegrist, L.F. Schneemeyer, D.W. Murphy, R.J. Cava, B. Batlogg, R.B. van Dover, R.M. Fleming, S.H. Glarum, S. Nakahara, R. Farrow, J.J. Krajewski, S.M. Zahurak, J.V. Waszczak, J.H. Marshall, P. Marsh, L.W. Rupp, Jr., and W.F. Peck, *Phys. Rev.* **B38** 893 (1988).

[88] E. Chavira, R. Escudero, D. Ríos-Jara and L.M. León, *Phys. Rev.* **B38** 9272 (1988).

[89] B. Jayaram, P.C. Lanchester, M.T. Weller, J.R. Grasmeder, P.A.J. de Groot and G. P. Rapson, *J. Phys. Condens. Matter*, **1** 477 (1989).

[90] B. Zhu, L. Lei, S.L. Yuan, S.B. Tang, W. Wang, G.G. Zheng, W.Y. Guan and J.Q. Zheng, *Physica* **C157** 370 (1989).

[91] H.B. Liu, L.Z. Cao, L. Zhou, Z.Q. Mao, X.X. Li, Z.D. Yu, B. Xue, X.L. Mao, G.E. Zhou, Y.Z. Run, Z.J. Chen and Y.H. Zhang, *Solid State Commun.* **69** 867 (1989).

[92] S.X. Dou, H.K. Liu, N.X. Tan, Y.J. Sheng and W.K. Jones, *Physica* **C158** 97 (1989).

[93] W. Peng, R.H. Hannon, H. Lee, A.P. Genis, V.J. Melim, C.W. Kimball, B. Dabrowski and D. G. Hinks, *Phys. Lett.* **139A** 91 (1989).

[94] J.S. Luo, D. Michel and J-P. Chevalier, *Appl. Phys. Lett.* **55** 1448 (1989).

Part II

Scientific Papers

Paper 1

Physica C **160** 461-465 (1989)

Vibrations of a Magnet Levitated over a Flat Superconductor,

Z.J. Yang, T.H. Johansen, H. Bratsberg, G. Helgesen and A.T. Skjeltorp.

Physica C 160 (1989) 461–465
North-Holland, Amsterdam

VIBRATIONS OF A MAGNET LEVITATED OVER A FLAT SUPERCONDUCTOR

Z.J. YANG, T.H. JOHANSEN, H. BRATSBERG and G. HELGESEN
Department of Physics, University of Oslo, Oslo, Norway

A.T. SKJELTORP
Institute for Energy Technology, N-2007 Kjeller, Norway

Received 12 August 1989

Based on a dipole–dipole interaction model, we discuss the levitation force and related vibration problems to understand the effects of flux pinning in type-II superconductors, and the applications of levitation in superconducting systems.

A very important property of superconductors is their ability to levitate a magnet. The low T_c of conventional superconductors limits the applications of this phenomenon in many aspects. Because the high cost of cooling systems with liquid helium, the levitation train and similar other superconducting machines are almost impossible from the economical point of view. The discovery of the high T_c oxide superconductors exhibits the possibility to apply superconductors systems in popular technology, even in daily life.

Recently, Brandt [1] reviewed levitations in several physical systems, and stressed in particular the superconductor system. So far, several groups [2–6] have reported investigations on the levitation force, and a new model was suggested for calculating the levitation distance [2].

Vibrations are very common in engineering and techniques. Sometimes, they are so severe that constructions may be damaged. It is very important to avoid resonances in designing a new machine and to reduce vibrations in machine making.

The purpose of this letter is to apply a dipole–dipole interaction model to: (i) analyse levitation forces; (ii) study vibrations in connection with levitation; (iii) utilize the vibrations to type-II superconductors for exploring the physical properties of flux pinning. The method, given here for studying the intrinsic vibrations of these kinds of systems, is also believed to be suitable for engineering design.

We consider the configuration that a permanent magnetic ball is levitating over an infinite plane of a superconductor. The system has a minimum potential energy when the polarization of the ball is directed parallel to the superconducting plane as shown in fig. 1(a).

Without loss of universality, we compare two configurations as shown in fig. 1: the magnetic moment is parallel to the plane (a), and perpendicular to the plane (b). For situation (a), there is an anti-symmetrical plane σ perpendicular to the magnetic moment and superconducting plane. If we assume that the image method is valid for studying the interaction, it is then easy to show that the potential energy (by using following eq. (1)) in (a) is just one half of that in (b). In addition, there is also a symmetrical axis along the magnetic moment in (b). In order to obtain a more clear physical picture, we analyse configuration (b) instead of (a) for type-II superconductors.

When the levitation distance z_0 is much larger than the diameter a of a sphere, the dipole model is good approximation for dealing with this kind of problem [7]. We therefore limit our discussion to this condition.

i) Type-I superconductor. Due to the perfect diamagnetism ($\mu=0$) of a superconductor in the Meis-

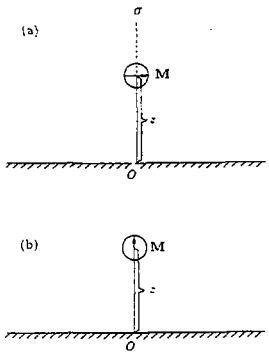

Fig. 1. A permanent magnetic sphere is levitating over an infinite superconductor plane. (a) magnetic moment is parallel with the plane, and (b) magnetic moment is perpendicular to the plane.

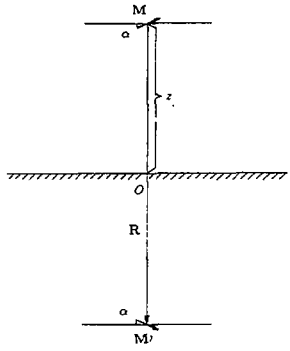

Fig. 2. The configuration of a dipole with moment M and its image dipole with moment M'.

sner state, the interaction energy between the permanent magnetic sphere and an infinite superconducting plane can be described by the dipole–dipole interaction as shown in fig. 2. Here, M' is the image dipole of M and $|M'|=|M|=M$.

The interaction between the pair of dipoles shown in fig. 2. is given by

$$V=\frac{\mu_0}{8\pi}\left[\frac{M'\cdot M}{(2z)^3}-\frac{3(M'\cdot R)(M\cdot R)}{(2z)^5}\right]$$
$$=\frac{\mu_0}{8\pi}\frac{M^2}{(2z)^3}(\cos 2\alpha+3\sin^2\alpha)\,. \qquad (1)$$

As there is no horizontal force in the system, we omit the horizontal movement of the dipoles. Furthermore, there is no horizontal torsion, and we therefore omit the rotation around the z-axis. For similar reason, the spin term around the polarization direction is omitted. In this case, the Lagrangian of the system can be written as follows:

$$L=\tfrac{1}{2}m\dot{z}^2+\tfrac{1}{2}I\dot{\alpha}^2-mgz-\frac{\mu_0}{8\pi}\frac{M^2}{8z^3}(\cos 2\alpha+3\sin^2\alpha) \qquad (2)$$

where m and I are the mass and inertia of the magnetic sphere, respectively.

It is easy to obtain the Euler–Lagrange equations for z and α:

$$m\ddot{z}+mg-\frac{\mu_0}{8\pi}\frac{3M^2}{8z^4}(\cos 2\alpha+3\sin^2\alpha)=0 \qquad (3)$$

and

$$I\ddot{\alpha}+\frac{\mu_0}{8\pi}\frac{M^2}{8z^3}\sin 2\alpha=0\,. \qquad (4)$$

The last term in eq. (3) is the force between the sphere and the superconductor, and this falls off with the distance as $F\sim z^{-4}$.

The condition for levitation can be expressed as

$$\partial V_{\mathrm{eff}}/\partial q_i=0 \qquad (5)$$

Here q_i are the dynamical variables z and α, and the effective potential is given by:

$$V_{\mathrm{eff}}=mgz+\frac{\mu_0}{8\pi}\frac{M^2}{8z^3}(\cos 2\alpha+3\sin^2\alpha)\,. \qquad (6)$$

We then obtain

$$mg-\frac{\mu_0}{8\pi}\frac{3M^2}{8z_0^4}(\cos 2\alpha_0+3\sin^2\alpha_0)=0 \qquad (7)$$

and

$$\sin 2\alpha_0 = 0 . \tag{8}$$

The solutions for the equilibrium position are thus:

$$\alpha_0 = 0 \tag{9}$$

and

$$z_0 = \left(\frac{\mu_0}{8\pi}\frac{3M^2}{mg}\right)^{1/4} . \tag{10}$$

As we are only interested in small vibrations, we let

$$z = z_0 + \rho \tag{11}$$

and

$$\sin\alpha = \alpha . \tag{12}$$

The linearization of eqs. (3) and (4) yields the decoupled equations:

$$m\ddot{\rho} + \frac{\mu_0}{8\pi}\frac{3M^2}{2z_0^5}\rho = 0 \tag{13}$$

and

$$I\ddot{\alpha} + \frac{\mu_0}{8\pi}\frac{M^2}{4z_0^3}\alpha = 0 . \tag{14}$$

These equations describe simple harmonical vibrations, and the solution are:

$$\rho = \rho_0 \sin(\Omega_1 t + \delta_1) \tag{15}$$

and

$$\alpha = \alpha_1 \sin(\Omega_2 t + \delta_2) . \tag{16}$$

Here ρ_0, α_1, δ_1 and δ_2 are constants determined by the initial conditions, and Ω_1 and Ω_2 are the vibrational frequencies given by

$$\Omega_1 = \left(\frac{\mu_0}{8\pi}\frac{3M^2}{2mz_0^5}\right)^{1/2} = \left(\frac{4g}{z_0}\right)^{1/2} \tag{17}$$

and

$$\Omega_2 = \left(\frac{\mu_0}{8\pi}\frac{M^2}{4Iz_0^3}\right)^{1/2} = \left(\frac{2mz_0 g}{3I}\right)^{1/2} = \left(\frac{m}{6I}\right)^{1/2} z_0\Omega_1 . \tag{18}$$

ii) Type-II superconductor. Let us assume that the dipole is lowered towards the superconductor from $z=\infty$. As discussed previously, we study the configuration as shown in fig. 1(b) without loss of universality. The field of a dipole along its axis may be expressed as $H \sim z^{-3}$. If $H < H_{c1}$ (H_{c1} = lower critical field), the superconductor shows perfect diamagnetism. We will now be interested in the situation for which $H_{c1} < H < H_{c2}$ (H_{c2} = upper critical field). For a free dipole with magnetic moment M (without the superconducting plane), the magnetic field at the origin point O is given by:

$$|H| = \frac{\mu_0}{4\pi}\frac{2M}{z^3} . \tag{19}$$

We now define

$$z_1 = \left(\frac{\mu_0}{4\pi}\frac{2M}{H_{c1}}\right)^{1/3} \tag{20}$$

and introduce the corresponding dimensionless distance ζ

$$\zeta = z/z_1 . \tag{21}$$

As ζ decreases from 1, the flux pinning begins and the pinning area expands axisymmetrically from the center point O. We can now divide the superconducting plane into two regions: a circular area centered at O with radius r_{Hc_1} and the remaining part as shown in fig. 3(b). The circle with radius r_{Hc_1} is the boundary between the flux pinning area and the pinning free area so that r_{Hc_1} increases as ζ decreases. Because the outside area ($r > r_{Hc_1}$) shows perfect diamagnetism in the Meissner state, the interaction between the dipole and this area is almost the same as in the case of a type-I superconductor. It is then possible to express the interaction as the difference between a dipole with an infinite type-I superconductor plane and a dipole with a disk area with radius r_{Hc_1} of type-II superconductor. However, the latter interaction is very difficult to deal with. To our knowledge, so far no theory can describe this very well.

Instead of calculating the interactions discussed above, we propose to use a semi-empirical formula to represent the interaction between a dipole and an infinite type-II superconductor plane when flux pinning begins. For this, we select a power law to describe the force $F_\perp$ between the magnet and super-

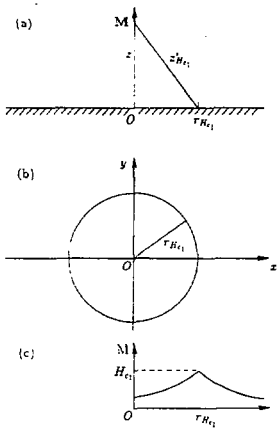

Fig. 3. (a) A magnetic dipole with moment M over an infinite type-II superconductor plane. $z'_{H_{c_1}}$ is a critical measure for the magnetic field (corresponding to H_{c_1}) on the superconductor. (b) The type-II superconductor plane is divided into two parts: the circular part with radius $r_{H_{c_1}}$ has $H > H_{c_1}$, and the rest part has $H < H_{c_1}$. (c) The magnetization curve of the superconductor as a function of distance r from the center.

conductor as follows:

$$F_{\perp} = C\zeta^{-\gamma} . \tag{22}$$

Here C is a constant determined by the dipole and γ is a function of the magnetic field at point O. We expect the exponent to satisfy

$$\gamma = \begin{cases} 4 & \text{if } \zeta > 1 , \\ > 0 \text{ and } < 4 & \text{if } \zeta < 1 . \end{cases} \tag{23}$$

This assumption has been proved by different groups [4,6].

As discussed previously, if the magnetic moment is parallel to the plane, the force $F_{\parallel}$ should be half of that of a dipole perpendicular to the plane i.e.

$$F_{\parallel} = \tfrac{1}{2}F_{\perp} = C_1\zeta^{-\gamma} \tag{24}$$

where $C_1 (= \frac{1}{2}C)$ is also a constant.

Now we study the small vibrations in z-direction. Without loss of universality, we choose $\alpha = 0$ (dipole is parallel with the plane). By substituting eq. (24) into eq. (3) for the interaction term one obtains:

$$m\ddot{z} + mg - C_1(z/z_1)^{-\gamma(z)} = 0 . \tag{25}$$

At the equilibrium position $z = z_0$, one thus obtains:

$$mg - C_1(z_0/z_1)^{-\gamma(z_0)} = 0 . \tag{26}$$

This equation thus determins z_0. It may not be possible to find $\gamma(z)$ analytically, but as discussed below, this may be found from vibration experiments.

For small vibrations we use the same variable transformation expressed in eq. (11), and by using the approximations:

$$\gamma(z) = \gamma(z_0) = \gamma \tag{27}$$

and

$$z^{-\gamma} = (z_0 + \rho)^{-\gamma} = z_0^{-\gamma}(1 - \gamma\rho/z_0) \tag{28}$$

we obtain from eq. (25):

$$m\ddot{\rho} + \gamma C_1 z_1^{\gamma} z_0^{-\gamma-1}\rho = 0 . \tag{29}$$

The solution of this is

$$\rho = \rho_1 \sin(\Omega_3 t + \delta_3) . \tag{30}$$

Here ρ_1 and δ_3 are constants determined by the initial conditions, and Ω_3 is the vibration frequency given by (using eq. (26)):

$$\Omega_3 = \left(\frac{\gamma C_1 z_1^{\gamma}}{m z_0^{\gamma+1}}\right)^{1/2} = \left(\frac{\gamma g}{z_1}\right)^{1/2}\left(\frac{mg}{C_1}\right)^{1/2\gamma} . \tag{31}$$

If we consider small angular vibrations as for the situation described previously for type-I superconductor, we can use the same approximation as in eq. (12), and this leads to

$$I\ddot{\alpha} + C_2(z_0/z_1)^{1-\gamma}\alpha = 0 . \tag{32}$$

here C_2 is a constant determined by the dipole (independent of z_0).

The solution to the equation is

$$\alpha = \alpha_2 \sin(\Omega_4 t + \delta_4) . \tag{33}$$

Here α_2 and δ_4 are constants determined by the initial conditions, and Ω_4 is the vibration frequency given by

$$\Omega_4 = \left[\frac{C_2}{I}\left(\frac{z_0}{z_1}\right)^{1-\gamma}\right]^{1/2} = \left[\frac{C_2}{I}\left(\frac{C_1}{mg}\right)^{1-\gamma/\gamma}\right]^{1/2} . \tag{34}$$

The flux pinning in type-II superconductors produces magnetic hysteresis and therefore damps vibrations. Due to this magnetic hysteresis, the force describing the dipole moving away from a superconductor must also be expressed by a different power law than for a dipole moving towards it, i.e.

$$F_m(\zeta) = C_3 \zeta^{-\gamma_1}. \tag{35}$$

Due to the fact that some flux lines are frozen, there will be an attractive force between the dipole and the superconductor. This means that if the dipole is at a distance z from the superconductor, the outward moving force F_m is lower than the inward moving force F. In vibration experiments around the same equilibrium position z_0, we should therefore obtain two different frequencies corresponding to inward and outward motions.

From eqs. (22), (24), (32) and (35), we see that parameters C_1, C_2 and C_3 are determined by the magnetic properties of a dipole. From formulae (31) and (34), the vibration frequencies Ω_3 and Ω_4 are controlled by magnetic parameters C_1, C_2 and z_1, inertial parameters m and I, and power index γ of the force. Conversely, we can also select a series of magnetic spheres with the same magnetic characteristics but different inertial parameters, or with the same inertial parameters but different magnetic characteristics, to investigate the vibrations. By measuring the frequencies Ω_3 and Ω_4, one should therefore obtain much knowledge of the interaction in these kinds of systems, and further understand the effects of flux pinning on the interactions.

Preliminary experiments in our laboratory showed the vibrations of a magnetic sphere over a superconducting plane in the z-direction.

This investigation is important for both physical research and applied engineering. For high-T_c superconductors, the investigations have a close relationship to the vortex studies. When a magnet is levitated over a high-T_c superconductor, the field in the superconductor is always higher than H_{c1}. Thus, the vibrations will certainly result in some motions of the flux lines. The vibration investigations will help us to understand the vortex behavior and its physical meaning.

Due to the discovery of oxide superconductors, an attractive application is levitation in engineering. Earlier research work about stable levitation by using superconductors was studied [8], but they did not investigate the resonances in the stable levitation states. As we know, resonances are very severe problems in engineering applications, which may damage the constructions. Therefore, it is a big challenge to find out how to avoid resonances occurring in system design. Our models and calculations should be suitable for such considerations.

In summary, we have analysed levitation forces of a magnet over a superconducting plane, calculated vibrations near equilibrium positions, and briefly discussed the importance of vibration investigations for understanding physical properties and applications of levitation.

Acknowledgements

One of the authors (ZJY) would like to thank Professor C.P. Bean for helpful discussion; three of the authors (ZJY, THJ and GH) would like to acknowledge the NAVF for supporting their research work, and the authors would like to thank B. Berling for drawing the figures.

References

[1] E.H. Brandt, Science 243 (1989) 349.
[2] F. Hellman, E.M. Gyorgy, D.W. Johnson Jr., H.M. O'Bryan and R.C. Sherwood, J. Appl. Phys. 63 (1988) 447.
[3] H. Kitaguchi, J. Takada, K. Oda, A. Osaka and Y. Miura, Physica C 157 (1989) 267.
[4] F.C. Moon, M.M. Yanoviak and R. Ware, Appl. Phys. Lett. 52 (1988) 1534,
D.B. Marshall, R.E. DeWames, P.E.D. Morgan and J.J. Ratto, Appl. Phys. A48 (1989) 87. In these papers the authors did not investigate the power law of force, but if we use eq. (22) to represent their results and plot γ as a function of distance z, we find that their data satisfy the condition described in eq. (23).
[5] E.H. Brandt, Appl. Phys. Lett. 53 (1988) 1554;
L.C. Davis, E.M. Logothetis and R.E. Soltis, J. Appl. Phys. 64 (1988) 4212.
[6] T.H. Johansen, Z.J. Yang et al., to be published.
[7] D. Bedeaux, M.M. Wind and M.A. van Dijk, Z. Phys. B68 (1987) 343.
[8] G.J. Homer, T.C. Randle, C.R. Walters, M.N. Wilson and M.K. Bevir, J. Phys. D10 (1977) 879.

Paper 2

Journal of Applied Physics **68** 3761-3762 (1990)

Comment on "Lateral Restoring Force on a Magnet Levitated above a Superconductor"

[J. Appl. Phys. **67** 2631 (1990)],

Z.J. Yang, T.H. Johansen, H. Bratsberg, G. Helgesen and A.T. Skjeltorp.

Comment on "Lateral restoring force on a magnet levitated above a superconductor" [J. Appl. Phys. 67, 2631 (1990)]

Z. J. Yang, T. H. Johansen, H. Bratsberg, and G. Helgesen
Department of Physics, University of Oslo, Oslo, Norway

A. T. Skjeltorp
Institute for Energy Technology, N-2007 Kjeller, Norway

(Received 9 April 1990; accepted for publication 21 June 1990)

Based on Davis' model for the lateral restoring force on a magnet levitated above a superconductor [J. Appl. Phys. 67, 2631 (1990)], we calculate the restoring force as a function of lateral displacement for a more realistic magnetic field profile.

Referring to Williams and Matey's[1] experiments on the lateral restoring force on a small Sm-Co bar magnet levitated over a disk of $Y_1Ba_2Cu_3O_7$ superconductor, Davis[2] has, in a recent paper, calculated the restoring force as a function of displacement from its original position at rest. The calculation is based on Bean's critical-state model to describe flux pinning.

Williams and Matey found that the force is linear for small displacements x_0 (~ 1 mm) from the original position (near the center of the superconducting disk). Similar behavior was observed by Moon, Yanoviak, and Ware.[3] Davis' model provides a clear interpretation for the linear behavior. Davis has obtained the following expression for the force:

$$F_x(x_0) = -\frac{\mu_0}{4J_c}\left[H_0^2(0) - \int_{-\infty}^{0} dx\left(H_0(x-x_0)\frac{\partial H_0^2(x)}{\partial x} + H_0^2(x-x_0)\frac{\partial H_0(x)}{\partial x}\right)\right], \quad (1)$$

where $H_0(x)$ is the field profile produced by the magnet at the lateral displacement x.

Davis evaluated the force numerically using the field profile

$$H_0(x) = H_0(0)h^2/(h^2+x^2), \quad (2)$$

where x is the lateral displacement and h is the height of the field source from the superconductor.

In this comment, we would like to point out that: (i) with the field profile described by Eq. (2), which contains the main physical feature corresponding to the field for a line current wire, Eq. (1) can be calculated analytically. The result is

$$\frac{-F_x(x)}{\mu_0 H_0^2(0)/4J_c} = \frac{(x/h)^2}{1+(x/h)^2} + \frac{(x/h)[20+(x/h)^2]}{[4+(x/h)^2]^3}\left(\pi - \arctan\frac{x}{h}\right) - \frac{4-5(x/h)^2}{[1+(x/h)^2][4+(x/h)^2]^2} - \frac{4[4+5(x/h)^2]}{(x/h)^2[4+(x/h)^2]^3}\ln[1+(x/h)^2], \quad (3)$$

(ii) Davis' model can be applied to more realistic magnet configurations.

Let us consider a permanent magnetic bar infinitely long in the y direction and $x \times z$ dimensions of $2l \times 2w$, respectively. Assuming that the magnet bar is magnetized homogeneously along the x direction, the magnetic field outside the bar can be described as the sum of contributions from the dipoles with volume moment density m_v in the bar. After integration over the bar volume, the x component of the field can be expressed as

$$H_x = 2m_v\left(\arctan\frac{h-w}{x-l} + \arctan\frac{h+w}{x-l} - \arctan\frac{h-w}{x-l} - \arctan\frac{h+w}{x+l}\right), \quad (4)$$

where h is the distance from the center of the bar magnet to the superconductor surface. Substituting this field, instead of Eq. (2), into Eq. (1), we evaluate the force numerically. Choosing different values for parameters l and w, the resulting forces are shown in Fig. 1. One can see that, for the field profile given by Eq. (2), the restoring force [Fig. 1(a)] increases monotonically and finally approaches the saturation value. For the fields expressed by Eq. (4), a peak appears in the force curves [Figs. 1(c), 1(d), and 1(e)]. At the limit, $l = w = 0$, we obtain the dipole-line case: an infinite long dipole-line polarized transversely, Fig. 1(b). The force is not very sensitive to the cross section of the magnet bar. With an increase in the size of the cross section, the peak value of the force shifts to the left but very slowly. Only when the magnet is very close to the superconductor ($w/h \sim 1$), the shift is pronounced [Fig. 1(e)].

High-resolution measurement of the restoring force[4] by use of a mechanical pendulum shows that the force increases dramatically for small x. Compared with the analytical result [Eq. (3)], the experimental data show a much steeper

 0021-8979/90/193761-02$03.00

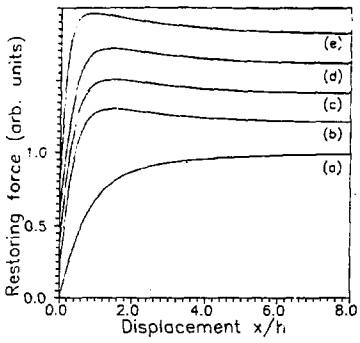

FIG. 1. Comparisons of restoring forces $-F_x/\{\mu_0 H_0^2(0)/4J_c\}$ as a function of displacement x/h: (a) analytical result expressed by Eq. (3), (b) the dipole-line model, (c) the dipole-bar model with $l/h = w/h = 0.1$, (d) the dipole-bar model with $l/h = w/h = 0.5$, and (e) the dipole-bar model with $l/h = w/h = 0.9$. The curves are shifted relative to each other by 0.2 in the y direction.

behavior, and is close to the curve given by the dipole-line model [Fig. 1(b)]. The physical reason for the peaks in the force curves is that the field changes sign. Since flux penetration takes place only when the field is larger than H_{c_1}, the real integral in Eq. (1) needs a cutoff x value. And if the extreme value of negative field is less than H_{c_1}, there is no contribution of negative field to the force, so that the force peaks will not appear in such cases. Quantitatively, we employ the dipole-line model, which gives a better approximation to the experimental field profile, to explain the observed force. The x component of magnetic field produced by a dipole line (polarized along the x direction and transverse to the line direction) can be expressed as

$$H_x = 2m_l\{(x^2 - h^2)/(x^2 + h^2)^2\}, \tag{5}$$

where m_l is the dipole-moment linear density (per unit length), x is the lateral displacement, and h is the height of the dipole line above the superconductor. When $x = h$, the field changes sign, and when $x = \sqrt{3}h$, the negative field reaches the extreme value: $|H_{\min}| = \frac{1}{8}|H_{\max}|$, so that, if $|H_{\min}| < H_{c_1}$, the negative part of the field does not contribute to the restoring force. However, when $|H_{\min}| \gg H_{c_1}$, the force should show a peak.

Finally, we would like to point out that even for a spherical magnet our previous studies[5] show that the restoring forces are different for motion parallel with and perpendicular to the magnetic moment M. The details of investigations about *effective force* and *effective potential* will be published elsewhere.[6]

The research was supported in part by the Norwegian Research Council for Science and the Humanities (NAVF). The authors would like to thank J. Yao for confirming the calculations, and L. C. Davis for sending his preprint and his comment.[7]

[1] R. Williams and J. R. Matey, Appl. Phys. Lett. 52, 751 (1988).
[2] L. C. Davis, J. Appl. Phys. 67, 2631 (1990).
[3] F. C. Moon, M. M. Yanoviak, and R. Ware, Appl. Phys. Lett. 52, 1534 (1988).
[4] T. H. Johansen, Z. J. Yang, H. Bratsberg, G. Helgesen, and A. T. Skjeltorp (to be published).
[5] Z. J. Yang T. H. Johansen, H. Bratsberg, G. Helgesen, and A. T. Skjeltorp, Physica C 165, 397 (1990).
[6] Z. J. Yang, T. H. Johansen, H. Bratsberg, G. Helgesen, and A. T. Skjeltorp (to be published).
[7] It would be pointed out that Eq. (1) is not a universal description of the lateral restoring force for any kind of field profile.

Paper 3

Applied Physics Letters **58** 179-181 (1991)

The Lateral Force on a Magnet Placed above a Planar $YBa_2Cu_3O_x$ *Superconductor*,

T.H. Johansen, **Z.J. Yang**, H. Bratsberg, G. Helgesen and A.T. Skjeltorp.

Lateral force on a magnet placed above a planar $YBa_2Cu_3O_x$ superconductor

T. H. Johansen, Z. J. Yang, H. Bratsberg, G. Helgesen, and A. T. Skjeltorp
Department of Physics, University of Oslo, P. O. Box 1048, Blindern, 0316 Oslo 3, Norway

(Received 10 September 1990; accepted for publication 16 October 1990)

The lateral force interaction between a permanent bar magnet and a large slab of high T_c superconductor has been investigated at 77 K, under conditions of a constant vertical separation of 2 mm. The restoring force as a function of lateral displacement rises very steeply, and reaches 90% of its saturation value, 5.1 mN, after 1.8 mm. The profile of the force-displacement curve is in qualitative agreement with the existing theory. A significant quantitative discrepancy is interpreted as due to a theoretical penetration depth exceeding the sample thickness. The lateral magnetic stiffness or spring constant, is found to be independent of displacement away from lateral equilibrium.

The levitation of a permanent magnet above a superconductor is classically explained as a consequence of the perfect diamagnetism possessed by the superconducting material. Surface currents are induced so that the external magnetic field is expelled from the interior of the sample (Meissner effect). When this repelling interaction balances the weight of the magnet it can levitate.

The discovery of the high T_c oxide superconductors has made it possible to study the forces acting on a levitating magnet quite conveniently at liquid-nitrogen temperature. During the last few years numerous articles have reported experiments that address this subject. A majority of these investigations has been concerned with the levitating component of the force.[1-6] The quantitative results of these experiments show that the image dipole interaction, which is expected from the Meissner effect alone, does not fully describe the observed behavior. This is interpreted as due to partial flux penetration and pinning, i.e., type-II behavior of the ceramic superconductors.

An even stronger manifestation of the flux pinning in these materials is the considerable lateral stability of the levitating magnet. In fact, a diamagnetic planar disk of finite size will not be able to provide such stability at all.[7] Since most thinkable applications of the levitation phenomenon will rely on this lateral stability, it is important to understand the underlying physical mechanisms. Until very recently, a theory for the origin and magnitude of the restoring lateral force did not exist for type-II materials. Now, a detailed calculation of this force has been presented by Davis.[8]

Experimentally, only very few attempts have been made to reveal the behavior of the lateral interaction.[1,9] In order to render a proper theoretical analysis, such experiments should be performed with constant vertical separation between the magnet and the superconducting slab. Moreover, the sample should be large enough to avoid finite size effects.

In this communication we report high-resolution measurements of the static lateral force and also dynamic stiffness as function of lateral displacement. Direct comparison with theory will be made.

We have used an apparatus shown in Fig. 1. A planar disk of $YBa_2Cu_3O_x$ is placed on a block of aluminum in a polystyrene container filled with liquid nitrogen. The top surface of the sample is aligned with the horizontal plane. The container rests on an electrically movable table. A step motor can displace the sample 1.25 μm per step in the lateral x direction. The table can also be lifted vertically by a manual micrometer.

A Nd-Fe-B permanent magnet, M, is attached to the lower end of a quartz rod, which is free to move as a

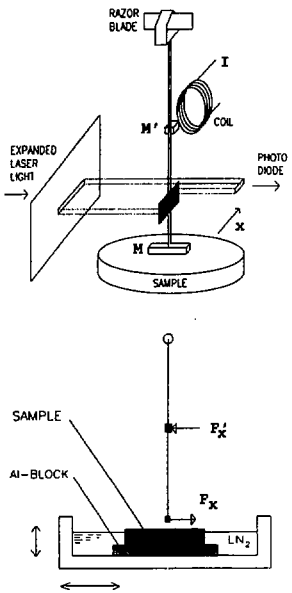

FIG. 1. Experimental arrangement for the lateral force measurements (upper). Schematic picture of the pendulum with the torques that are acting upon it in the balance position (lower).

 0003-6951/91/020179-03$02.00

vertical planar pendulum. The horizontal position of the magnet is detected by a photodiode placed in the focus of a laser beam that is partly intersected by the pendulum.

When the sample is in the superconducting state we observe that as it is moved laterally, the interaction causes the magnet to follow. In order to measure this force, F_x, we insist on keeping the diode signal constant, i.e., fix the magnet's position while the sample is displaced. For this purpose a balancing force, F'_x, is generated by applying a field gradient to a second small permanent magnet, M', attached near the center of the rod. At balance, F'_x will be proportional to the current, I, supplied to the electromagnet. Since the torques of the two forces now must be equal, one has $F_x \propto I$. Thus, the lateral force, $F_x(x)$, produced by the superconductor can be found by measuring the current in the coil. Note that since the pendulum remains fixed, these measurements are performed with a constant vertical distance.

For optimal performance, the system is fully computerized so that the control action of the coil current is automatically updated. More details about the design, instrumentation, and operation of this apparatus can be found elsewhere.[10]

The magnet close to the sample was 9 mm long and had a square cross section of 2×2 mm^2. Figure 1 shows the orientation of the magnet, which was polarized parallel to the x direction. A Hall probe gave 1.3 kG for the field intensity at a point along the x-oriented symmetry axis 1 mm away from the poles.

The sintered sample of $YBa_2Cu_3O_x$ was shaped as a planar circular disk of 7 mm thickness and 70 mm diameter. The superconducting material, which has a density of 90% of the theoretical value and $T_c = 90$ K, was provided by Kali–Chemie Aktiengesellschaft, Hannover, West Germany.

All the experiments started by cooling the sample when it was placed far below the magnet. In this way essentially no flux was frozen into the superconductor initially. The movable table was then lifted so that the distance from the sample top surface to the lower side of the magnet was 1.0 mm.

Curve 1 in Fig. 2 shows the observed lateral force as a function of unidirectional horizontal displacement covering a total of 6 mm. The force, which is restoring in its nature, rises very steeply during the first small fraction of a millimeter. As the displacement increases the slope decreases monotonically, and the curve approaches asymptotically a plateau. The force reaches 90% of its saturation value, 5.1 mN, after 1.8 mm displacement. The behavior was independent of the starting point of the motion as long as the magnet was held away from the edge of the sample.

We find that the overall profile of the curve is quite similar to the behavior predicted by Davis.[8] These calculations are based on Bean's critical-state model, and assume a magnet of infinite length in the transverse y direction. They give the following expression for the lateral force per unit length of the magnet

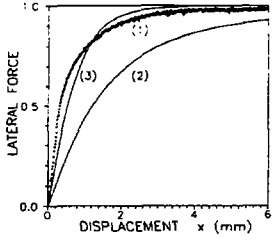

FIG. 2. Normalized lateral force F_x as function of horizontal displacement. The experimental curve (1) rises to $F_x^{\max} = 5.1$ mN. The curves (2) and (3) show the theoretical force behavior for the cases $H_0(x) = H_0(0)/(1+X^2)$ and $H_0(x) = H_0(0)/(1+X^2)^3$, respectively.

$$\frac{F_x(x)}{L_y} = -\frac{\mu_0}{4J_c}\left[H_0^2(0) - \int_{-\infty}^{0} dx'\left(H_0(x'-x)\times\frac{\partial H_0^2}{\partial x'}(x') + H_0^2(x'-x)\,\frac{\partial H_0}{\partial x'}(x')\right)\right]. \quad (1)$$

Here $H_0(x)$ is the tangential field distribution at the surface of the superconductor, and J_c is the effective critical current density. As suggested by Davis, the case of a magnet polarized parallel to the lateral displacement can be well approximated using the simple profile

$$H_0(x) = H_0(0)/(1+X^2), \quad X = x/h, \quad (2)$$

which corresponds to the field a distance h away from a straight wire carrying a current. Very recently, Yang *et al.*[11] found the analytical solution for this force

$$\frac{-F_x(x)/L_y}{\mu_0 H_0^2(0)/4J_c} = \frac{4+7X^2+X^4}{(4+X^2)^2} + X\frac{20+X^2}{(4+X^2)^3} \times(\pi - \arctan X) - \frac{4(4+5X^2)}{X^2(4+X^2)^3} \times\ln(1+X^2). \quad (3)$$

For comparison, this function has been plotted in Fig. 2, curve 2, using $h = 2$ mm, equal to the distance from the superconductor surface to the center of the magnet.

It is evident that the theoretical curve rises much more slowly than the observed behavior. One possible cause for this discrepancy is the choice of model for the field profile. It is clear that with H_0 falling off with x more quickly than described by Eq. (2) it is possible to get a steeper initial slope in the force. Indeed, we have solved the force integral numerically for many such field distributions, however, without being able to reproduce the experimental behavior. As an example, curve 3 of Fig. 2 shows the force for the case $H_0(x) = H_0(0)/(1+X^2)^3$, which describes to a good approximation the decay of the field produced by an infinite line of transversely polarized dipoles. The resulting increased initial slope has the additional effect of driving the force to a saturation at a too small displacement.

From Eq. (1) it follows that the saturation force is given by

$$F_x^{\text{sat}} = -\mu_0[H_0^3(0)/4J_c]L_y \tag{4}$$

a result that is independent of the particular choice of the field distribution. In order to estimate this saturation value we use $J_c = 100$ A/cm^2 and a maximum surface tangential field of 1 kG. Equation (4) then gives a force of 1.6 N, which is almost three orders of magnitude larger than the observed F_x^{sat}.

From this discussion it is clear that Davis' model does not give a satisfactory quantitative description of the force measurements reported in this work. The reason for this we believe is the large current penetration depth $\delta_0(x) = H_0(x)/J_c$ in materials with low J_c. In fact, using the same numerical values as above one finds a maximum depth of $\delta_0(0) = 8$ cm, i.e., more than ten times the thickness d of the sample. As pointed out by Davis, in such cases the basis of his calculations is no longer valid. However, if one assumes that the saturation force is monotonically increasing with the surface field also when $\delta_0(0) > d$, one can use the model to estimate a lower bound for F_x^{sat}. The result of Eq. (4) is applicable for fields up to $H_0(0) = J_c d$. One therefore expects the saturation force to satisfy

$$|F_x^{\text{sat}}| \geq \mu_0 J_c^2 d^3 L_y/4.$$

In our case, the lower bound amounts to 1 mN. Thus, the present measurements are not inconsistent with Davis' theory.

The magnetic stiffness associated with the lateral interaction is defined by

$$k_{xx} = dF_x/dx.$$

It is a dynamic quantity that governs oscillatory types of motion. If the lateral force were reversible, k_{xx} would simply equal the slope of the force-displacement curve. However, earlier measurements[1,10] have shown that major loops in lateral displacement, are highly hysteretic. The determination of the stiffness therefore requires separate experiments.

In this work, the stiffness measurements were performed by letting the unidirectional motion of the sample regularly be interrupted by periods of 0.1 mm backwards motion. The resulting behavior of the force is shown in Fig. 3.

We observe that as the motion is reversed the force decreases very quickly. Then the displacement again is set forward, the force reversibly returns to the point where the reversal started. These experiments clearly demonstrate that the slope of these reversible lines remains constant, independent of how far from the origin the minor loop takes place. The lateral stiffness $k_{xx}(x)$, taken as these

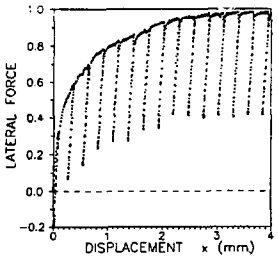

FIG. 3. Measurement of the lateral force stiffness. The set of parallel lines is the result of periodically reversing the displacement. The slope of the lines give $k_{xx} = 26$ N/m.

slopes, is therefore independent of the displacement. This surprising result is quite different from the behavior of the analogue quantity for the vertical direction, $k_{zz}(z)$, which depends strongly upon the separation z.[2,6]

We do not at present have an explanation for why the lateral stiffness is invariant. We believe, however, that this result is of considerable significance, both from a theoretical as well as practical point of view. To improve our understanding of the lateral interaction more experimental information about its characteristics is needed. A series of investigations is ongoing in our laboratory.

The authors wish to thank A. Haug for helpful discussions and P. Hatlestad for building part of the electronic equipment. The financial support of the Norwegian Council of Natural Sciences (NAVF) is gratefully acknowledged.

[1] F. C. Moon, M. M. Yanoviak, and R. Ware, Appl. Phys. Lett. 52, 1534 (1988).
[2] F. C. Moon, K-C. Weng, and P-Z. Chang, J. Appl. Phys. 66, 5643 (1989).
[3] D. B. Marshall, R. E. DeWames, P. E. D. Morgan, and J. J. Ratto, Appl. Phys. A 48, 87 (1989).
[4] D. E. Weeks, Rev. Sci. Instrum. 61, 197 (1990).
[5] T. H. Johansen, H. Bratsberg, Z. Yang, and G. Helgesen, *Europhysics Conference Abstracts. 10th General Conference of the Condensed Matter Division of the EPS*, 9–12 April, 1990, Lisbon, Portugal (European Physical Society, 1990), Vol. 14 A, p. 10.
[6] B. R. Weinberger, L. Lynds, and J. R. Hull, Supercond. Sci. Technol 3, 381 (1990).
[7] L. C. Davis, E. M. Logothetis, and R. E. Soltis, J. Appl. Phys. 64, 4212 (1988).
[8] L. C. Davis, J. Appl. Phys. 67, 2631 (1990).
[9] R. Williams and J. R. Matey, Appl. Phys. Lett. 52, 751 (1988).
[10] T. H. Johansen, H. Bratsberg, Z. J. Yang, G. Helgesen, and A. T. Skjeltorp, Rev. Sci. Instrum. (to be published).
[11] Z. J. Yang, T. H. Johansen, H. Bratsberg, G. Helgesen, and A. T. Skjeltorp, J. Appl. Phys. 68, 3761 (1990).

Paper 4

Physica C **165** 397-403 (1990).

Investigation of the Interaction between a Magnet and a Type-II Superconductor by Vibration Methods,

Z.J. Yang, T.H. Johansen, H. Bratsberg, G. Helgesen and A.T. Skjeltorp.

Physica C 165 (1990) 397–403
North-Holland

INVESTIGATION OF THE INTERACTION BETWEEN A MAGNET AND A TYPE-II SUPERCONDUCTOR BY VIBRATION METHODS

Z.J. YANG, T.H. JOHANSEN, H. BRATSBERG, G. HELGESEN and A.T. SKJELTORP [a]
Department of Physics, University of Oslo, Oslo, Norway
[a] *Institute for Energy Technology, N-2007 Kjeller, Norway*

Received 24 November 1989

Vibration methods are used to investigate the interaction between a magnet and a type-II superconductor on the basis of a dipole–dipole interaction model. For this purpose, a compound pendulum was constructed for studying the interaction between a magnet and a high-T_c superconductor. The experiments show that the damping of the pendulum is much larger when the motion is parallel to the direction of the magnetic moment than when it is perpendicular. This novel result is discussed in relation to the model and movements of flux lines.

1. Introduction

In connection with the application of levitation in superconducting systems, it is very important to understand the interaction between a magnet and a superconductor [1–4]. The interaction between a magnet and a type-I superconductor is well understood by means of perfect diamagnetism of the superconductor in the Meissner state. A dipole–dipole model is very good to describe the interaction [1–5]: the potential energy $V \sim z^{-3}$ and force $F \sim z^{-4}$ with z the distance between the magnet and superconductor. However, due to the flux pinning of type-II superconductors when $H > H_{c_1}$ (H_{c_1} = lower critical field), the interaction between a magnet and a type-II superconductor is, to our knowledge, not clear so far [1]. Hellman and co-workers [2] have suggested a flux pinning model, which yields, in the range of $H_{c_1} < H < H_{c_2}$ (H_{c_2} = upper critical field) and under certain conditions, $V \sim z^{-1}$ and $F \sim z^{-2}$.

Moon et al. and Marshall et al. [3] have reported experimental investigations of the force in this range, but they did not investigate the power law behaviour of the interaction. In an earlier paper we reported [4] the investigations of the force between a permanent magnetic sphere and an oxide superconductor as a function of separation z. We employed a power law to describe the force, $F \sim z^{-\gamma(z)}$, with $\gamma(z)$ satisfying $0 < \gamma(z) < 4$. Based on these experimental results, we studied the vibrations of a magnet levitated over a flat superconductor using a Lagrangian dynamical method [6].

The purpose of this letter is to suggest a vibration method based on a dipole–dipole interaction model, developed from our previous research [6], to investigate the interaction between a magnetic system and a type-II superconductor.

2. Description of the methods

Consider a permanent magnetic sphere with moment M over a flat superconductor as shown in fig. 1.

For type-I superconductors, (or when $H < H_{c_1}$ for type-II superconductors), we can use a dipole–dipole model and the image method to deal with it. The interaction between a dipole and an infinite superconducting plane can thus be expressed by:

$$V = \frac{\mu_0}{8\pi}\left[\frac{\boldsymbol{M}\cdot\boldsymbol{M}'}{(2z)^3} - \frac{3(\boldsymbol{M}'\cdot\boldsymbol{n})(\boldsymbol{M}\cdot\boldsymbol{n})}{(2z)^3}\right]$$

$$= \frac{\mu_0}{8\pi}\frac{|\boldsymbol{M}||\boldsymbol{M}'|}{(2z)^3}\left[\cos(\alpha+\alpha') + 3\sin\alpha\sin\alpha'\right] \quad (1)$$

where $\boldsymbol{M}'$ is the image dipole of the dipole $\boldsymbol{M}$ and

0921-4534/90/$03.50

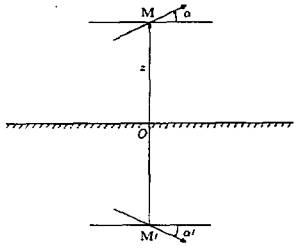

Fig. 1. The configuration of a dipole with moment M and its image dipole with moment M'.

$|M| = |M'|$. n is the unit vector along the line connecting the dipoles, and $\alpha' = \alpha$. The potential can then be written

$$V = \frac{\mu_0}{32\pi} \frac{|M||M'|}{2z^3} (1 + \sin^2 \alpha) . \tag{2}$$

The force along the z-direction is then given by:

$$F_z = -\frac{\partial V}{\partial z} = \frac{\mu_0}{32\pi} \frac{3|M||M'|}{2z^4} (1 + \sin^2 \alpha) . \tag{3}$$

The equilibrium position, corresponding to the minimum in potential energy, occurs for $\alpha = 0$.

Let us consider a dipole moving towards an infinite type-II superconductor plane from $z = \infty$. When $H < H_{c_1}$, eq. (1) is an almost exact representation of the interaction. For decreasing z, eq. (1) is not valid below a certain value, $z = z_1$, as the field will be higher than H_{c_1}. On the basis of our experimental results [4] as well as results due to others [3], we use a power law to describe the force (for $\alpha = 0$):

$$F = C(z/z_1)^{-\gamma(z)} \tag{4}$$

(if we let $\alpha = \pi/2$, the right hand side of eq. (4) should be multiplied by 2) where C and z_1 are constants determined by the magnetic properties of the magnet and the superconductor and z_1 defined by:

$$z_1 = \left(\frac{\mu_0}{4\pi} \frac{2M}{H_{c_1}} \right)^{1/3} . \tag{5}$$

$\gamma(z)$ is a monotonic decreasing function of z satisfying

$$0 < \gamma(z) < 4 . \tag{6}$$

Due to the fact that flux pinning causes magnetic hysteresis, the force describing a dipole moving away from the superconductor is expressed by a different power law from that for a dipole moving towards it, i.e. $F_m \sim z^{-\gamma_1(z)}$, and $\gamma(z) \neq \gamma_1(z)$, but $\gamma_1(z)$ also needs to satisfy $0 < \gamma_1(z) < 4$.

2.1. Determination of the force exponent from spring vibrations

Let us consider a system shown in fig. 2. A magnetic sphere of mass m_1 and magnetic moment M is attached to a spring with mass m_2 and spring constant k and hanging over an infinite superconducting plane. The equilibrium situation is with M parallel to the plane.

The equation of motion for this mass-spring system acted upon only by gravitation without magnetic interaction may be expressed as:

$$(m_1 + \tfrac{1}{3}m_2)\ddot{x} + kx = 0 \tag{7}$$

where x is the coordinate from the equilibrium position. A small extension, Δx, of the spring is given by $\Delta x = (m_1 + \frac{1}{3}m_2)g/k$. The solution to eq. (7) is

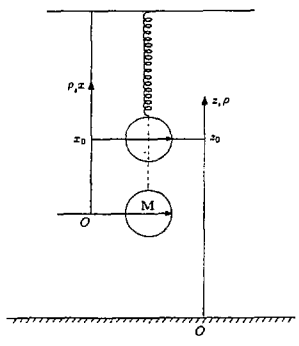

Fig. 2. A magnetic dipole with mass m_1 and moment M, connected by a string with mass m_2 and force constant k, above an infinite type-II superconductor plane.

$$x = x_{00}\sin(\Omega_0 t + \delta_0) \tag{8}$$

where x_{00} and δ_0 are constants determined by the initial conditions, and Ω_0 is the inertia vibrational frequency given by:

$$\Omega_0 = \left(\frac{k}{m_1 + \frac{1}{3}m_2}\right)^{1/2}. \tag{9}$$

We now want to study the effect of the superconductor on the *inertia system*. Let us assume that the force between the magnet and the superconductor may be described by eq. (4), and by substituting eq. (4) into eq. (7) a new dynamical equation is obtained:

$$(m_1 + \tfrac{1}{3}m_2)\ddot{x} + kx - C(z/z_1)^{-\gamma(z)} = 0. \tag{10}$$

The new equilibrium position z_0 (the distance from the surface to the center of the magnet) and x_0 (the distance from the old equilibrium position to the new equilibrium position) should satisfy:

$$kx_0 - C(z_0/z_1)^{-\gamma(z_0)} = 0 \tag{11}$$

where x_0 and z_0 can be measured directly.

Introducing a new argument, ρ, defined by

$$x = x_0 + \rho \quad \text{and} \quad z = z_0 + \rho, \tag{12}$$

and using the approximations

$$\gamma(z) \simeq \gamma(z_0) \tag{13}$$

and

$$z^{-\gamma(z)} = (z_0 + \rho)^{-\gamma(z_0+\rho)} \simeq z_0^{-\gamma(z_0)}\left[1 - \gamma(z_0)\frac{\rho}{z_0}\right] \tag{14}$$

the linearization of eq. (10) yields:

$$(m_1 + \tfrac{1}{3}m_2)\ddot{\rho} + k\rho + \frac{\gamma(z_0)}{z_0} C\left(\frac{z_0}{z_1}\right)^{-\gamma(z_0)}\rho = 0. \tag{15}$$

With the use of eqs. (9) and (11), eq. (15) is changed to:

$$\ddot{\rho} + \left[\Omega_0^2 + \gamma(z_0)\Omega_0^2\frac{x_0}{z_0}\right]\rho = 0. \tag{16}$$

The solution of this is:

$$\rho = \rho_0 \sin[\Omega_1(z_0)t + \delta_1] \tag{17}$$

where ρ_0 and δ_1 are constants determined by the initial conditions. The new vibrational frequency $\Omega_1(z_0)$ depends on the equilibrium position z_0 and is given by:

$$\Omega_1(z_0) = \Omega_0\left[1 + \gamma(z_0)\frac{x_0}{z_0}\right]^{1/2}. \tag{18}$$

This equation yields

$$\gamma(z_0) = \frac{z_0}{x_0}\left\{\left[\frac{\Omega_1(z_0)}{\Omega_0}\right]^2 - 1\right\}. \tag{19}$$

All the parameters of the right side of this equation can be measured directly. The exponent $\gamma(z_0)$ can thus be obtained precisely by measuring z_0, x_0, Ω_0 and $\Omega_1(z_0)$.

2.2. The potential function investigated for a stiff pendulum

Since the exponent $\gamma(z)$ in the force function $F(z)$ is a function of distance z, it is not possible to obtain the exponent function of the *potential function* by integrating the force function $F = C(z/z_1)^{-\gamma(z)}$. Thus, it is not possible to obtain the potential function using the vibration method described earlier. Instead, we now want to discuss how it is possible to measure the potential function using a rigid pendulum.

For this, let us assume that we have a similar system as in the spring vibration: the spring is changed to a rigid rod. The pendulum is placed over an infinite type-II superconductor plane as shown in fig. 3. Let us assume that the diameter a of the sphere is much smaller than the length l of the rod, i.e. $a \ll l$. Without the magnetic interaction, the dynamical equation of motion for the compound pendulum acted upon by gravitation may be expressed by (omitting the spin term of the ball in kinetic energy):

$$(m_1 + \tfrac{1}{3}m_3)l^2\ddot{\alpha} + (m_1 + \tfrac{1}{2}m_3)gl\sin\alpha = 0. \tag{20}$$

Let us consider a small angle approximation, i.e. $\sin\alpha \simeq \alpha$. The linearized equation may then be expressed as:

$$(m_1 + \tfrac{1}{3}m_3)l\ddot{\alpha} + (m_1 + \tfrac{1}{2}m_3)g\alpha = 0. \tag{21}$$

The solution to this equation is:

$$\alpha = \alpha_{00}\sin(\Omega_2 t + \delta_2) \tag{22}$$

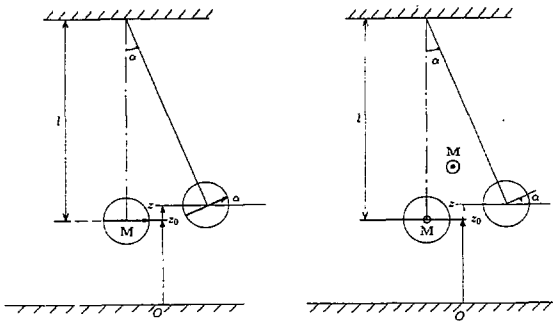

Fig. 3. A magnetic dipole with mass m_1 and moment M, connected by a rigid rod with mass m_3 and length l, above an infinite type-II superconductor plane. (a): The moment M is parallel with the motion direction, and (b): the moment M is perpendicular to the motion direction.

where α_{00} and δ_2 are constants determined by the initial conditions, and Ω_2 is the inertia compound pendulum frequency given by

$$\Omega_2=\left(\frac{m_1+\frac{1}{2}m_3g}{m_1+\frac{1}{3}m_3\,l}\right)^{1/2}. \tag{23}$$

We now want to consider the effect of the interaction between the permanent magnetic sphere and the superconductor on the *inertia compound pendulum*. Let us assume that the potential function can be described as follows:

$$V=C_1(z/z_1)^{\gamma_2(z)}(1+\sin^2\alpha) \tag{24}$$

where z_1 is defined previously by eq. (5). C_1 is a constant determined by the magnetic properties of the ball and the superconductor, and $\gamma_2(z)$ is a function of the distance z. If $\gamma_2(z)$ is independent of z, $\gamma(z)$ in eq. (4) will also be independent of z. We then obtain the following relationships: $\gamma_2=\gamma+1$ and $C=C_1\gamma_2$ (actually, these relationships are not valid for a type-II superconductor). In this case, we assume that the angular part in eq. (2) is valid (i.e. we still use the image method and that the absolute value, $|M|$, of the image dipole M' is reduced, but its angle is unchanged).

Let us assume that the vertical displacement $(z-z_0=l(1-\cos\alpha))$ of the pendulum is much smaller than the distance z_0, i.e. $l(1-\cos\alpha)\ll z_0$. As a first approximation the new dynamical equation of motion of the compound pendulum system, corresponding to the configuration of fig. 3a, can be expressed by:

$$(m_1+\tfrac{1}{3}m_3)l^2\ddot{\alpha}+(m_1+\tfrac{1}{2}m_3)gl\alpha +2C_1(z_0/z_1)^{-\gamma_2(z_0)}\alpha+lC(z_0/z_1)^{-\gamma(z_0)}\alpha=0\,. \tag{25}$$

The last term is the force function $F(z)$ [#1,2]. At least

[#1] Here we omit one term (assume $\partial\gamma_2(z)/\partial\alpha=0$). If we still formally use eq. (24) to dedude eq. (25), the force function $F_1(z)$ is different from the force function described in eq. (4). The formal result of the force function in eq. (25) should be:

$$F_1(z)=C_1\left(\frac{z}{z_1}\right)^{-\gamma(z)}\left[\frac{\gamma_2(z)}{z_1}\left(\frac{z}{z_1}\right)^{-1}+\ln\left(\frac{z}{z_1}\right)\frac{\partial\gamma_2(z)}{\partial z}\right].$$

In the following we also need to use $F_1(z)$ instead of $F(z)$. The final results are all consistent in eqs. (30), (32) and (33).

[#2] It should be pointed out that here the force function F only has an effective meaning. The effective force thus changes sign from "−" (repulsive force) to "+" (attractive force) when the field H is below or above H_{c_1} respectively. As the details of the dynamical processes are very complicated, the potential function, $V(z)$, and the force function, $F(z)$, are only phenomenological.

three methods can be employed to determine $F(z)$. The first method was discussed above. We may also connect the other end of the rod to a balance and measure $F(z)$ directly. Later we will describe the third method.

The solution to eq. (25) is

$$\alpha=\alpha_0 \sin[\Omega_3(z_0)t+\delta_3] \tag{26}$$

where α_0 and δ_3 are constants determined by the initial conditions, and $\Omega_3(z_0)$ is a function of distance z_0. The new vibration frequency $\Omega_3(z_0)$ depends on the distance z_0 and is given by:

$$\Omega_3(z_0)=\left[\Omega_2^2+\frac{2}{l^2(m_1+\frac{1}{3}m_3)}V(z_0)+\frac{F(z_0)}{l(m_1+\frac{1}{3}m_3)}\right]^{1/2} \tag{27}$$

where $V(z)$ is the potential function defined by

$$V(z)=C_1(z/z_1)^{-\gamma(z)}. \tag{28}$$

eq. (27) yields

$$V(z_0)=\tfrac{1}{2}l^2(m_1+\tfrac{1}{3}m_3)[\Omega_3^2(z_0)-\Omega_2^2]-\tfrac{1}{2}lF(z_0). \tag{29}$$

This potential function can thus be obtained by measuring $\Omega_3(z)$, Ω_2 and $F(z)$ directly.

Now we consider the third method to measure the force function $F(z)$. We can use the same rigid compound pendulum as discussed above, but with a different configuration: the moment M of the permanent magnetic sphere is now parallel to the rotation axis of the pendulum as shown in fig. 3b. By using the same approximations as before the potential term will vanish and the dynamical equation of motion of the pendulum can be simplified to

$$(m_1+\tfrac{1}{3}m_3)l\ddot{\alpha}+(m_1+\tfrac{1}{2}m_3)g\alpha+C(z_0/z_1)^{-\gamma(z_0)}\alpha=0. \tag{30}$$

The solution to this equation is

$$\alpha=\alpha_1 \sin[\Omega_4(z_0)t+\delta_4] \tag{31}$$

where α_1 and δ_4 are constants determined by the initial conditions. The new vibrational frequency $\Omega_4(z_0)$ with z_0 the equilibrium position is given by

$$\Omega_4(z_0)=\left[\Omega_2^2+\frac{F(z_0)}{l(m_1+\frac{1}{3}m_3)}\right]^{1/2}. \tag{32}$$

This equation yields

$$F(z_0)=l(m_1+\tfrac{1}{3}m_3)[\Omega_4^2(z_0)-\Omega_2^2]. \tag{33}$$

As may be seen from eqs. (27) and (33), it is possible to obtain the force function $F(z)$ and potential function $V(z)$ from precise measurements of the frequencies Ω_2, $\Omega_3(z)$ and $\Omega_4(z)$ for a stiff compound pendulum [#3]. To our knowledge, this offers a new experimental approach to analyse the properties of type-II or high-T_c superconductors.

3. Experiments and discussions

Based on the above suggestions, we have constructed a rigid compound pendulum for investigating the interaction between a magnet and a high-T_c superconductor. For this purpose, a cylindrical Nd–Fe–B permanent magnet with diameter 9.5 mm and length 10 mm was mounted at the end of a quartz rod hanging by a knife's edge. The pendulum was placed above an $YBa_2Cu_3O_x$ superconducting disk with diameter 69 mm and thickness 6.8 mm emerged in liquid nitrogen. An optical system was employed to monitor the time dependence of the amplitudes of the oscillations. The pendulum intersected a fraction of a laser beam and the transmitted light detected by a photodiode was proportional to the amplitude. Via an IBM DACA sampling card, the signals from the diode were transfered into an IBM PC-AT for data treatment.

Preliminary experiments were performed for examining the changes of amplitudes and frequencies of the pendulum. The damping of the free pendulum without the superconductor is very small and negligible. When the distance from the superconducting surface to the bottom of the magnet is relatively large (typical value is larger than 25 mm), the influence of the magnetic interaction on the amplitude and

[#3] If we phenomenologically introduce the damping terms $\Gamma_3\dot{\alpha}$, $\Gamma_4\dot{\alpha}$ to eqs. (25) and (30), respectively, the frequencies $\Omega_3(z)$ and $\Omega_4(z)$ need to be corrected. The new corrected frequencies $\Omega_3'(z)$ and $\Omega_4'(z)$ can be obtained by:

$\Omega_3'(z)=[\Omega_3^2(z)]-\Gamma_3^2]^{1/2}$ and $\Omega_4'(z)=[\Omega_4^2(z)]-\Gamma_4^2]^{1/2}$, respectively.

frequency is very weak. As the distance decreases, one can clearly observe changes of both amplitude and frequency. An unexpected and novel observation was that the oscillations in the two configurations, with the moment M parallel with and perpendicular to the direction of motion (fig. 3), are very different as displayed in fig. 4. There is also an increase of the frequencies for both configurations relative to the free pendulum. This is in qualitative agreement with our model. As seen in fig. 4, the parallel motion (fig. 3a) shows much stronger damping than the perpendicular motion (fig. 3b). In the *image* picture, the motions of the magnet cause movements of the flux lines in the superconductor. For the same amplitudes, even though the motions in both configurations affect the same quantities of moving flux lines, a simple calculation for the field distribution of a dipole shows that not only the quantities of moving flux lines, but also the interactions among the flux lines contribute to the damping differently in the two configurations. The experiments yield the results in qualitative agreement with our calculation. This difference in damping for different configurations will also obviously have important consequences in levitation applications. Besides the frequencies change in both configurations, the frequencies were also seen to increase slightly with time. This feature is beyond the description of our model. It is not surprising that our simple model is unable to contain all the characteristic features for such a rich physics system. This would probably be improved in future work.

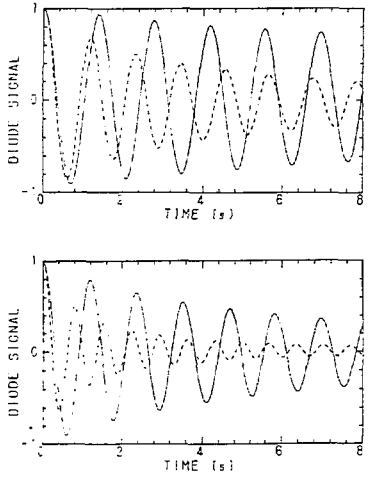

Fig. 4. Two measurements of the amplitudes (proportional to the diode signals) vs. time with different distances between the magnet and the superconductor. (a): $z=14.5$ mm (frequencies $f=0.725$ Hz and 0.920 Hz, and damping factors $\Gamma=0.033\ s^{-1}$ and $0.1\ s^{-1}$, respectively), and (b) $z=11.5$ mm (frequencies $f=0.870$ Hz and 1.44 Hz, and damping factors $\Gamma=0.1\ s^{-1}$ and $0.3\ s^{-1}$, respectively). The solid lines show the responses for M perpendicular to the motion direction (fig. 3a) and the dashed lines for M parallel with the motion direction (fig. 3b).

4. Summary and conclusion

The preliminary experiments of our pendulum show very high sensitivity for examining the interaction. As the motion of flux lines (lattice) depends on temperature, an obvious extension of our experiments would be to improve the set-up and measure the melting and creeping of flux lines. This is of particular interest as the melting and creeping are the main reasons for a low critical current density. The model and experiments also offer efficient tools to study the dynamical behaviour of flux lines in superconductors, which has not been understood very well so far. The interaction is attractive due to the fact that some flux lines are frozen. This means that the force, $F_m(z)$, acting on a dipole moving away from the superconductor at a distance z is lower than the force, $F(z)$, acting on the dipole moving toward it. The resulting potential function is therefore also different for these two situations. By measuring the vibration frequencies for these inward and outward motions we are therefore able to map the potential function. Such investigation will be of interest both for characterization of the superconductor itself as well as for applications.

Acknowledgements

The research was supported in part by the Norwegian Research Council for Science and Humanities (NAVF). One of the authors (ZJY) would like to thank Prof. C.P. Bean for a helpful discussion, and the authors also acknowledge the assistance for the experiments from B. Berling, J. Yao, K. Nilsen, P.M. Hatlestad and T. Foss.

References

[1] E.H. Brandt, Appl. Phys. Lett. 53 (1988) 1554;
L.C. Davis, E.M. Logothetis and R.E. Soltis, J. Appl. Phys. 64 (1988) 4212.

[2] F. Hellman, E.M. Gyorgy, D.W. Johnson Jr., H.M. O'Bryan and R.C. Sherwood, J. Appl. Phys. 63 (1988) 447;
H. Kitaguchi, J. Takada, K. Oda, A. Osaka and Y. Miura, Physica C 157 (1989) 267.

[3] F.C. Moon, M.M. Yanoviak and R. Ware, Appl. Phys. Lett. 52 (1988) 1534;
D.B. Marshall, R.E. DeWames, P.E.D. Morgan and J.J. Ratto, Appl. Phys. A48 (1989) 87.
In these papers the authors did not investigate the power law for the force, but if we use eq. (5) to represent their results and plot γ as a function of distance z, we find that their data satisfy the condition described in eq. (6).

[4] T.H. Johansen, Z.J. Yang, H. Bratsberg, G. Helgesen and A.T. Skjeltorp, to be published.

[5] D. Bedeaux, M.M. Wind, M.A. van Dijk, Z. Phys. B68 (1987) 343.
This paper contains calculation of the perturbation terms of the electrical dipole–dipole interaction which is also valid for the magnetic interactions considered here.

[6] Z.J. Yang, T.H. Johansen, H. Bratsberg, G. Helgesen and A.T. Skjeltorp, Physica C 160 (1989) 461.

Paper 5

Superconductor Science and Technology **3** 591-597 (1990)

Potential and Force between a Magnet and a Bulk $Y_1Ba_2Cu_3O_{7-\delta}$ Superconductor Studied by a Mechanical Pendulum,

Z.J. Yang, T.H. Johansen, H. Bratsberg, G. Helgesen and A.T. Skjeltorp.

Supercond. Sci. Technol. 3 (1990) 591–597. Printed in the UK

Potential and force between a magnet and a bulk $Y_1Ba_2Cu_3O_{7-\delta}$ superconductor studied by a mechanical pendulum

Z J Yang†, T H Johansen†, H Bratsberg†, G Helgesen† and A T Skjeltorp‡

† Department of Physics, University of Oslo, Oslo, Norway
‡ Institute for Energy Technology, N-2007 Kjeller, Norway

Received 20 August 1990, in final form 12 November 1990

Abstract. The interaction between a magnet and a high T_c superconductor (HTSC) is investigated by a novel method. A permanent magnet mounted at one end of a stiff rod hanging by a knife's edge forms a mechanical pendulum. When a HTSC is placed below the magnet the frequency ν and damping factor Γ will be changed due to the interaction between the magnet and the HTSC. The experiments show that, as the separation between the magnet and the HTSC decreases, the flux lines start to penetrate the sample via intergranules and grain boundaries, which results in a horizontal restoring force even for the field range $B << B_{c_1}$. The present experimental results are consistent with the theoretical model of weak links for bulk HTSC. The power-law-like *potential*, $V_{\rm eff}$, and *force*, $F_{\rm eff}$, are introduced to describe the *interaction*. The behaviour of $V_{\rm eff}$ and $F_{\rm eff}$ obtained from the present measurements is in disagreement with the dipole-image model even for the field range $B << B_{c_1}$.

1. Introduction

In connection with the application of levitation and superconducting bearings by using high T_c superconductors (HTSC), several groups have reported their results of theoretical analysis and force measurements [1–8]. In particular, Williams and Matey [5] have measured the lateral force acting on a small permanent magnet levitated above an HTSC disc and tried to obtain the potential as a function of horizontal displacement. Based on Beans' model of hard superconductors, Davis [6] has calculated the lateral restoring force. High resolution measurements of the lateral force [7] are only in qualitative agreement with Davis' results. At present there is therefore relatively little quantitative information or basic understanding of the interaction between a magnet and an HTSC. The purpose of this paper is to use a mechanical pendulum [8] to investigate the interaction between a small magnet and a large $Y_1Ba_2Cu_3O_{7-\delta}$ (Y123) superconductor disc, and to introduce phenomenologically the *potential* $V_{\rm eff}$ and *force* $F_{\rm eff}$ to describe the *interaction* in this system. These studies enable us to investigate the dynamic behaviour of flux lines in a Y123 superconductor [9]. The present results show new features distinctly different to those obtained from previous studies on conventional superconductors [10–12] and HTSC [13].

2. Experiment

The experimental set-up is shown schematically in figure 1. A Nd–Fe–B permanent magnet (M) (manufactured by Sumitomo Special Metals Co. Ltd. Japan) was cut into a cube-like shape ($6.5 \times 6.5 \times 7.5$ mm^3) with rounded edges and attached to the end of a 55 cm long quartz tubular rod hanging by the edge of a razor blade. The magnet was magnetized with a 1.3 T field along the longest side. The maximum remanent field on the surface of the magnet was measured to be 0.4 T using a Hall probe. The magnet could be set in oscillations above the sample, a Y123 superconducting disc with diameter 69.3 mm and thickness 6.8 mm. (The sample was manufactured by KaliChemie Aktiengesellschaft. Germany with $T_c \sim 90$ K and a density more than 90% of the theoretical density.) The sample was immersed in liquid nitrogen (77 K) and the distance z between the sample and permanent magnet could be adjusted by moving up and down the nitrogen reservoir containing the sample. An optical system was employed to monitor the time dependence of the 'horizontal displacement' of the oscillations as follows. The pendulum intersected a fraction of a spread light beam from a laser. The signal from a photodiode detecting the focused passing light beam was thus proportional to the horizontal position of the magnet. A controlled and reproducible initiation

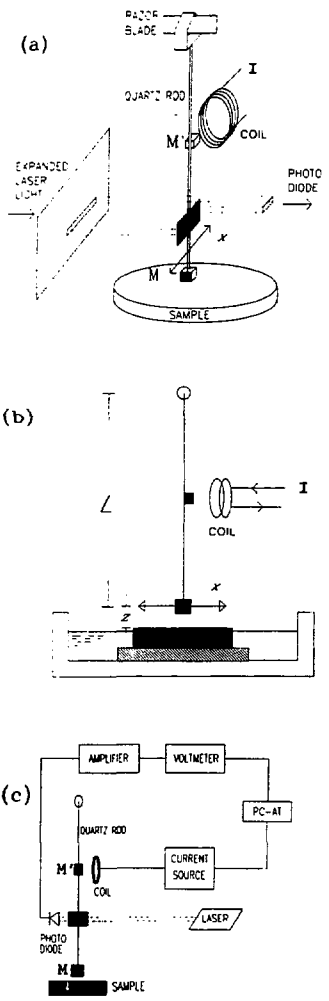

Figure 1. Schematic diagram of the experimental set-up: (a) perspective view, (b) front view, and (c) block diagram of the instrument connections. The permanent magnet M attached to the end of a tubular quartz rod swings above the sample in the x direction. An expanded laser beam is sent through an aperture with a rectangular cross section. Part of this light beam is intersected by the pendulum and focused by a lens onto the photodiode. The diode signal is amplified and recorded by a PC/AT. The oscillations are started by turning off the supply current in the coil attracting the small permanent magnet M' (see text).

of the oscillation was achieved by using a small permanent magnet (M' in figure 1) attached to the middle part of the quartz tube. The tube could thus be pulled out to a fixed position (< 0.4° from vertical) by supplying current to an adjacent coil. By turning off the current, the oscillations were started. The whole set-up was automated using a PC/AT data-logging system. In the experiments the direction of the magnetic moment $\boldsymbol{M}$ could be made either normal (N configuration) or parallel (P configuration) to the direction of the oscillations of the pendulum.

The performance of the pendulum was also checked with the sample in the normal state. It was found that the damping Γ_0 was very small in this case ($\Gamma_0 \sim 0.011\ s^{-1}$) and negligible compared to the damping Γ in the presence of the superconducting sample ($\Gamma \sim 0.1\ s^{-1}$, typically). Also, no change in the oscillation frequency ν_0 ($\nu_0 = 0.798$ Hz) of the free pendulum was observed. Thus, by using a relatively rapid

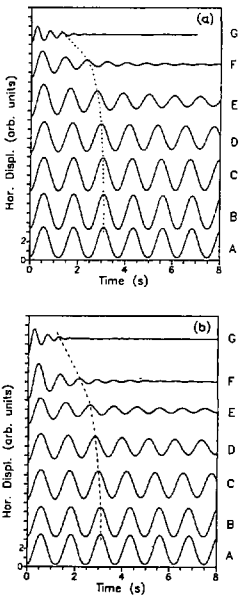

Figure 2. Typical measurements of the horizontal displacements (proportional to the diode signals) against time for decreasing distances between the magnet and the superconductor: (a) for the N configuration, and (b) for the P configuration. Curves A show the free oscillations. The distances are z = 37 mm (B); 25 mm (C); 21 mm (D); 17 mm (E); 13 mm (F); and 9 mm (G). The broken curves indicate the frequency shift. A sampling rate of 188 s^{-1} was used.

sampling rate (188 s^{-1}) of the amplitude signal (pendulum position), we could therefore deduce information about the magnet–superconductor interactions from frequency and damping changes.

3. Results and discussion

Figure 2 shows the typical response curves: horizontal displacements against time for the N and P configurations with different distances z between the magnet and the superconductor. It may be seen that the oscillations are damped and there is also a frequency shift. In order to confirm that the frequency shift was a specific effect of pinned flux lines in HTSC, normal metals and alloys (copper, aluminium, brass, etc) were used as a substitute for the superconductor. A damping was also observed for these, but frequency changes were never observed. The damping caused by normal metals is due to eddy currents. However, there is no force to pin the field lines, and damping is therefore no physical reason for a frequency change. (The present results were also confirmed by measurements on other Y123 samples with various sizes supplied by other manufacturers.)

By fitting parabolas to the extrema of the response curves, the positions and values of the peaks were accurately determined, and the frequency ν and damping factor Γ were calculated precisely (see appendix A). The frequency shift $\nu_i - \nu_0$ against z is shown in figure 3 ($i = 1$ for the N configuration and $i = 2$ for the P configuration). It can be seen that these shifts increase drastically for decreasing distance z. The differences between the two configurations will be discussed below. It may also be seen that there is pronounced hysteresis for both configurations.

Figures 4 and 5 show log–log plots of the quantities $|\nu_i^2 - \nu_0^2|$ and $|\nu_2^2 - \nu_1^2|$ against distance z. It can be seen that the curves are approximately linear, signifying a power-law dependence. The slopes thus produce exponents for the *force* and *potential* as discussed below.

At a given distance z the experiments also show that, as the amplitude decreases with time, the frequency initially increases slightly and then saturates. Meanwhile, the damping factor decreases slightly in the beginning and then reaches a constant level. This behaviour is distinctly different from results obtained for the conventional tin superconductor using a torsion pendulum [10].

It may be shown that the field produced around a homogeneously polarized spherical permanent magnet (SPM) with moment M is the same as that created by a point dipole with moment M located at the centre of the sphere. To the first approximation we may also use a sphere approximation instead of the cube-like magnet to evaluate the field on the HTSC disc (see appendix B). The maximum field on the surface of an SPM with moment M and radius r_0 is given by $B_{max} = \mu_0|M|/2\pi r_0^3$ (SI units hereafter). Let us consider an SPM placed above the centre of a large HTSC disc with the moment M parallel to the upper surface of the superconductor. We define a critical separation, $z_1 = (B_{max}/2B_{c_1})^{1/3} r_0$, for which $B = B_{c_1}$ at the centre of the superconductor surface. (For this configuration one can show that the maximum field on the superconductor is $\mu_0|M|/4\pi z^3$). We can estimate the field range for our experiments with the parameters chosen: $B_{max} = 0.4$ T, $B_{c_1} = 0.01$ T and $r_0 = 4.2$ mm

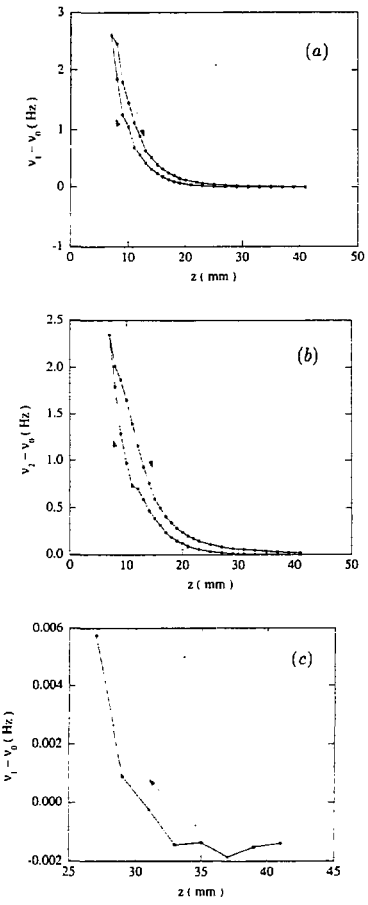

Figure 3. The frequency shift, $\nu_i - \nu_0$, against distance z for: (a) the N configuration ($i = 1$); (b) the P configuration ($i = 2$); and (c) detail of (a) in the range $z = 41$— 27 mm for decreasing z (virgin curve). The corresponding fields at the centre of the HTSC were estimated to be 2.2×10^{-4} T ($z = 41$) → 7.7×10^{-4} T ($z = 27$ mm) using the magnetic sphere approximation.

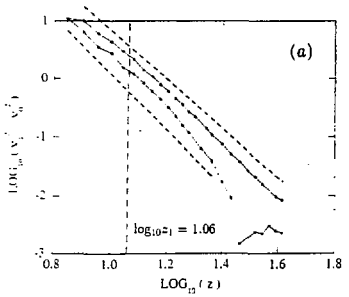

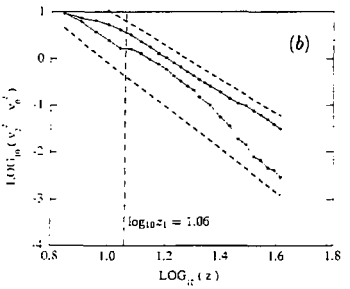

Figure 4. The log–log plots of the quantity $|\nu_i^2 - \nu_0^2|$ against distance z for: (a) the N configuration ($i = 1$), and (b) the P configuration ($i = 2$). The least-squares fits to the straight parts as indicated by the dashed lines (shifted up and down for clarity) produce the following slopes: -4.7 ± 0.1 (decreasing z) and -4.5 ± 0.1 (increasing z) for the N configuration, and -4.7 ± 0.1 (decreasing z) and -3.7 ± 0.1 (increasing z) for the P configuration. The vertical broken lines show the position of z_1.

($r_0 = (3\times6.5\times6.5\times7.5/4\pi)^{1/3}$ is the equivalent radius of a sphere with the same volume as the cube-like magnet), and then $z_1 = 11.4$ mm ($\log_{10} z_1 = 1.06$).

Consider an SPM with moment $\boldsymbol{M}$ over an infinite flat superconductor as shown in figure 6. For type I superconductors, (or when $B < B_{c_1}$ for conventional type II superconductors), the dipole-image method can be used to explain the potential as:

$$V = \frac{\mu_0}{8\pi}\frac{|\boldsymbol{M}||\boldsymbol{M}'|}{(2z)^3}[\cos(\alpha+\alpha') + 3\sin\alpha\sin\alpha'] \qquad (1)$$

where $\alpha' = \alpha$ is the vertical inclining angle, $\boldsymbol{M}'$ the image dipole of the dipole $\boldsymbol{M}$ and $|\boldsymbol{M}| = |\boldsymbol{M}'|$. The potential can then be written as

$$V = \frac{\mu_0}{64\pi}\frac{|\boldsymbol{M}||\boldsymbol{M}'|}{z^3}(1+\sin^2\alpha) \qquad (2)$$

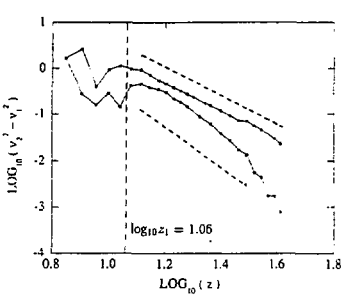

Figure 5. The log–log plots for the quantity $|\nu_2^2 - \nu_1^2|$ against distance z. The least-squares fits to the straight parts as indicated by the dashed lines (shifted up and down for clarity) produce the following the slopes: -4.2 ± 0.1 (decreasing z) and -3.1 ± 0.1 (increasing z), which give the exponents of the *potential*, V_{eff}, as discussed in the text.

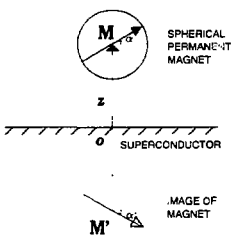

Figure 6. The configuration of a spherical permanent magnet with moment $\boldsymbol{M}$ and an infinite flat superconductor.

with a minimum for $\alpha = 0$, which is the equilibrium position. The force on the magnet is then given by

$$\boldsymbol{F} = -\nabla V = \frac{3\mu_0}{64\pi}\frac{|\boldsymbol{M}||\boldsymbol{M}'|}{z^4}\boldsymbol{k} \qquad (3)$$

where $\boldsymbol{k}$ is the unit vector in the z direction. One can see that there is no lateral restoring force for an SPM freely placed above a type I superconductor, but only a vertical force reducing the gravitational force.

If the superconducting disc is in the perfect diamagnetic state, the repelling force due to the Meissner effect should only cause a decrease in frequency for the present pendulum system. Using the dipole–dipole model, at the critical distance z_1, the vertical repelling force is estimated to be ~2.5 g or about 10% of the weight of the pendulum. This should reduce the pure inertia frequency ν_0 by approximately 5%. However, the present experiments show that the frequency increases even for separations much larger than the critical distance z_1. Figures 3 and 4 show that $\nu_1 - \nu_0 \simeq 0$ for $z_0 = 30.0$ mm

($\log_{10} z_0 = 1.48$). Using the sphere approximation discussed above, the corresponding field at this separation is estimated to be $B(z_0) = 5.6 \times 10^{-4}$ T $<< B_{c_1}$. It is therefore clear that the dipole-image potential described by equations (1)–(3) cannot provide a physical interpretation for the frequency increase.

The frequency increase must therefore be due to some kind of attractive forces with lateral or vertical components. The bulk sample used in the experiments contains voids and grain boundaries. The flux lines may thus penetrate into the sample via these defects even for fields much lower than the lower critical field B_{c_1}. The flux lines will thus be pinned and cause an attractive force between the magnet and the sample. This would explain the frequency increase. The gradual flux penetration for fields below B_{c_1} may also be detected indirectly from magnetization measurements. For conventional type II superconductors, a distinct deviation from a linear M–B relationship identifies B_{c_1}. What is observed for the present HTSC materials is a gradual deviation from a linear M–B curve [14, 15], signifying a gradual flux penetration even for fields below B_{c_1}.

It is generally accepted that the magnetic properties of the bulk HTSCs are dominated by the weak links between the granules at low external fields. The lower critical field of intergranules is $B_{c_{1J}} << B_{c_1}$ (the lower critical field of the intragranules). Tinkham and Lobb [16] have estimated $B_{c_{1J}} \sim 0.5 \times 10^{-4}$ T for a three-dimensional weak link cubic array model. Clem [17] has obtained the result $B_{c_{1J}} \sim 1 \times 10^{-4}$ T using the weak link Josephson coupling parameters. The present experimental results seem to be consistent with such a model. Since the vertical repelling force only contributes to the reduction of frequencies, the penetration takes place even for $z > z_0 = 30.0$ mm ($B(z_0) = 5.6 \times 10^{-4}$ T), i.e. $B_{c_{1J}} < B(z_0)$.

For the virgin process (magnet approaching the HTSC disc) the experimental results may be interpreted as follows: (i) When $z > z_{1J}$ (defined by $B(z_{1J}) = B_{c_{1J}}$), the frequency is only reduced by the vertical repelling force. (ii) When $z < z_{1J}$, the frequency shift is controlled by the competition between the vertical repelling force and the lateral attractive force resulting from the flux penetration. The former dominates the effect for $z > z_0$ and the latter dominates the effect for $z < z_0$. (iii) When $z \leq z_1$, the attractive lateral force will increase due to the intragranular penetration.

As all the measurements were performed with small amplitudes (< 1 mm or < 0.4° from vertical), we may use the linear approximation (checked also in lateral force measurements [7]) for the equation of motion of the mechanical compound pendulum (without the superconductor):

$$\ddot{\alpha} + \Gamma_0 \dot{\alpha} + 4\pi^2 \nu_0^2 \alpha = 0 \qquad (4)$$

where α is the deflection angle, Γ_0 is the mechanical damping factor, and the intrinsic frequency of inertia is $\nu_0 = (1/2\pi)(lgM_{\text{eff}}/I)^{1/2}$ (g is the graviational constant). Here, I is the moment of inertia which can be measured or calculated, M_{eff} is the effective mass of the inertia compound pendulum and l is the length of the pendulum rod. The solution of equation (4) is

$$\alpha(t) = \alpha_0 \exp(-\Gamma_0 t/2) \cos(2\pi \nu_{0,\text{meas}} t + \delta_0) \qquad (5)$$

where α_0 is the initial angle, δ_0 is the initial phase, and the measured frequency is $\nu_{0,\text{meas}} = \sqrt{\nu_0^2 - (\Gamma_0/4\pi)^2} \simeq \nu_0$ for $4\pi\nu_0 >> \Gamma_0$, which is satisfied for the present measurements.

In the presence of the superconductor, the equation of motion is given by

$$\ddot{\alpha} + \Gamma_i \dot{\alpha} + 4\pi^2 \nu_i^2 \alpha = 0 \qquad (6)$$

where $i = 1$ for the N configuration and $i = 2$ for the P configuration. Here, the damping faccors Γ_i and frequencies ν_i are determined by both the mechanical system and the magnet–superconductor interaction. The solutions are

$$\alpha_i(t) = \alpha_{i,0} \exp(-\Gamma_i t/2) \cos(2\pi \nu_{i,\text{meas}} t + \delta_i) \qquad (7)$$

where $\alpha_{i,0}$ ($i = 1, 2$) is the initial angle, δ_i ($i = 1, 2$) is the initial phase and the measured frequency is $\nu_{i,\text{meas}} = \sqrt{\nu_i^2 - (\Gamma_i/4\pi)^2}$.

The quantities $\nu_i^2 - \nu_0^2$ and $\Gamma_i - \Gamma_0$ express the contributions of the interaction to the elastic and dissipative parts, respectively. Classically, the parameter $\nu_i^2 - \nu_0^2$, which is proportional to the change of the stiffness constant, is a measure of the energy changes from the pure inertia pendulum. The kinetic energy for the system described by equation (6) is $T_i \sim 2\pi^2 \nu_i^2 \exp(-\Gamma_i t)$, and the potential is $V_i \sim 2\pi^2 \nu_i^2 \exp(-\Gamma_i t)$. The total energy is $E_i \sim 4\pi^2 \nu_i^2 \exp(-\Gamma_i t)$, and the relevant energy loss per period is $\exp(-\Gamma_i/\nu_i)$. Since $\Gamma_i/\nu_i \leq 0.1 << 1$ for most cases in our measurements, the interaction between the magnet and the superconductor mainly contributes to the elastic part. It is then reasonable to assume that the parameter $\nu_i^2 - \nu_0^2$ is a measure of the interaction in this system.

Phenomenologically, and guided by the dipole-image picture, the *force* $F_{\text{eff}}(z)$ and *potential* $V_{\text{eff}}(z)$ may be expressed [8] as a power law:

$$F_{\text{eff}}(z) = \begin{cases} C_0 (z/z_1)^{-\gamma_0(z)} & \text{decreasing } z \\ C_1 (z/z_1)^{-\gamma_1(z)} & \text{increasing } z \end{cases} \qquad (8)$$

and

$$V_{\text{eff}}(z) = \begin{cases} C_2 (z/z_1)^{-\gamma_2(z)} (1 + \sin^2 \alpha) & \text{decreasing } z \\ C_3 (z/z_1)^{-\gamma_3(z)} (1 + \sin^2 \alpha) & \text{increasing } z \end{cases} \qquad (9)$$

where $z_1 = (|M|/B_{c_1})^{1/3}$. The parameters C_0, C_1, C_2 and C_3 are independent of distances. However, these parameters as well as the exponents $\gamma_0(z)$, $\gamma_1(z)$, $\gamma_2(z)$ and $\gamma_3(z)$ should be temperature and sample dependent.

Substituting equations (8) and (9) into equation (6), one may obtain for the N configuration

$$I\ddot{\alpha} + I\Gamma_1 \dot{\alpha} + [4\pi^2 \nu_0^2 I + lF_{\text{eff}}(z)]\alpha = 0 \qquad (10a)$$

and for the P configuration

$$I\ddot{\alpha} + I\Gamma_2\dot{\alpha} + [4\pi^2\nu_0^2 I + lF_{\text{eff}}(z) + 2V_{\text{eff}}(z)]\alpha = 0. \quad (10b)$$

By neglecting the effects of damping, one obtains

$$\begin{aligned} F_{\text{eff}} &= C_{0,1}(z/z_1)^{-\gamma_{0,1}} = 4\pi^2 I(\nu_1^2 - \nu_0^2)/l \\ V_{\text{eff}} &= C_{2,3}(z/z_1)^{-\gamma_{2,3}} = 2\pi^2 I(\nu_2^2 - \nu_1^2). \end{aligned} \quad (11)$$

This functional form is consistent with the linear dependence in the log–log plots in figure 4(*a*), and from the linear regions the following values for the exponents were obtained: $\gamma_0 = 4.7$, $\gamma_1 = 4.5$, and from figure 5 $\gamma_2 = 4.2$ and $\gamma_3 = 3.1$.

It is interesting to note that the effects of the *potential* on the frequency shift become less and less for decreasing z. This is shown in figure 7. When $z \leq z_1$ (the corresponding field is $B > B_{c_1}$) there appear to be no effects from V_{eff}.

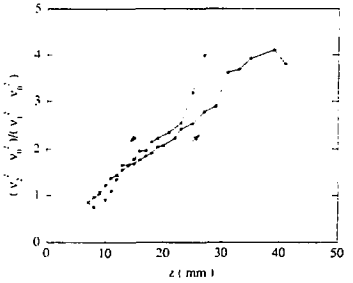

Figure 7. The quantity $(\nu_2^2 - \nu_0^2)/(\nu_1^2 - \nu_0^2)$ against distance z (omitting the negative starting points for decreasing z in the virgin curve).

It should be pointed out that the present measurements were performed in the field range around B_{c_1}. We believe that our method should also be applicable to the higher fields, but this is limited by the maximum fields obtained for the best permanent magnets on the market (1.0 T on the surface of an Nd–Fe–B sphere). Since the measurement of frequency responses is a very sensitive technique, it is believed that an improved pendulum could also be applied to investigate the dynamic behaviour of the isolated fluxoids in HTSC films. The characteristic frequency [18] of collective vibrations of flux-lines in HTSCs may be measured by the use of forced oscillations and this is currently being pursued in our laboratory.

4. Summary and conclusion

In summary, the main results reported here are: (i) construction of a mechanical pendulum to study the interaction between a small permanent magnet and a big high-T_c superconductor; (ii) introduction of the functional form of a *potential* and *force* to describe the interaction; and (iii) experiments showing that the flux lines penetrate into the HTSC even for external fields lower than the lower critical field B_{c_1}, which is consistent with the theoretical model of weak links for bulk HTSCs. Since the intergranular penetration is very pronounced, the present investigations are quite important for superconducting bearings and similar applications.

Acknowledgments

The research was supported in part by the Norwegian Research Council for Science and the Humanities (NAVF). The authors would also like to acknowledge assistance from P M Hatlestad, K Nilsen and J Yao in the experiments.

Appendix A

All response curves are closely described by a damped harmonic function, i.e. the deflection angle, α, is given by (equations (5) and (7)):

$$\alpha(t) = \alpha_0 \exp(-\Gamma t/2)\cos(2\pi\nu_{\text{meas}}t + \delta)$$

where α_0 is the initial angle, Γ is the damping factor, ν_{meas} is the measured frequency, and δ is the initial phase.

The extrema satisfy the following equation (where we have that $\dot{\alpha}(t_{\text{extr}}) = 0$):

$$\begin{aligned} -\alpha_0 e^{-\Gamma t_{\text{extr}}/2}[\tfrac{1}{2}\Gamma\cos(2\pi\nu_{\text{meas}}t_{\text{extr}} + \delta) \\ + 2\pi\nu_{\text{meas}}\sin(2\pi\nu_{\text{meas}}t_{\text{extr}} + \delta)] = 0 \end{aligned}$$

and then we have

$$2\pi\nu_{\text{meas}}t_{\text{extr},n} = -\tan^{-1}(\Gamma/4\pi\nu_{\text{meas}}) - \delta + n\pi. \quad (12)$$

Thus, the time difference between two extrema is $\Delta t_{\text{extr}} = 1/2\nu_{\text{meas}} = T/2$ and therefore precisely the half period.

Appendix B

The magnetic field around a permanent magnetic rectangular parallelepiped with dimension $2l \times 2h \times 2w$ (figure 8) homogeneously polarized along the x direction is calculated to be

$$\begin{aligned} B_x &= -\frac{\mu_0 m}{4\pi}[F_1(-x,y,z) + F_1(-x,y,-z) \\ &\quad + F_1(-x,-y,z) + F_1(-x,-y,-z) + F_1(x,y,z) \\ &\quad + F_1(x,y,-z) + F_1(x,-y,z) + F_1(x,-y,-z)] \\ B_y &= \frac{\mu_0 m}{4\pi}\ln\left(\frac{F_2(-x,-y,z)F_2(x,y,z)}{F_2(-x,y,z)F_2(x,-y,z)}\right) \\ B_z &= \frac{\mu_0 m}{4\pi}\ln\frac{F_3(-x,y,-z)F_3(x,y,z)}{F_3(-x,y,z)F_3(x,y,-z)} \end{aligned} \quad (13)$$

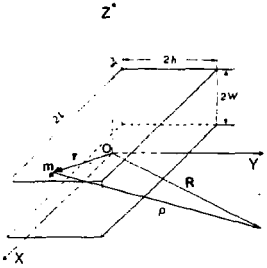

Figure 8. Schematic diagram for calculating the magnetic field around a homogeneously polarized magnetic rectangular parallelepiped with dimensions $2l \times 2h \times 2w$ and moment density m.

where $m = |\boldsymbol{m}|$ is the moment density, and functions F_1 and F_2 are defined by

$$F_1(x,y,z) = \tan^{-1}\frac{(h+y)(w+z)}{(l+x)\sqrt{(l+x)^2+(h+y)^2+(w+z)^2}} \tag{14}$$

$$F_2(x,y,z) = \frac{\sqrt{(l+x)^2+(h+y)^2+(w-z)^2}+w-z}{\sqrt{(l+x)^2+(h+y)^2+(w+z)^2}-w-z} \tag{15}$$

The magnetic field around a permanent magnetic sphere with an equivalent radius $r_{eq} = (3V/4\pi)^{1/3} = (6lhw/\pi)^{1/3}$ homogeneously polarized along the x direction is calculated to be

$$B_x = \frac{\mu_0 m}{4\pi}\frac{8lhw\cdot(3x^2-R^2)}{R^5} = \frac{\mu_0 m r_{eq}^3}{3}\frac{3x^2-R^2}{R^5}$$
$$B_y = \frac{\mu_0 m}{4\pi}\frac{24lhw\cdot xy}{R^5} = \frac{\mu_0 m r_{eq}^3}{3}\frac{3xy}{R^5} \tag{16}$$
$$B_z = \frac{\mu_0 m}{4\pi}\frac{24lhw\cdot xz}{R^5} = \frac{\mu_0 m r_{eq}^3}{3}\frac{3xz}{R^5}.$$

We may choose $l = h = w = 1$ (cube) to evaluate the difference between the cubic and spherical magnets, and numerical calculations show that when $R > 2$ this difference is $< 5\%$. The sphere model is thus a good approximation for evaluating the field distribution.

$$F_3(x,y,z) = \frac{\sqrt{(l+x)^2+(h-y)^2+(w+z)^2}+h-y}{\sqrt{l+x)^2+(h+y)^2+(w+z)^2}-h-y}. \tag{16}$$

References

[1] Brandt E H 1988 *Appl. Phys. Lett.* **53** 1554
[2] Hellman F, Gyorgy E M, Johnson D W Jr, O'Bryan H M and Sherwood R C 1988 *J. Appl. Phys.* **63** 447
Harter W G, Hermann A M and Sheng Z Z 1988 *Appl. Phys. Lett.* **53** 1119
[3] Moon F C, Yanoviak M M and Ware R 1988 *Appl. Phys. Lett.* **52** 1534
Marshall D B, DeWames R E, Morgan P E D and Ratto J J 1989 *Appl. Phys.* A **48** 87
Kitaguchi H, Takada J, Oda K, Osaka A and Miura Y 1989 *Physica* C **157** 267
Moon F C, Weng K-C and Chang P-Z 1989 *J. Appl. Phys.* **66** 5643
Chang P-Z, Moon F C, Hull J R and Mulcahy T M 1989 *Appl. Phys. Lett.* submitted
Weeks D E 1989 *Appl. Phys. Lett.* **55** 2784
Shapira Y, Huang C Y, Mcniff E J Jr, Peters P N, Schwartz B B and Wu M K 1989 *J. Magn. Magn. Mat.* **78** 19
[4] Brandt E H 1989 *Science* **243** 349
Moon F C and Chang P-Z 1990 *Appl. Phys. Lett.* **56** 397
[5] Williams R and Matey J R 1988 *Appl. Phys. Lett.* **52** 751
[6] Davis L C 1990 *J. Appl. Phys.* **67** 2631
Davis L C, Logothetis E M and Soltis R E 1988 *J. Appl. Phys.* **64** 4212
[7] Johansen T H, Bratsberg H, Yang Z J, Helgesen G and Skjeltorp A T 1990 *Rev. Sci. Instrum.* in press
Johansen T H, Yang Z J, Bratsberg H, Helgesen G and Skjeltorp A T 1990 to be published
[8] Yang Z J, Johansen T H, Bratsberg H, Helgesen G and Skjeltorp A T 1989 *Physica* C **160** 461; 1990 *Physica* C **165** 397
[9] Yang Z J, Bratsberg H, Johansen T H, Helgesen G and Skjeltorp A T 1990 to be published
[10] Houston W V and Smith D R 1967 *Phys. Rev. Lett.* **16** 516
[11] Kaper J P, Zweers H A, Dekking P and van Beelen H 1971 *Physica* **53** 60
[12] Wraight P C 1971 *Phil. Mag.* **23** 1261
[13] Longo A S and Kumar B 1989 *J. Supercond.* **2** 241
[14] Yan S H, Liang S C, Ma H, Fenp Q R, Sun Y X, Gao Y and H Zhang 1989 *Solid State Commun.* **70** 553
[15] Phillips J C 1989 *Physics of High-T_c Superconductors* (New York: Academic) p 272 and references therein
[16] Tinkham M and Lobb C J 1989 *Solid State Phys.* **42** 91
[17] Clem J R 1990 *Physics and Materials Science of High-Temperature Superconductors* ed R Kossowsky, S Methfessel and D Wohlleben (Dordrecht: Kluwer) p 79
[18] Dew-Hughes D 1988 *Cryogenics* **28** 674

Paper 6

Japanese Journal of Applied Physics **30** L92-L95 (1991).

Effect of Current on Collective Motion of Flux Lines in a Bulk $Y_1Ba_2Cu_3O_{7-\delta}$ Superconductor,

Z.J. Yang, H. Bratsberg, T.H. Johansen, G. Helgesen and A.T. Skjeltorp.

JAPANESE JOURNAL OF APPLIED PHYSICS
Vol. 30, No. 1B, JANUARY, 1991, pp. L 92-L 95

Effect of Current on Collective Motion of Flux Lines in a Bulk $Y_1Ba_2Cu_3O_{7-\delta}$ Superconductor

Z. J. YANG, H. BRATSBERG, T. H. JOHANSEN,
G. HELGESEN and A. T. SKJELTORP*

Department of Physics, University of Oslo, Oslo, Norway
**Institute for Energy Technology, N-2007 Kjeller, Norway*

(Received November 9, 1990; accepted for publication December 3, 1990)

When a permanent magnet, placed above a high temperature superconductor (HTSC), is moved by an external force, the flux lines in the HTSC will follow the magnet and perform a collective motion due to the interaction between the flux lines and the magnet. Here, the collective motion of flux lines in an $Y_1Ba_2Cu_3O_{7-\delta}$ (Y123) HTSC is studied by a mechanical pendulum method for various transport currents I through the sample. The magnet is set in low frequency (typically 1 Hz) oscillations with a mechanical pendulum, and the current I is flowing perpendicular to the direction of the magnet motion.

The experiments show that the shift of the stiffness (corresponding the shift of the frequency squared) exhibits a cross-over phenomenon: from independence to power law-like dependence for increasing currents. The results are compared with the theories of collective flux creep in HTSCs.

KEYWORDS: high-T_c superconductor, fluxoid pinning, flux collective motion, magnet-superconductor interaction, quasistatic magnetic field response, transport current effect, superconducting bearing

§1. Introduction

Flux line (fluxoid) dynamics in type-II superconductors reveals information about the motion of vortices as influenced by various pinning effects from physical defects like inhomogeneities, strains, and vacancies. These effects are important for the depinning critical current and possible applications of high T_c superconductors (HTSC). Traditional a.c. susceptibility and magnetization measurements have revealed giant thermal flux creep in these materials.[1-9]

Related with the dynamics of fluxoids in HTSCs, a currently interesting topic is to find the relationship between the transport currents and the pinning barrier. Several experimental[10,11] and theoretical[12-17] papers have been published in journals and proceedings. All of these reports have shown high frequency responses of fluxoids and focused on the behavior of the intragranules, i.e. the physical properties of single crystals and highly orientated thin films. This research is very important for the applications in microelectronics. The application of the bulk HTSC materials is equally important in other fields of science and technology, in particular, the levitation and magnetic bearings. It is generally accepted that Josephson weak links of the intergranules dominate the physical properties in the bulk HTSCs at a weak field.[18,19] The lower critical field of the intergranules ($H_{c_{1j}} \sim 1$ Oe) is much lower than the lower critical field of the intragranules ($H_{c_1} \sim 100$ Oe for the Y-Ba-Cu-O and 20 Oe for the Bi(Pb)-Sr-Ca-Cu-O). When a relative weak external field H in the range $H_{c_{1j}} < H < H_{c_1}$ is applied to a bulk HTSC sample, the penetration takes place via intergranules. The low frequency responses of the flux lines related with pinning properties in this field range have not been understood.

We have previously designed a novel mechanical pendulum technique to investigate the interaction between a permanent magnet and a large HTSC disc.[20,21] By extending the application of the pendulum, we have studied the effect of the transport currents on the quasistatic responses (typically 1 Hz) of the flux lines in a bulk $Y_1Ba_2Cu_3O_{7-\delta}$ (Y123) HTSC in the field range of $H_{c_{1j}} < H < H_{c_1}$. In this letter, we report experimental results and interpretation based on the collective flux creep theory recently introduced by Feigel'man *et al.*[12]

§2. Experimental

The experimental setup is shown schematically in Fig. 1. A cube-like Nd-Fe-B permanent magnet (M) ($6.5 \times 6.5 \times 7.5$ mm^3)* with rounded edges was attached to the end of a 55 cm tubular quartz rod hanging by the edge of a razor blade. The polarization direction was along the longest side of the magnet. The magnet could be set in oscillations above the sample, a bulk Y123 HTSC disc ($T_c \sim 90$ K and $\rho > 90\%$ of the theoretical density)** with diameter 69.3 mm and thickness 6.8 mm. The sample was immersed in liquid nitrogen (77 K) and the distance between the sample and the magnet could be adjusted. An optical system was employed to monitor the time dependence of the horizontal displacement of the oscillations as follows: the pendulum intersected a fraction of a rectangular light-beam from a laser. The signal from a photodiode detecting the focused light-beam was thus proportional to the position of the magnet. A controlled and reproducible initiation of the oscillation was obtained using a small permanent magnet (M' in Fig. 1) attached to the middle of the quartz rod.

*The unmagnetized Nd-Fe-B bar was manufactured by *Sumitomo Special Metals Co. Ltd.* (Japan). The magnet was magnetized with a 1.3 T field.

**The $Y_1Ba_2Cu_3O_{7-\delta}$ superconducting ceramics disc was manufactured by *Kali-Chemie Aktiengesellschaft* (W. Germany).

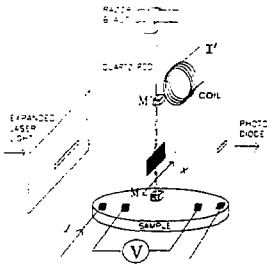

Fig. 1. Schematic diagram of the experimental setup. The permanent magnet M attached to the end of a quartz rod, swings above the HTSC sample. An expanded Laser beam is sent through an aperture to form a homogeneous light beam with rectangular cross-section. Part of this light beam is intersected by the pendulum and focused by a lense onto a photodiode. The diode signal, linearly proportional to the horizontal displacement of the pendulum, is amplified and sent to a PC/AT. The oscillations are started by switching off the supply current I' to the coil attracting the small permanent magnet M' as discussed in the text.

The rod could thus be pulled out to a fixed position ($-0.4°$ from vertical) by supplying current to an adjacent coil. By turning off the current, the oscillation started. The whole setup was automated using a PC/AT data-logging system.

A standard four-lead setup with indium contacts was used to supply current (I) to the sample and monitor the superconducting state of the sample. In all the experiments, the sample current direction was parallel with the light beam, and perpendicular to the direction of the motion of the magnet. Thus, the current could be in one direction (positive) or reversed (negative).

In the experiments the direction of the magnetic moment could be made parallel (P configuration) or normal (N configuration) to the direction of oscillations of the pendulum. The maximum field on the surface of the magnet was measured to be 4×10^3 Oe with a Hall-probe.

The interaction between a free-swinging permanent magnet and a superconducting disk leads to frequency change and strong damping.[20,21] As shown below, this may be related to the flux bundle activation barrier U.[12,22] Specifically, we find that the predicted power-law dependence: $U(I) \propto I^{-\alpha}$ describes the data well for a wide range of currents.

The performance of the pendulum was also checked with the sample in the normal state. It was found that the free-damping (Γ_0) was very small ($\Gamma_0 \sim 0.011\ s^{-1}$) and negligible compared to the damping caused by the superconducting sample. Moreover, no change in the oscillation frequency ν_0 of the free pendulum ($\nu_0 = 0.798$ Hz) was observed. Thus, by relatively rapid sampling (188 s^{-1}) of the amplitude signal, we could extract information directly about the magnet-superconductor interactions from the shifts in frequency and damping. As discussed elsewhere,[20] we have developed quite generally the force and potential for changes in the separation between a magnet and a type-II superconductor. This has enabled us to undertake the present study.

§3. Results and Discussion

The measurements of the oscillation frequency ν and damping factor Γ of the pendulum with sample currents from 0 A to 5 A in steps of 0.5 A were performed with various distances between the magnet and the superconductor. Some typical pendulum oscillations are shown for increasing sample currents $I = 0$ A–5 A in Figs. 2(a)–2(b) for the N and P configurations, respectively. The distance from the center of the magnet to the surface of the superconductor was 14 mm. In this case the magnetic field at the center of the sample was estimated to be 54 Oe using a sphere approximation.[20,21] As may be seen, there are significant changes in both frequency and damping with currents.

By fitting parabolas to the peak regions of the response curves, the frequencies ν and damping factors Γ were obtained precisely.[20,21]

Figure 3 shows typical experimental results for the quantity $\nu^2 - \nu_0^2$ against the sample current I in a log–log

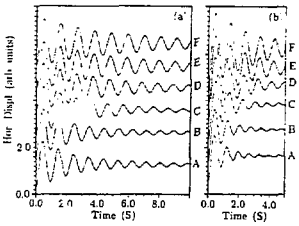

Fig. 2. Horizontal displacements of the magnet versus time for various sample currents: (a) for the N configuration, and (b) for P configuration. Here the separation $d = 14$ mm measured from the center of the magnet to the surface of the sample. A: $I = 0$ A, B: $I = 1.0$ A, C: $I = 2.0$ A, D: $I = 3.0$ A, E: $I = 4.0$ A and F: $I = 5.0$ A. The dashed lines show the frequency shift with an increase in current.

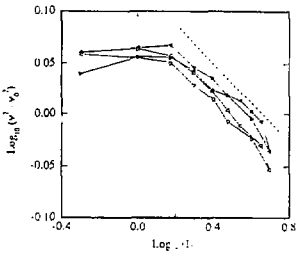

Fig. 3. Typical log–log plot of the quantity $\nu^2 - \nu_0^2$ versus sample current I in the P configuration cycled between 0 A and 5 A (up-down marked by arrows) at $d = 18$ mm (the maximum field was estimated to be $H_{max} = 25.4$ Oe on the sample). ▲ is for positive and ▽ for reversed currents. The dashed line (shifted upwards for clarity) with slope $\alpha = 0.19$ represents the average high current behaviour for all the measurements.

plot (the reason for this model of presentation will become clear below).

A characteristic feature of the frequency change with sample current I, was a cross-over effect: for low I, ν was almost independent of I, followed by a decrease in ν for increasing I. This effect reflects the reduced interaction strength due to sample currents as discussed below.

The experiments also show that, for increasing field (reduced distance), there is a shift in cross-over region to the left corresponding to smaller sample currents.

Using the same pendulum we have measured the horizontal restoring force on a long permanent magnet bar due to the interaction at liquid nitrogen temperatures[23,24] The lateral force is, to a very good approximation (<5%), linear when the horizontal displacement is less than 1 mm which is satisfied by the present experiments. The direct force measurements permit us to use a linear approximation to analyse the experimental data.

In a linear approximation (the maximum deflection angle is $\theta_{max} < 0.4°$ for our experiments) the motion of the compound pendulum can be described by the following equation:

$$\ddot{\theta} + \Gamma\dot{\theta} + 4\pi^2\nu^2\theta = 0, \tag{1}$$

where θ is the deflection angle, Γ is the damping factor, and ν is the oscillation frequency. Both Γ and ν contain contributions from the graviation and the magnet-HTSC interaction. The solution to this equation is

$$\theta(t) = \theta_0 \exp(-\Gamma t/2) \cos(2\pi\nu_{meas} t + \delta), \tag{2}$$

where $\nu_{meas} = \sqrt{\nu^2 - (\Gamma/4\pi)^2}$ (ν_{meas} is equal to the measured frequency), θ_0 is the initial deflection angle, and δ is the initial phase factor. The response curves of the experiments are consistent with this linear approximation.

As discussed previously,[20,21] the quantities $4\pi^2(\nu^2 - \nu_0^2)$ and $\Gamma - \Gamma_0$ express the contributions of the interaction to the elastic part and dissipation part, respectively. Classically, the energy of this pendulum is $E \sim 4\pi^2\nu^2 \exp(-\Gamma t)$, and the relevant energy loss per period is $\exp(-\Gamma/\nu)$. So that, the quantity $\nu^2 - \nu_0^2$ is a measure of the energy change from the pure inertia pendulum. Some normal metals and alloys (copper, aluminium, brass, etc.) were chosen as substitutes for the HTSC for clarifying the physical origins of the interaction. The damping was observed for these also, but no frequency shift was observed. This could be understood as that the eddy-current is responsible for the damping, and the frequency shift is due to the pinning of flux lines. Since $\Gamma/\nu < 0.1 \ll 1$ for our measurements, the magnet-HTSC interaction mainly contributes to the elastic part. It is then reasonable to assume that the parameter $\nu^2 - \nu_0^2$ is a measure of the interaction in this system.

When the magnet is moved by the graviational force, the fluxoids will follow the magnet and perform a collective motion (hopping). The collective motion needs to overcome the pinnings at randomly distributed defects such as the interfaces of the intergranulars. The pinned fluxoids attract the magnet, and as a consequence, the frequency ν increases due to the collective pinning of weak disorder. The frequency shift is thus a measure of the collective pinnings. From a classical point of view, $4\pi^2(\nu^2 - \nu_0^2)$ expresses the energy gain of the pendulum due to the collective pinnings in the HTSC sample. Therefore, we argue that the quantity $\delta\nu^2 = \nu^2 - \nu_0^2$ is proportional to the bundle activation energy U.

The collective pinning barrier U is of the order of the elastic energy of hopping flux bundles.[12,22] When a current is passed through the sample, the Lorentz force $\boldsymbol{F} = \boldsymbol{I} \times \boldsymbol{B}$ enhances the collective flux motion, which is equivalent to reducing the collective pinning barrier U. As a result of the reduced magnet-HTSC interaction, the stiffness of the pendulum is also reduced lower.

Feigel'man *et al.*[12] have studied the flux-creep phenomena in the case of collective pinning by weak randomly distributed defects. Based on the Anderson concept of flux bundle,[22] they have shown that the bundle activation barrier U has a power-law dependence on current I: $U(I) \propto I^{-\alpha}$: For different regimes of currents, α changes from 1/7 to 7/9. Since the physical basis of this theory is the pinning of weak disordered defects, the results should also be applicable for analysing the present experimental data although they obtained the theory based on the consideration of single crystals. The physical reason for the present results is also the randomly distributed pinning centers.

The transport current in the superconductor creates a magnetic field parallel with the direction of the pendulum motion. For the P configuration, the direction of the current has no effect on the barrier exponent α. For the N configuration α is affected by the direction of the current when the field is relative weak. The relative effect on the different current directions decreases with increasing field.

The field dependence of the barrier exponent α is also investiged and this is shown in Fig. 4, which is in qualitative agreement with Feigel'man *et al.*'s theory.

When the magnet approaches the superconductor, we observe that the frequency ν decreases slightly and then increases monotonically for the transport-current-free oscillation. This may be interpreted as follows: when $\nu = \nu_0$ (ν_0 is the free pendulum frequency), the flux lines start to penetrate into the sample and $H = H_{c_1}$ (the detail

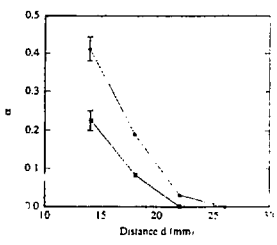

Fig. 4. The variation of the slope α with magnet-superconductor separation d for the P configuration (●), and the N configuration (○). The maximum fields on the HTSC sample were estimated to be 8.4 Oe (d = 26 mm), 13.9 Oe (d = 22 mm), 25.4 Oe (d = 18 mm), and 54 Oe (d = 14 mm) using a sphere approximation.

was discussed in ref. 20, 21) We found that the effect of sample currents on the frequency and damping is very different for weak fields ($H \sim H_{c_1}$ corresponding to $\nu \sim \nu_0$ without sample current and only a few penetrating flux lines present) and strong fields ($H \gg H_{c_1}$ corresponding to $\nu \gg \nu_0$ without sample current and with a certain amount of flux lines). It appears that when $H \leq H_{c_1}$, the frequency and damping factors are almost independent of sample currents. It seems to us that a very small increase in frequency with an increase in sample current can be observed, but this is on the level of our experimental resolution. However, when the field is much higher than H_{c_1}, the effect of sample currents is significant.

Kes and co-workers[17] have shown that the activation barrier U is independent of the field for thermally assisted flux flow (TAFF) at small driving forces. Kes *et al.*'s theory is a good description for isolated fluxoids. For the TAFF, the hopping of fluxoids is governed by the convensional linear diffusion equation. In this case, the fluxoids relax individually, and the correlation of the fluxoids does not play an important role. The present experiments at low fields are consistent with Kes *et al.*'s theory. In the case of low fields, the fluxoid-fluxoid interaction is very weak since only a few fluxoids are present in the sample. The motion of fluxoids is similar to the TAFF in this case. However, when the fields are high enough, the correlation of fluxoids is more pronounced. As a consequence, the motion of fluxoids becomes collective, i.e. the flux-"creep" in the case of collective pinnings by weak disorders, which is beyond the description of Kes *et al.*'s TAFF theory. As a result of an increase in fluxoid-fluxoid correlation, the barrier exponent α increases monotonically with increasing fields.

The experiments also show that for the P and N configurations α has different field-dependence, which is consistent with the current-free experiments.[20,21] Phenomenologically, the parallel motion has an extra contribution of the magnetic moment M compared with the normal motion. Therefore, the former needs more energy to overcome the barrier.

It should be pointed out that the present investigation is mainly about the physical properties for bulk HTSCs at low fields. It is believed that the present method can also be applied to studying the HTSC films and single crystals at high fields, which is ongoing at our laboratory.

§4. Summary and Conclusion

The main results reported here are the investigation about the effect of transport currents on the collective motion of flux lines in a bulk Y123 HTSC by using a mechanical pendulum. The experiments show a crossover behavior for the current assisted flux line creep in a bulk sample in the field range of $H_{c_1} < H < H_{c_2}$. The stiffness of the pendulum is unchanged when using a small feeding current, and shows a power law-like decrease with increasing feeding current I. The field dependent exponents for high current region were obtained by the present experiments. The experimental results are interpreted in terms of the current theories of collective flux creep.

Acknowledgement

The research was supported in part by the Norwegian Research Council for Science and the Humanities (NAVF). The authors acknowledge the assistance for the experiments from P. M. Hatlestad, K. Nilsen and J. Yao.

References

1) K. A. Muller, M. Takashige and J. G. Bednorz: Phys. Rev. Lett. **58** (1987) 1143.
2) Y. Yeshurum and A. P. Malozemoff: Phys. Rev. Lett. **60** (1988) 2202.
3) A. F. Malozemoff, L. Krusin-Elbaum, D. C. Cronemyer, Y. Yeshurum and F. Holtzberg: Phys. Rev. **B38** (1988) 6940.
4) T. T. M. Palstra, B. Batlogg, L. F. Schneemeyer and J. V. Waszczak: Phys. Rev. Lett. **60** (1988) 1662.
5) M. Tinkham: Phys. Rev. Lett. **60** (1988) 1658.
6) T. T. M. Palstra, B. Batlogg, R. B. van Dover, L. F. Schneemeyer and J. V. Waszczak: Phys. Rev. **B41** (1989) 6621.
7) J. D. Hettinger, A. G. Swanson, W. J. Skocpol, J. S. Brooks, J. M. Graybeal, P. M. Mankiewich, R. E. Howard, B. L. Straughn and E. G. Burkhardt: Phys. Rev. Lett. **62** (1989) 2044.
8) Z. J. Sun, K. Char, M. R. Hahn, T. H. Geballe and A. Kapitulnik: Appl. Phys. Lett. **54** (1989) 663.
9) A. Gupta P. Esquinazi, H. F. Braun and H.-W. Neumuller: Phys. Rev. Lett. **63** (1989) 1869.
10) E. Zeldov, N. M. Amer, G. Koren, A. Gupta, M. W. McElfresh and R. J. Gambino: Appl. Phys. Lett. **56** (1990) 680.
11) R. C. Budhani, D. O. Welch, M. Suenaga and R. L. Sabatini: Phys. Rev. Lett. **64** (1990) 1666.
12) M. V. Feigel'man, V. B. Geshkenbein, A. I. Larkin and V. M. Vinokur: Phys. Rev. Lett. **63** (1989) 2303.
13) M. V. Feigel'man, V. B. Geshkenbein and A. I. Larkin: Physica **C167** (1990) 177.
14) V. M. Vinokur, P. H. Kes and A. E. Koshelev: Physica **C168** (1990) 29.
15) R. Griessen: Phys. Rev. Lett. **64** (1990) 1674.
16) B. I. Ivlev and N. B. Kopnin: Phys. Rev. Lett. **64** (1990) 1828.
17) P. H. Kes, J. Aarts, J. van den Berg, C. J. van der Beek and J. A. Mydosh: Supercond. Sci. and Technol. **1** (1989) 242.
18) M. Tinkham and C. J. Lobb: Solid State Phys. **42** (1989) 91, and references therein.
19) J. R. Clem: in *Physics and Materials Science of High-Temperature Superconductors*, ed. R. Kossowsky, S. Methfessel and D. Wohlleben (Kluwer Academic Publishers, Dordrecht, 1990) p. 79, and references therein.
20) Z. J. Yang, T. H. Johansen, H. Bratsberg, G. Helgesen and A. T. Skjeltorp: Physica **C165** (1990) 397.
21) Z. J. Yang, T. H. Johansen, H. Bratsberg, G. Helgesen and A. T. Skjeltorp: to be published in Supercond. Sci. Technol. (1990).
22) P. W. Anderson: Phys. Rev. Lett. **9** (1962) 309.
23) T. H. Johansen, H. Bratsberg, Z. J. Yang, G. Helgesen and A. T. Skjeltorp: to be published in Rev. Sci. Instrum. (1990).
24) T. H. Johansen, Z. J. Yang, H. Bratsberg, G. Helgesen and A. T. Skjeltorp: to be published in Appl. Phys. Lett. (1990).

Paper 7

Physica **C 162-164** 1587-1588 (1989)

The Effect of Pb-doping in Bi-Sr-Ca-Cu-O and Sb-doping in Bi-Pb-Sr-Ca-Cu-O Superconductors,

Z.J. Yang, H. Bratsberg, T.H. Johansen, N. Norman, J. Taftø, G. Helgesen, I. Lorentzen and A.T. Skjeltorp.

Physica C 162-164 (1989) 1587-1588
North-Holland

The effect of Pb-doping in Bi-Sr-Ca-Cu-O and Sb-doping in Bi-Pb-Sr-Ca-Cu-O superconductors

Z.J.Yang[1], H.Bratsberg[1], T.H.Johansen[1], N.Norman[1], J.Tafts[1], G.Helgesen[1], I.Lorentzen[2] & A.T.Skjeltorp[3]

[1]: Department of Physics, University of Oslo, Oslo, Norway
[2]: Department of Chemistry, University of Oslo, Oslo, Norway
[3]: Institute for Energy Technology, N-2007 Kjeller, Norway

A series of samples with nominal starting compositions $Bi_{1.4}Pb_{0.6}Sr_2Ca_3Cu_4O_x$ and $Bi_2Pb_{2x}Sr_2Ca_3Cu_4O_x$ $(0.1 \leq x \leq 0.4)$ were prepared using dry and wet methods. X-ray emission studies of SEM and TEM show that most of the Pb-doping is lost during sintering, but Pb apparently acts as a catalyst to form the high-T_c phase. Another series of samples with starting compositions $Bi_{2(1-x)}Pb_{2x(1-y)}Sb_{2xy}Sr_2Ca_3Cu_4O_x$ $(0.2 \leq x \leq 0.3$ and $0.2 \leq y \leq 0.7)$ and $Bi_{2(1-x)}Pb_{2x}Sb_{2y}Sr_2Ca_3Cu_4O_x$ $(0.2 \leq x \leq 0.3$ and $0.03 \leq y \leq 0.08)$ were prepared by the wet method. Susceptibility measurements indicate a range of Sb-doping levels producing a well developed high-T_c phase. The superconducting transition of Sb-doped Bi-Pb-Sr-Ca-Cu-O specimens is very sensitive to the strength of a.c. measurement fields and external d.c. fields.

1. INTRODUCTION

It has been revealed that *Pb*-doping of *Bi-Sr-Ca-Cu-O* superconductors enhances the high-T_c phase formation[1]. Despite numerous work[2-4] there are conflicting results whether *Pb* occupies the Ca or Bi sites[2] or whether the final *Pb*-content and post-sintering procedure play important roles in the superconductivity[3,4]. The present paper reports a brief summary of the effects of *Pb*-doping and various heat treatment conditions. In another series of experiments the effects of *Sb*-doping of the *Bi-Pb-Sr-Ca-Cu-O* system were studied. The objective was to find out to what extent *Sb*-doping enhances or decreases T_c as speculated in earlier reports[5,6].

2. EXPERIMENTAL

Two groups of *Pb*-doped samples were prepared using the dry and wet methods: $Bi_{1.4}Pb_{0.6}Sr_2Ca_3Cu_4O_x$ (sample type A1) and $Bi_2Pb_{2x}Sr_2Ca_3Cu_4O_x$ with $0.1 \leq x \leq 0.4$ (sample types A21-A24). In the dry method the mixed powders of nominal composition were heated at 845°C for 120 hours. The heated powder was ground and compressed at about 15 kbars into pellets which were sintered at 850°C for about 130 hours and quenched in air. In the wet method the mixed powders were dissolved in nitric acid and the solution was heated at about 600°C for about 40 hours. The dry powder was ground and compressed at about 15 kbars into pellets which were sintered for about 110 hours and quenched in air. For the *Sb*-doped samples, also two groups were prepared (wet method): $Bi_{2(1-x)}Pb_{2x(1-y)}Sb_{2xy}Sr_2Ca_3Cu_4O_x$ with $0.2 \leq x \leq 0.3$ and $0.2 \leq y \leq 0.7$ (sample types B11-B16) and $Bi_{2(1-x)}Pb_{2x}Sb_{2y}Sr_2Ca_3Cu_4O_x$ with $0.2 \leq x \leq 0.3$ and $0.03 \leq y \leq 0.08$ (sample types B21-B27). The samples were investigated using X-ray diffraction, SEM, TEM and a.c. susceptibility measurements (χ' and χ'', $f = 75$ Hz).

TABLE 1

Superconducting transition temperatures of *Pb*-doped specimens. The data shown in columns 3 and 4 are peak temperatures $T_c(K)$ / half-height width (K) of χ''.

Samples	Pb_α	Bi_γ	
	α	$\gamma = 1.40$	$\gamma = 2.00$
A1	.60	105.5/5.0	
A21	.20		77.0/-
A22	.40		72.0/7.0
A23	.60		99.0/4.6
A24	.80		63.0/-

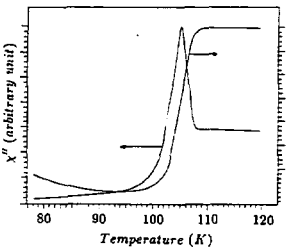

FIGURE 1

a.c. susceptibility vs. temperature for specimen A1.

0921-4534/89/$03.50 © Elsevier Science Publishers B.V
(North-Holland)

3. RESULTS

For the type A samples X-ray emission shows that *Pb* disappears during sintering. The variation of T_c (defined as the inflection point in χ' vs. T data) for the different nominal starting compositions are collected in Table 1. Figure 1 shows the results of a.c. susceptibility measurements for the best sample with $T_c = 105.5K$. Table 2 summarizes the results for the type B samples. The highest T_c seen for group B1 is $108.4K$ for the B14 sample with $x = 0.3$ and $y = 0.2$, and $T_c = 105.5K$ for the B22 sample with $x = 0.2$ and $y = 0.05$ for group B2. The corresponding a.c. susceptibility measurements are shown in Figure 2.

The superconducting transition of *Sb*-doped *Bi-Pb-Sr-Ca-Cu-O* specimens is sensitive to the strength of a.c. measurement fields and external d.c. fields. A very weak d.c. magnetic field results in a large shift in the transition to lower temperatures.

4. CONCLUSIONS

The present results show that *Pb*-doping of *Bi-Sr-Ca-Cu* oxides is important for achieving T_c above $100K$, but *Pb* appears to be lost in the final composition. It is suggested that *Pb* acts as a catalyst in stabilization of the high-T_c phase. *Sb*-doping of the *Bi-Pb-Sr-Ca-Cu* oxides is shown to enhance and sharpen the superconducting transition. A *Sb* substitution of about 5% favours forming the 2223 phase which is contrary to some other report[6].

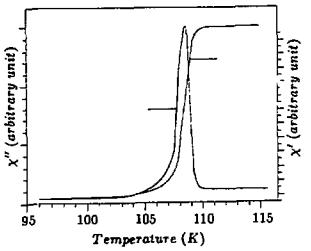

FIGURE 2

a.c. susceptibility vs. temperature for specimen B14.

TABLE 2

Superconducting transition temperatures of *Sb*-doped specimens. The data shown in columns 4 and 5 are peak temperatures $T_c(K)$ / half-height width (K) of χ''.

Samples	Pb_α	Sb_β	Bi_γ	
	α	β	$\gamma = 1.40$	$\gamma = 1.60$
B11	.32	.08		103.7/4.4
B12	.24	.16		102.6/4.7
B13	.12	.28		65.0/-
B14	.48	.12	108.4/1.0	
B15	.36	.24	76.0/13.3	
B16	.18	.42	< 65.0	
B21	.40	.08	104.5/1.6	
B22	.40	.10	105.5/1.0	→
B23	.40	.12	104.4/1.5	
B24	.40	.16	103.4/1.5	
B25	.60	.06		105.8/1.5
B26	.60	.08		← 105.4/1.4
B27	.60	.10		105.3/1.0

ACKNOWLEDGEMENT

This work was supported in part by the Norwegian Council for Science and Humanities (NAVF).

REFERENCES

1. S. A. Sunshine, T. Siegrist, L. F. Schneemeyer, D. W. Murphy, R. J. Cava, B. Batlogg, R. B. van Dover, R. M. Fleming, S. H. Glarum, S. Nakahara, R. Farrow, J. J. Krajewski, S. M. Zahurak, J. V. Waszczak, J. H. Marshall, P. Marsh, L. W. Rupp, Jr., and W. F. Peck, Phys. Rev. **B38** 893-896(1988)

2. E. Chavira, R. Escudero, D. Ríos-Jara and L. M. León, Phys. Rev. **B38** 9272-9275(1988)

3. B. Zhu, L. Lei, S. L. Yuan, S. B. Tang, W. Wang, G. G. Zheng, W. Y. Guan and J. Q. Zheng, Physica **C157** 370(1989)

4. P. V. P. S. S. Sastry, I. K. Gopalakrishnan, J. V. Yakhmi and R. M. Iyer, Physica **C157** 491(1989)

5. H. B. Liu, L. Z. Cao, L. Zhou, Z. Q. Mao, X. X. Li, Z. D. Yu, B. Xue, X. L. Mao, G. E. Zhou, Y. Z. Ruan, Z. J. Chen and Y. H. Zhang, Solid State Commun. **69** 867(1989)

6. S. X. Dou, H. K. Liu, N. X. Tan, Y. J. Sheng and W. K. Jones, Physica **C158** 97(1989)

Paper 8

Journal of Magnetism and Magnetic Materials **89** 309-314 (1990)

Preparation and Magnetic Properties of the Sb-doped Bi-Pb-Sr-Ca-Cu-O Superconductors,

Z.J. Yang, H. Bratsberg, T.H. Johansen, N. Norman, J. Taftø, G. Helgesen and A.T. Skjeltorp.

Journal of Magnetism and Magnetic Materials 89 (1990) 309–314
North-Holland

PREPARATION AND MAGNETIC PROPERTIES OF THE Sb-DOPED Bi–Pb–Sr–Ca–Cu–O SUPERCONDUCTORS

Z.J. YANG, H. BRATSBERG, N. NORMAN, T.H. JOHANSEN, J. TAFTØ, G. HELGESEN
Department of Physics, University of Oslo, Oslo, Norway

and

A.T. SKJELTORP
Institute for Energy Technology, N-2007 Kjeller, Norway

Received 28 December 1989; in final form 14 May 1990

Two groups of samples were prepared by the wet method with nominal composition $Bi_{x_1}Pb_{x_2}Sb_{x_3}Sr_2Ca_3Cu_4O_z$. In the first group $x_1 + x_2 + x_3 = 2$. Here x_1 ranges from 1.2 to 1.6 with x_2 varying from 0.72 to 0.12. The second group is characterized by $x_1 + x_2 = 2$. Here x_1 was chosen to be 1.4 and 1.6 while x_3 ranges from 0.08 to 0.16. The results show: (i) high Sb content reduces the transition temperature; (ii) for small Sb contents the transition temperature is relatively constant but the transition becomes sharper, (iii) the best sample (with $x_1 = 1.4$, $x_2 = 0.48$ and $x_3 = 0.12$) exhibits a very sharp transition with a peak in the imaginary component of the ac susceptibility at 108.4 K; and (iv) the transition of lightly Sb-doped material is strongly influenced by small external magnetic fields.

1. Introduction

The discovery of superconductivity in the Bi–Sr–Ca–Cu–O system by Maeda et al. [1] has touched off a flurry of research [2–16]. Tarascon and co-workers [2] have identified three superconductors in the Bi–Sr–Ca–Cu–O family referred to by their cation ratios as 2201, 2212 and 2223. Formation of the highest T_c (110 K) phase, 2223, has been hampered by the relatively high stability of the 2212 (85 K) phase [2–16]. Sunshine and co-workers [3] have discovered that the addition of Pb enhances the content of the 2223 phase, but the mechanism for this is not yet understood. Although different groups have reported some conflicting results, the conclusion that lead-doping of starting compositions favours the forming of the 2223 phase is confirmed by all reports.

Furthermore, more and more groups [17–21] have reported the effect of Sb-substitution in Bi-based superconductors. Their results are not consistent [17–21].

In this letter we report investigations about the Sb-doped Bi–Pb–Sr–Ca–Cu–O superconductors. The wet method was employed for sample preparations and X-ray emission (SEM studies) was used to analyze the Pb content. AC susceptibility measurements were used to show the effects of Sb-doping on the superconducting transition and the influences of external ac and dc magnetic fields.

2. Experimental

In order to mix the powders completely, the wet method was used for sample preparation. Powders of Bi_2O_3, PbO_2, Sb_2O_3, $SrCO_3$, $CaCO_3$ and CuO were completely dissolved in nitric acid. The solution was heated to 800 °C and baked for 7 h. The dry powder was ground and compressed at about 10 kbar. After sintering at 850 °C in air for about 150 h, the specimens were quenched in liquid nitrogen.

0304-8853/90/$03.50

Table 1
Superconducting transition temperatures of specimens with different starting compositions: $Bi_{x_1}Pb_{x_2}Sb_{x_3}Sr_2Ca_3Cu_4O_z$. The data shown are $T_{0.5}$ (temperatures when $\chi' = -0.5$)/$T_{0.1}$ (temperatures when $\chi' = -0.1$)

Samples	Pb_{x_2}	Sb_{x_3}	Bi_{x_1}			
	x_2	x_3	$x_1 = 1.20$	$x_1 = 1.40$	$x_1 = 1.60$	$x_1 = 2.00$
SB22	0.32	0.08			105.8/108.4	
SB24	0.24	0.16			103.7/106.6	
SB27	0.12	0.28			< 65.0	
SB32	0.48	0.12		108.0/109.5		
SB34	0.36	0.24		91.0/95.0		
SB37	0.18	0.42		75.8/84.9		
SB31	0.54	0.06		106.7/108.3		
SB41	0.72	0.08	107.2/108.5			
PSB204	0.40	0.08			105.0/107.3	
PSB205	0.40	0.10			105.7/107.4	
PSB206	0.40	0.12			104.4/106.5	
PSB208	0.40	0.16			103.7/105.6	
PSB303	0.60	0.06		105.8/107.8		
PSB304	0.60	0.08		105.4/107.6		
PSB305	0.60	0.10		105.3/106.7		
PB1	0.60	0		102.7/109.5		
PB2	0.60	0				101.6/109.7

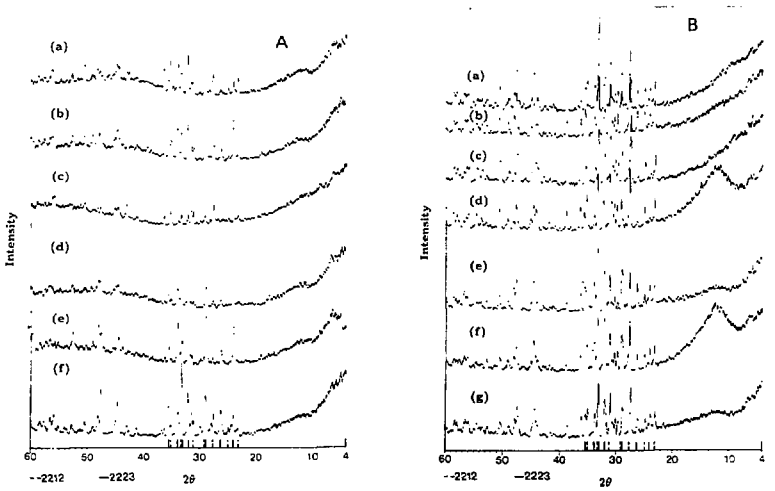

Fig. 1. (A) X-ray diffraction patterns of the specimens: (a) SB22, (b) SB24, (c) SB27, (d) SB32, (e) SB34 and (f) SB37. Positions of diffraction peaks corresponding to the 2212 and 2223 phases are indicated with dashed and solid markers, respectively; (B) X-ray diffraction patterns of the specimens: (a) PSB204, (b) PSB205, (c) PSB206, (d) PSB208, (e) PSB303, (f) PSB304 and (g) PSB305.

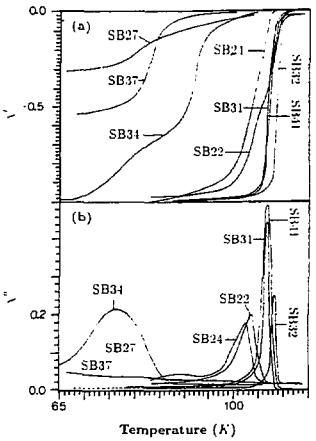

Fig 2. AC susceptibility vs. temperature for the specimens in the first group (table 1): (a) real parts and (b) imaginary parts.

Two groups of samples were prepared to give a nominal composition $Bi_{x_1}Pb_{x_2}Sb_{x_3}Sr_2Ca_3Cu_4O_z$ as starting material. In the first group some of the Bi was substituted by Pb and Sb so that $x_1 + x_2 + x_3 = 2$. The samples in the first group are denoted SB**. In the second group some of the Bi was substituted by Pb and an additional amount of Sb introduced. Thus in this group $x_1 + x_2 = 2$, and these samples are denoted PSB***. Using the same wet method, we also prepared the Sb-free $Bi_{x_1}Pb_{x_2}Sr_2Ca_3Cu_4O_z$ samples denoted PB*.

The diffraction patterns were obtained from an X-ray diffractometer using crystal monochromatized Cu K_α radiation. A JEOL-35 scanning electron microscope (SEM) was employed for element analysis. The ac susceptibility measurements were performed inside a high permeability magnetic shield to reduce the earths magnetic field. In the experiments the ac field was about 30 mG, and the voltage from two opposing secondary coils was measured with a PAR 2-phase lock-in amplifier (model 5204).

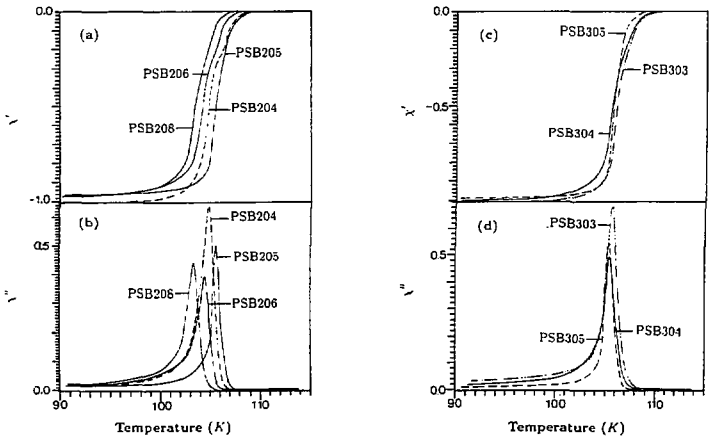

Fig 3. AC susceptibility vs. temperature for the specimens in the second group (table 1): (a) and (c) real parts, (b) and (d) imaginary parts.

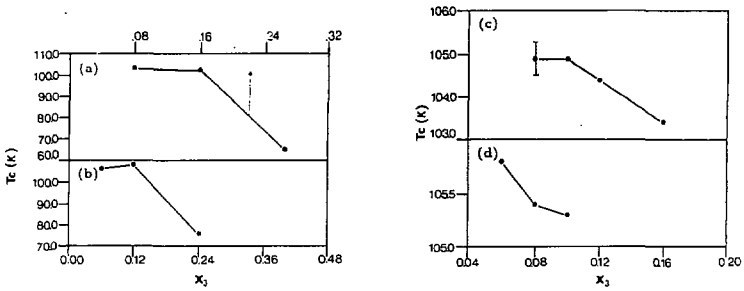

Fig. 4. Superconducting transition temperatures, T_c (defined as the temperature when χ'' reaches its maximum), vs. antimony contents, x_3, for the specimens with certain nominal lead(antimony) contents (starting compositions as discussed in the text): (a) 20%-Pb(Sb) ($x_2 + x_3 = 0.4$), (b) 30%-Pb(Sb) ($x_2 + x_3 = 0.6$) substituting bismuth in the first group; and (c) 20%-Pb ($x_2 = 0.4$), (d) 30%-Pb ($x_2 = 0.6$) substituting bismuth in the second group.

3. Results and discussion

Fig. 1 shows the X-ray diffraction patterns of the specimens. For many specimens the crystalline reflections are rather weak. However, the diffractograms seem to indicate that all the specimens contain both the 2212 and the 2223 phases. At the same time the high background indicates the existence of a large fraction of amorphous material.

Table 1 summarizes the superconducting transition temperatures for all Sb-doped and undoped specimens prepared by the same wet method, figs. 2 and 3 show the ac magnetic susceptibilities of selected specimens given in table 1, and fig. 4 displays the variation of T_c with Sb content for different nominal Pb contents.

It may be seen that the transition is sharp, and T_c is rather insensitive to Sb-doping for Sb: Bi(Pb) ratio up to about 5%. Above this doping, there is a drastic reduction in T_c and broadening of the transition. Our results thus show that there is some (but not remarkable) improvement in superconducting transition for low Sb-doping level. Compared with the conflicting results in literature [17–21], the present results are consistent with Luo et al.'s results [21] for low Sb-doping level.

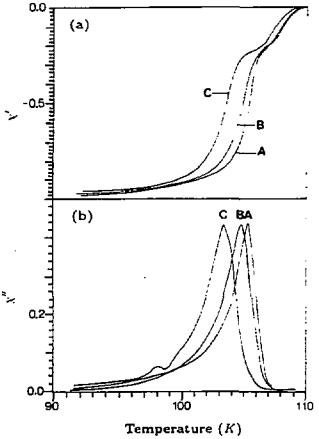

Fig. 5. AC susceptibility vs. temperature for specimen PSB204 for various ac fields (H_{ac}) and dc fields (H_{dc}) as discussed in the text: (a) real parts and (b) imaginary parts. A: H_{ac} = 0.032 Oe. H_{dc} = 0.00 Oe; B: H_{ac} = 0.053 Oe, H_{dc} = 0.00 Oe; and C: H_{ac} = 0.032 Oe, H_{dc} = 0.53 Oe.

and Dou et al.'s results [19] for relatively high Sb-doping level.

The specimen SB32 exhibits the highest T_c (108.4 K) and sharpest transition (half-height width of χ'', $\Delta T = 1.0$ K, see fig. 2). It is interesting to note that this sample has a very high fraction of amorphous material as indicated in fig. 1A, curve d.

The Sb-doped Bi–Pb–Sr–Ca–Cu–O superconductors are very sensitive to both the strength of the ac measurement fields and the external dc fields. As shown in fig. 5, a slight increase in the ac field (≈ 0.02 Oe amplitude) can cause the transition to shift to significantly lower temperatures, and very weak external dc magnetic fields (≈ 0.5 Oe) produce similar trends. This suggests that it is the intergranular coupling which is influenced by small Sb amounts as these fields are far less than the established value of H_{c_1}.

The quantitative results of the X-ray emission from SEM for the SB206 sample indicate that 90% of the lead in the starting composition disappears during the preparation. Checks on specimen SB204 show similar results. It seems that in order to obtain the highest T_c, it is very important that the starting composition contains 20–30% of lead substituting bismuth. It seems probable that the lead does not enter the superconducting phase, but may play a catalytic role in forming the 2223 phase. The role of "lead-doping" is still an interesting and open question to answer. The investigation of this phenomenon is important for producing high quality Bi-superconductors.

4. Conclusion

. The present experiments indicate that the transition region is sharpened and T_c is relatively constant for Sb-doping of Bi–Pb–Sr–Ca–Cu–O superconductors when the substitution of Bi(Pb) by Sb is a few percent. For higher doping, T_c decreases dramatically and the transition broadens. For the Sb-doped Bi–Pb–Sr–Ca–Cu–O superconductors, lead appears to act as a catalyst in producing the 2223 phase. However, the precise role of lead is still an open question. Sb-doping also strongly affects the Bi(Pb)-superconducting phase formation, but the mechanism behind this is not clear at present.

Acknowledgements

This work was supported in part by the Norwegian Research Council for Science and the Humanities (NAVF). The authors would also like to thank J. Yao for drawing the figures.

References

[1] H. Maeda, Y. Tanaka, M. Fukutomi and T. Asano, Jpn. J. Appl. Phys. 27 (1988) L209.
[2] J.M. Tarascon, W.R. McKinnon, P. Barboux, D.M. Hwang, B.G. Bargley, L.H. Greene, G. Hull, Y. LePage, N. Stoffel and M. Giroud, Phys. Rev. B 38 (1988) 8885.
[3] S.A. Sunshine, T. Siegrist, L.F. Schneemeyer, D.W. Murphy, R.J. Cava, B. Batlogg, R.B. van Dover, R.M. Fleming, S.H. Glarum, S. Nakahara, R. Farrow, J.J. Krajewski, S.M. Zahurak, J.V. Waszczak, J.H. Marshall, P. Marsh, L.W. Rupp, Jr. and W.F. Peck, Phys. Rev. B 38 (1988) 893.
[4] S. Koyama, U. Endo and T. Kawai, Jpn. J. Appl. Phys. 27 (1988) L1861.
[5] R. Ramesh, G. Thomas, S. Green, C. Jiang, Y. Mei, M.L. Rudee and H.L. Luo, Phys. Rev. B 38 (1988) 7070.
[6] Q. He, D.A. Yu, S.A. Chang, R.K. Wang and H. Zhang, Phys. Lett. A 133 (1988) 441.
[7] E. Chavira, R. Escudero, D. Ríos-Jara and L.M. León, Phys. Rev. B 38 (1988) 9272.
[8] A. Manthiram and J.B. Goodenough, Appl. Phys. Lett. 53 (1988) 2695.
[9] N. Murayama, M. Awano, E. Sudo and Y. Torii, Jpn. J. Appl. Phys. 27 (1988) L2280.
[10] A. Oota, A. Kirihigashi, Y. Sasaki and K. Ohba, Jpn. J. Appl. Phys. 27 (1988) L2289.
[11] T. Kawai, S. Kawai, S. Tanaka, T. Horiuchi, S. Takagi, K. Ogura, S. Kambe and M. Kawai, Jpn. J. Appl. Phys. 27 (1988) L2296.
[12] H. Nobumasa, T. Arima, K. Shimizu, Y. Otsuka, Y. Murata and T. Kawai, Jpn. J. Appl. Phys. 28 (1989) L57.
[13] M. Wilhelm and O. Eibl, Solid State Commun. 70 (1989) 137.
[14] B. Zhu, L. Lei, S.L. Yuan, S.B. Tang, W. Wang, G.G. Zheng, W.Y. Guan and J.Q. Zheng, Physica C 157 (1989) 370.
[15] P.V.P.S.S. Sastry, I.K. Gopalakrishnan, J.V. Yakhmi and R.M. Iyer, Physica C 157 (1989) 491.
[16] L. Pierre, D. Morin, J. Schneck, J.C. Tolédano, J. Primot, C. Daguet, F. Glas, J. Etrillard and H. Savary, Solid State Commun. 69 (1989) 499.

[17] T. Komatsu, R. Sato, K. Matusita and T. Yamashita, J. J. Appl. Phys. 28 (1989) L1159.
[18] H.B. Liu, L.Z. Cao, L. Zhou, Z.Q. Mao, X.X. Li, Z.D. Yu, B. Xue, X.L. Mao, G.E. Zhou, Y.Z. Run, Z.J. Chen and Y.H. Zhang, Solid State Commun. 69 (1989) 867.
[19] S.X. Dou, H.K. Liu, N.X. Tan, Y.J. Sheng and W.K. Jones, Physica C 158 (1989) 97.
[20] W. Peng, R.H. Hannon, H. Lee, A.P. Genis, V.J. Melim, C.W. Kimball, B. Dabrowski and D.G. Hinks, Phys. Lett. A 139 (1989) 91.
[21] J.S. Luo, D. Michel and J-P. Chevalier, Appl. Phys. Lett. 55 (1989) 1448.